Montanuniversität Leoben

Dissertation

Recovery phenomena in severely deformed metals

Oliver Renk

Leoben, November 2015

This work was financially supported by the FWF Austrian Science fund under grant 24141–N19 and the European Research Council under ERC Grant No. 340185 USMS.

Erich Schmid Institute of Materials Science
Austrian Academy of Sciences
Jahnstrasse 12
A–8700 Leoben

This thesis was typeset by the use of KOMA-Script and LaTeX 2_ε.

Affidavit

I declare in lieu of oath, that I wrote this thesis and performed the associated research myself, using only literature cited in this volume.

Oliver Renk

Leoben, November 2015

Wo kämen wir hin, wenn jeder sagte, wo kämen wir hin und keiner ginge, um zu sehen, wohin wir kämen, wenn wir gingen.

KURT MARTI

Danksagung

Zuallererst möchte ich mich bei meinem Betreuer Prof. Dr. Reinhard Pippan für die Vergabe dieser Arbeit und deren Betreuung bedanken. Seine Erfahrung und der Blick aufs Wesentliche, vor allem aber der grenzenlose Optimismus, erleichterten vieles. Danke für die Geduld und Zeit, die zahlreichen Diskussionen, Ideen und die Möglichkeit für zahlreiche Reisen zu internationalen Tagungen. Die Betreuung abseits der Wissenschaft an den schönsten Kletterspots der Steiermark - all das machte die vergangenen vier Jahre ganz besonders!

Bei Toni Hohenwarter möchte ich mich für die ausgezeichnete Co-Betreuung, die kritischen Fragen zu allen experimentellen Befunden sowie die mentale Unterstützung in schwierigen Phasen der Arbeit bedanken. Ein Dankeschön geht auch an Stefan Wurster, für die vielen Diskussionen, das Dabeisein bei fragwürdigen Versuchen und seinen trockenen Humor.

Bei allen Kollegen am Erich-Schmid-Institut möchte ich mich für die tolle Atmosphäre und die Hilfsbereitschaft bedanken. Im Speziellen sei den Damen vom Sekretariat, Viktoria Schrutt, Daniela Brunner und Sabine Wilfling für die Erledigung von organisatorischen Arbeiten und Abrechnungen, sowie für die Hilfe beim Bewältigen von neu geschaffenen bürokratischen Hürden herzlich gedankt, dem Werkstättenteam, Franz Hubner und Robin Neubauer, für die stets gewissenhafte und prompte Erledigung von Arbeiten, Silke Modritsch und Gabi Felber für die metallografische Probenpräparation und die Unterstützung bei der Präparation von TEM Proben. Bei Peter Kutleša möchte ich mich besonders für seine helfende Hand bei Experimenten und seinen grenzenlosen Humor bedanken. Ein Dank gebührt auch meinen studentischen Mitarbeitern, Gerald Schaffar und Severin Jakob, für ihr Interesse und die gewissenhafte Erledigung der Arbeiten. Ich wünsche euch alles Gute für euer weiteres Studium!

Ein besonderer Dank geht auch an meine Bürokollegen Andreas Umgeher und Benjamin Schuh für die kurzweilige Bürozeit und die vielfältigen Diskussionen. Daniel Kiener und Verena Maier danke ich für Diskussionen, die schöne Zeit auf Konferenzen und einige gute Tropfen. Thomas Leitner und Karoline Kormout danke ich für die gemeinsamen Stunden auf Tagungen, die Hilfsbereitschaft und die "16:00 Uhr

bis später Diskussionsrunden". Xiang Zhou danke ich für die Motivation im gemeinsamen Endspurt. Im Übrigen gratuliere ich ihm zur gewonnenen Wette.

Ihr alle habt zum Gelingen dieser Arbeit beigetragen, nochmals ein ganz herzliches Danke.

Zum Schluss ein besonderer Dank an meine Familie. Danke für eure Unterstützung und euren Rückhalt - ihr habt dadurch vieles erst ermöglicht! Marlene danke ich für die wunderbare gemeinsame Zeit, das Verständnis und bei zu viel Motivation für die Arbeit, den Hinweis auf die wirklich wichtigen Dinge im Leben!

Abstract

In the last decades, methods of Severe Plastic Deformation (SPD), have received enormous scientific attention as they provide a simple tool to refine coarse grained materials to the submicron- or even nanoscale. Their outstanding physical and mechanical properties, such as high strength and low coercivity have been intensively studied and documented. Despite these efforts, certain subjects are still not well understood. In light of the extensive research that has been carried out, showing that fragmentation of the structure terminates after sufficient straining, the dynamic recovery processes that take place after large strains have not been directly investigated. Identifying and understanding these processes, that are necessary to enable the restoration of the microstructure is crucial for both, modeling activities and further microstructural design of such fine grained materials. Tantamount to this open question, during the early stages of recovery at relatively low annealing temperatures, unusual hardening phenomena have been reported. Different explanations for these unusual strengthening phenomena that cannot be exclusively attributed to the formation of additional phases have been proposed. Interestingly, this strengthening phenomena cannot be observed for severely deformed materials in general. The linking microstructural feature of both relatively new research fields is a metastable or non-equilibrium state of grain boundaries, leading in the first case under an external load to grain restoration processes, in the other case, during annealing, to a recovery hardening. In this thesis a unified experimental view on this cutting edge process is provided.

For the first time the dynamic restoration mechanisms, required for a dynamic equilibrium, have been directly identified with a so-called split specimen technique. With the chosen setup it was possible to study the microstructural changes of the structure by Electron Backscatter Diffraction (EBSD) on the grain scale during deformation. Grain boundary migration was identified to be the dominant mechanism that enables a dynamic equilibrium of microstructural features during deformation. Moreover, with a similar approach it was proven, that boundary migration takes also place after a strain path change to adjust and restore a new dynamic equilibrium. Since EBSD data provides the orientation of the grains with migrating boundaries, an estimation of the underlying driving forces will be presented. To understand why static recovery can lead in certain cases to a hardness increase, a comprehensive

experimental study on severely deformed metals, binary alloys and a commercially available austenitic steel was carried out. Effects of segregates to the strengthening were analyzed for specific samples using atom probe tomography. The results clearly show that a hardness increase during annealing is only possible when the grain size can be kept below a certain threshold. Below this limit, a grain size dependency of the hardening is observed.

Contents

1

Introduction and aim of the thesis

The following chapter will give a short introduction into the field of nanocrystalline (nc) and ultrafine-grained (UFG) metals. Interesting questions yet unsolved, concerning the microstructural changes during deformation of such structures and their response during early stages of recovery will be outlined. A major challenge of the thesis was to find suitable experiments to clarify these issues. The main results are then summarized in chapter 2. Details can be found in the enclosed publications, see publications A, B, C, D and E.

Nanocrystalline (nc) and ultrafine-grained (UFG) materials have been in the focus of basic research in the last three decades. Due to their enhanced mechanical properties such as strength or fatigue limit but also on account of their physical properties (e.g. low coercivity of nc magnetic materials) [1, 2] they are potential candidates for certain applications. Such fine grained materials can be synthesized by so called 'bottom-up' or 'top down' processes. While in 'top-down' processes such as inert gas condensation (IGC) the nanostructured material is built up atom by atom or layer by layer, top down processes use coarse grained starting materials which are heavily deformed to break up the coarse grained structure [3, 4]. Because none of the bottom-up processes was used in the present thesis, for details to this processes the reader is referred to [3]. The most popular 'top-down' approach is Severe Plastic Deformation (SPD) processing, where coarse grained samples are subjected to severe strains, that can easily reach several thousand percent, to generate nanostructured materials without changing the dimensions of the sample itself [5]. This definition of a constant sample shape is, however not a prerequisite to refine the microstructure to the nanoscale. Structures of similar dimensions are accessible by conventional cold rolling or wire drawing too [6–9], albeit the starting dimensions of the sample would be in the range of meters to reach strains, that are comparable to

SPD processes. The main advantage of SPD processes when comparing to bottom up processes is that relatively large, bulk samples without porosity or flaws can be generated, making all kinds of physical or mechanical testing possible. The main SPD methods that have been developed in the past decades are high pressure torsion (HPT) [10,11], accumulative roll bonding (ARB) [12,13] and equal channel angular pressing (ECAP) [14,15]. Beside this basic processes, a vast number of modifications or new processing routes have been developed in recent years, although the main principles remained unchanged, see for example [16,17]. As within this thesis HPT was used to synthesize nanostructured and ultrafine-grained materials, only this method will be described briefly within this section. For details to the other SPD processes the reader is referred to the references given above [12–15].

In HPT a cylindrical sample is placed between two anvils. Large hydrostatic pressures of several GPa are applied to enable severe torsional straining without cracking. In Fig. 1.1, a schematic of the quasi constrained HPT process is shown. With this setup large shear strains of several thousand percent can be applied easily. The shear strain γ, can be calculated by Eq. 1.1, where n denotes the number of revolutions, r the radius and t the specimen thickness. For comparison with other processes, an equivalence criterion such as the von Mises strain is introduced which can be calculated as given in Eq. 1.2.

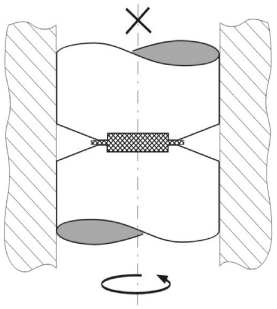

Figure 1.1 Schematic of the quasi constrained HPT process.

Simple inductive heating systems or cooling can further be applied to change the deformation temperature, see for example [10, 18] for details to the heating and cooling devices used.

$$\gamma = \frac{2\pi r n}{t} \tag{1.1}$$

$$\epsilon_{vM} = \frac{\gamma}{\sqrt{3}} = \frac{2\pi r n}{t} \tag{1.2}$$

During plastic deformation the density of stored dislocations is increasing with strain. It has been shown by intensive TEM studies, that the dislocations are not stored randomly in the material but in form of dislocation structures, with the size

and shape of these cells depending on the applied stress (strain) and deformation mode. Important findings of these studies and an overview may be found in [19–21]. The defect density within the cells is fairly low when compared to the cell walls. Deforming the material further, additionally to low angle boundaries (LAGB), high angle grain boundaries (HAGB) have to form and subdivide the original grain. With increasing strain, the size of the cells is decreasing and their misorientation is increasing [6,19,20,22,24]. This decrease in grain (cell) size is reflected in the increased flow stress of the material. While the decrease in cell size is effective at small degrees of deformation, the increment of structural size reduction and so the increase in flow stress per additional strain increment is gradually reduced [6, 22, 24]. The reasons for this reduced work hardening rate are dynamic recovery effects that balance part of the refinement. At very high strains, often referred to stage IV and V of work hardening, recovery equals work hardening or grain refinement. This regime often referred as steady state or saturation regime, can therefore be seen as a dynamic equilibrium between restoration or recovery mechanism (strain softening) and grain refinement (strain hardening). The fact that grain refinement 'terminates' after sufficient strain has been reported frequently for SPD processed materials [18, 24–27]. Beside the boundary spacing, also other structural features like aspect ratio, misorientation distribution or texture remain constant on average, see publication B and [24].

A saturated microstructure cannot exclusively be obtained by classic SPD processes. In fact, each deformation mode, where sufficient strain can be applied without failure, as for example cold rolling or wire drawing, leads to a certain steady state microstructure, see for example studies on severely cold rolled Ni or Al where grain refinement has almost diminished [6, 7]. The minimum grain size achievable, resulting from the dynamic equilibrium between restoration and refinement, was found to be mainly dependent on the deformation temperature and the purity level of the material. The strain rate and the applied hydrostatic pressure in HPT deformation affect the resulting grain size only marginally [18, 24]. Although the existence of a steady state is well known and a vast amount of experimental work has been performed, confirming a diminishing work hardening rate, the dynamic recovery processes that can completely equilibrate grain refinement, are still not understood. The main reason for this might be due to the lack of direct experimental results. So far, completely different approaches and results about the underlying mechanisms, and therefore contrary efforts to predict or model the minimum grain size in SPD have been made, see for example [28–31]. Therefore, in one part of the thesis a suitable experimental setup was looked for, to get direct and unbiased insights into the dynamic recovery mechanisms during severe deformation. The experimental setup used as well as the main results are discussed in chapter 2.1. Details can be found in publication B.

In addition to this experiment, samples with a saturated microstructure were subjected to a strain path change to get (i) a better understanding for the stability of the equilibrium state and (ii) to scrutiny if such a strategy could lead to further structural refinement. Preliminary results can be found in section 2.1.1.

Additionally to dynamic recovery processes occurring during plastic deformation of metals, static recovery of the deformed structure will proceed when the load is removed. Although such processes would require long periods of time when the samples are stored at the same temperature where they were deformed, even slight temperature increases may activate such processes to occur accelerated. Because recovery, recrystallization or grain growth processes reduce the density of defects stored within the material and thus the systems energy, nc and UFG metals seem to be rather unstable, as they obey a large fraction of crystal defects. The large fraction of free volume makes it easy for linear and point defects to annihilate and the small size of the crystallites offers large driving forces for grain growth. Taking into account only the energy being stored in form of grain boundaries, for metals with grain sizes in the 100 nm regime, yields a latent energy of several Jcm^{-3}. This value is about 2 – 3 orders of magnitude larger than in microcrystalline samples.
Indeed, several studies on pure nc or UFG copper showed recrystallization and massive grain growth even during storage at room temperature ($\approx 0.22\ T_m$) for several months, see for example [32,33]. It is well known that grain growth can be effectively hindered by adding particles or alloying elements to the sample [34–36].
With these approaches, nanocrystalline materials showed exceptional stability up to temperatures of about $0.30 - 0.50\ T_m$. Such strategies are often referred as thermodynamic (reducing the boundary energy by segregated solute) or kinetic approaches (reducing the boundary mobility with particles), see for details to the thermodynamic framework Refs. [34, 38–40].

Interestingly, several studies indicated, that whenever grain growth of the nanostructures could be avoided and only recovery of defects occurred, a gain of the yield strength or hardness have been measured [43–46]. Because, no additional phases formed during annealing other explanations than classical ones i.e. based on precipitation hardening, are required for these intriguing results. An increase in hardness solely caused by recovery processes, such as the reduction of defect density or slight (sub)grain growth seems astonishing, because classic recovery knowledge is usually found to decrease the materials strength [47, 48]. Although several explanations exist for the occurrence of this hardening phenomenon, the details have remained uncertain yet. One of the first proper descriptions claimed a starvation of dislocations [43], similar to that observed in single crystalline samples having dimension below a couple of microns, being proposed analytically by Ashby already in 1968 [49] and experimentally verified decades later [50, 51], to be responsible for the strengthening. The remaining dislocations may not be sufficient to realize the imposed deformation, thus sources have to be activated requiring enhanced stress levels. Unexpected strengthening was also observed in nc alloys such as an aluminium alloy and an austenitic steel [52,53]. In both cases segregated solute was detected by atom probe tomography (APT), hence the strengthening was attributed to a hindering or pinning of dislocation getting emitted from the boundaries [52, 53]. A different explanation, although based on segregated solute or impurities, would be that the segregates hinder the relaxation of lattice dislocations at the grain boundaries. This

situation is schematically shown in Fig. 1.2. Fig. 1.2a indicates a dislocation that has been emitted from a grain boundary. This dislocation will move further through the crystal due to the resulting shear stress on its glide plane. Fig. 1.2b shows the ideal case of dislocation segments that have been already deposited at the grain boundary. During a heat treatment impurity or solute atoms may segregate to the grain boundaries. This could lead to a retarded relaxation process of dislocation segments, as schematically shown in Fig. 1.2c. Such a behavior would result in an increased curvature of the dislocation, what requires a higher stress level to move it further than in the case of Fig. 1.2b.

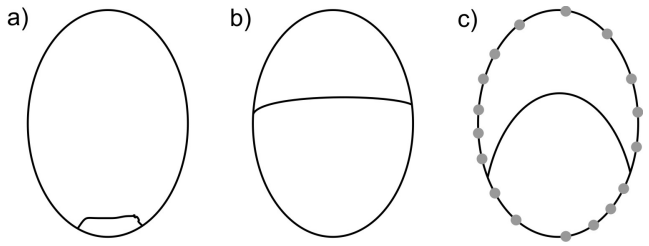

Figure 1.2 A possible explanation for the observed hardness increase during annealing. a) Schematics of a dislocation emitted from a grain boundary; b) During the movement of the dislocation through the grain, segments have to be deposited at the boundaries. c) This relaxation behavior might be retarded due to the presence of segregated solute, indicated with grey dots. In this case, the increased curvature of the dislocation line would require higher stress levels for further movement than in case b).

A MD simulation and an experimental study on ball milled powders point out into a similar direction [41, 42]. Due to the difficulty to separate possible contributions of these two explanations a detailed understanding of the underlying mechanisms has not evolved yet. Even in the purest material a certain amount of impurities will segregate to the vast number of boundaries, while on the other hand also dislocations will annihilate during the annealing in alloyed systems. Results of different SPD deformed metals showed that such hardness increases will not take place in all systems. This shows unambiguously that further studies are needed to understand this interesting strengthening mechanism in detail. In the second part of the thesis experiments were carried out to clarify the origin of hardening by annealing that might occur during the early stages of recovery in nc metals. Experiments on different binary alloys as well as pure Ni were carried out. Microstructural investigation and insights into the boundary chemistry by APT completed the picture. The results are summarized in section 2.2 and outlined in detail in publication C, D and E.

2

Summary of the experimental results

2.1 Dynamic recovery mechanisms in the steady state regime

To directly capture the dominant restoration mechanism in the steady state regime a split specimen technique was used. This approach uses two identical samples that are fitted together with the areas of interest brought into contact to imitate a bulk like behavior and to keep the surface roughness at a low level. Such a technique enables to capture the structural evolution during subsequent deformation steps. High purity Cu (99.99 %) was used as a model material. Because during HPT even small twist angles result in a relatively large strain, see Eq. 1.2, and thus large structural changes can be expected, the experiment was performed on severely cold rolled samples. Rolling allows to apply smaller deformation increments and is so perfectly suitable to follow the structural evolution in the steady state regime. To reduce the strain needed to reach a steady state upon cold rolling at RT, Cu with an UFG structure obtained by HPT, was used as a starting material. As the grain size was already refined to the submicron level, only the grain shape and the texture had to be changed from the state after HPT to the one after cold rolling. The normal direction (ND) of the cold rolled material was kept parallel to the former torsion axis and the long grain axis was alligned parallel to the rolling direction (RD) during the entire experiment. Microstructural investigations based on EBSD data and microhardness measurements showed that this transition and so a new steady state is created for rolling strains being larger than $\phi \geq 2$, see publication B.
For the split specimen, two small samples with a saturated microstructure ($\phi = 2$) were prepared for Electron Backscatter Diffraction (EBSD) on the RD-ND plane. These two samples were fitted into a brass sheet (see Fig. B.1 in publication B) and cold rolled to an additional thickness reduction of $\Delta\phi = 0.70$ in several passes, each of

them with a thickness reduction of $\Delta\phi \approx 0.15 - 0.20$. Between each strain increment an EBSD scan was performed to capture microstructural changes. The regions of interest were marked with a Focused Ion Beam (FIB) station. This facilitates finding the scanned areas again after the next rolling pass and in addition drift problems can be excluded if the height and width of the FIB markers are the same in the SEM image and the Orientation Imaging Microscopy (OIM) data. The structural evolution of one of these regions during additional 70 % deformation in the steady state is shown in Fig. 2.1. No clean-up algorithm was used in this Inverse Pole Figure (IPF) maps to avoid falsification of the results especially in the boundary regions.

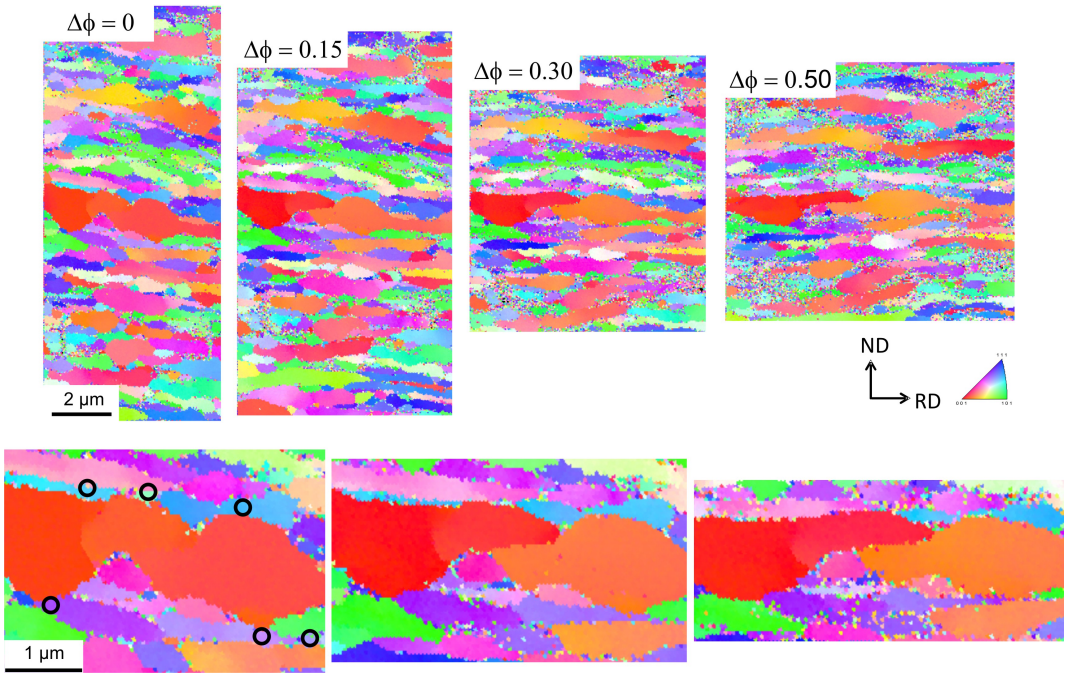

Figure 2.1 Inverse Pole Figure maps showing structural changes occurring during additional rolling deformation in the steady state regime. Positions where changes appeared are circled and shown in detail at the bottom.

In Fig. 2.1, regions where microstructural changes occurred are circled and shown in detail. From the experiments it can be seen that grain boundary sliding does not take place, at least at a length scale that is accessible by EBSD. Contrary, it can be seen that grain boundaries move in ND during cold rolling. This movement leads to a fragmentation of adjacent grains, followed by a complete disappearance in many cases. This grain boundary movement makes it possible to restore the microstructure as growing grains can balance the refinement due to rolling by consuming neighboring grains. Although the results of the split specimen show only a 2D picture, exactly similar processes occur in bulk samples. This can be seen in Fig. 2.2a, where a bulk sample, cold rolled to similar strains, has been investigated. Similar changes than

found in the split specimen can be identified. Grains that are getting fragmented are highlighted by arrows. Beside, a grain, colored in green in the IPF map, appeared to be already split into two parts. These two fragments are marked with black dots and their orientation is plotted in the IPF to the right. It can be clearly seen that the orientation of the two grains is almost identical, what indicates that these two grains formed a single grain before and that the processes, observed in the split specimen are really the ones responsible to recover a certain equilibrium microstructure during severe straining.

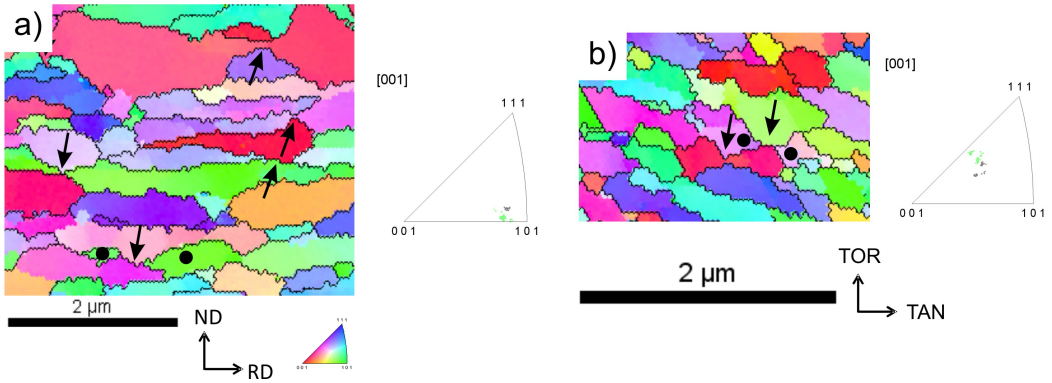

Figure 2.2 IPF maps of bulk samples of a) Cu (99.99 %) cold rolled to saturation and b) Ni (99.99 %) HPT deformed to saturation. In both cases the arrows indicate positions were structural changes occur. It can be seen, that also in the bulk case the fragmentation of grains due to the migration of boundaries occur. This is confirmed by plotting the orientation of two grain fragments, marked with black dots, in an IPF, showing almost identical orientations.

Up to now, structural investigations just focused on severe cold rolling. Therefore, it is of interest if similar processes take place under different loading conditions as well. For this reason IPF maps of pure Ni (99.99 %) samples, containing the HPT saturation microstructure, were carefully examined. Fig. 2.2b shows exemplarily such a sequence. Similar changes as already observed during cold rolling appeared and are highlighted by arrows. Again, two grains just fragmented are marked with black dots and their orientation is plotted in the standard triangle to the right. Summing up the results, it can be concluded that the motion of grain boundaries limits refinement at large strains and is responsible to restore a certain steady state microstructure. The movement of the boundaries limits not only the minimum spacing of the lamellae boundaries, by the fragmentation of neighboring grains, additionally the long axis of the grains will be frequently reduced and kept at a certain maximum level.
Recently, triple junction motion has been observed as a static recovery mechanism in severely cold rolled aluminium [54, 55]. Because thin grains have a small dihedral angle, being far off the equilibrium angles between three grains, (see Fig. 2.3b) a driving force towards larger angles occurs which is responsible for the movement of the junction to the right in this example [54]. In addition, this mechanism can

be seen as the first step to destroy the lamellar arrangement of grains, typically for a material deformed to severe strains, mandatory to form a recrystallization nuclei [56]. Further it was suggested, that the movement of triple junctions might also be responsible for the dynamic recovery of severely deformed structures [57]. Undoubtful, also the movement of triple junctions is an appropriate process to restore the microstructure, see schematics in Fig. 2.3b.

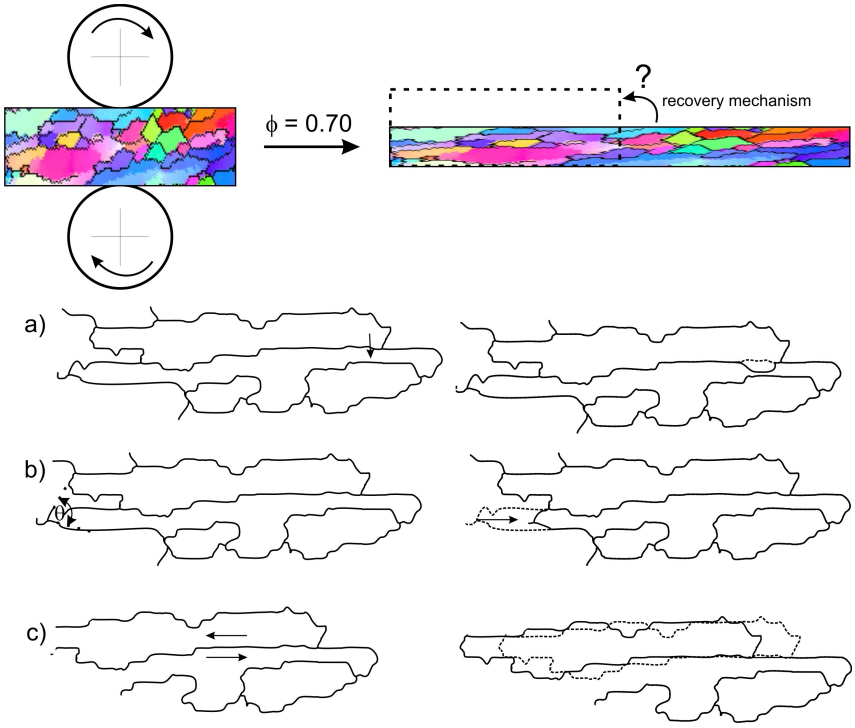

Figure 2.3 Schematics of potential restoration mechanisms with the structures taken from an EBSD scan: a) migration of boundaries b) movement of triple junctions, c) sliding of adjacent grains.

In Fig. 2.3, additionally to the migration of a triple junction two other possible restoration mechanisms, the migration of boundaries (Fig. 2.3a) and the sliding of adjacent grains (Fig. 2.3c) as discussed before, are shown. Although it was found that triple junction motion is a thermally activated process [55], thus taking place more frequently at elevated temperatures, it is reasonable that similar processes will occur just mechanically driven, as in the case of the observed motion of HAGB. However, a direct separation of these two mechanisms is not possible with the chosen split specimen technique as both, further migration of the grain boundary and a movement of the triple junction would result in the same picture in the IPF map. Nevertheless, in most cases observed, the initial step was found to be the movement of a boundary in ND. By this, an adjacent grain fragments and often forms a triple junction that would not have been there before. Only after that fragmentation process a movement of the triple junctions could take place. From this point of

view, the migration of grain boundaries seems to be the critical and rate determining dynamic recovery mechanisms after severe monotonic straining. This boundary migration does not only lead to a local growth of certain grains, it also leads to a fragmentation of shrinking grains and thus also limits the aspect ratio at a certain length. This finding is different to a grain size stabilizing mechanism discussed earlier in a review on saturation of fragmentation. There [24], it was proposed that a fragmentation of grains occurs by formation of LAGB perpendicular to the long grain axis which increase their misorientation with increasing strain. Although such a behavior was not observed experimentally, a thorough examination of the IPF maps was carried out in view of this proposed mechanism. Such boundaries of small misorientation, often termed interconnecting boundaries, can be frequently found in UFG structures. Despite that, they are not changing their misorientation considerably during deformation, as can be seen for both, cold rolled and HPT deformed structures where a LAGB was tracked over a certain strain interval. This is shown for the HPT case for three interconnecting LAGB in Fig. 2.4, before and after a strain increment of $\epsilon = 0.30$.

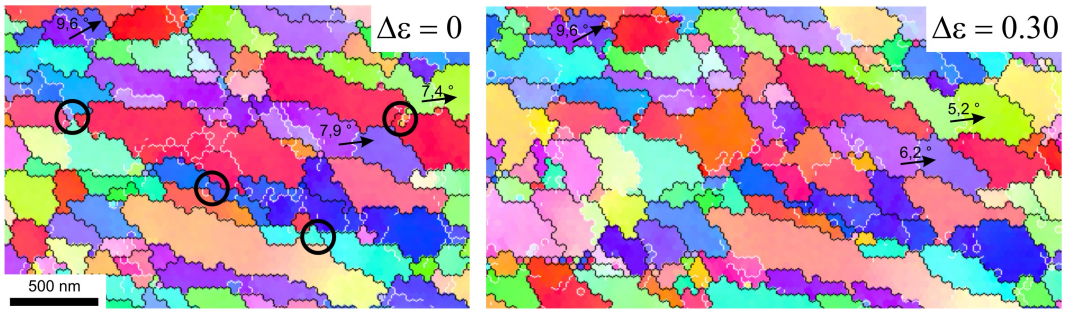

Figure 2.4 IPF maps of HPT deformed Ni before and after an additional strain increment of $\epsilon = 0.30$ in the saturation regime. Three LAGB are marked with arrows and their misorientation angle is indicated in both cases. The misorientation angle is not changing considerably during the applied strain increment. Positions were boundary migration and a fragmentation occurs are circled.

This result can be interpreted in a way that those LAGB realize a certain geometrically distortion required for the accommodation with the nearest neighbors. A substantial modification of this misorientation can therefore only be expected when the neighborhood of this grain changes. A distinct change of the neighborhood could be realized by the dissolution of adjacent grains as a consequence of boundary migration or by a change of the crystal orientation through lattice rotation. Otherwise, a change of the misorientation would require the deformation of the surrounding grains.

In summary, the experiments clearly showed that the dominant restoration mechanism during severe monotonic strains is the migration of grain boundaries that also limits the length of the grains by a splitting process. Because at a local scale grains tend to grow, while for sake of volume consistency others have to shrink, it is

interesting to understand which grains have a tendency for growth and what could be the underlying driving forces. This issue will be discussed in detail in section 2.1.2, as similar changes are also occurring during a strain path change, see next section. Due to the limitations of refinement after severe monotonic strains, it was of interest, if a strain path change could lead to further refinement. More specifically, UFG structures obtained by HPT were additionally cold rolled. This should, at least from a geometrical point of view, lead to additional refinement when the long grain axis is aligned in rolling direction. Furthermore, a general understanding of the structural changes that might occur due to a strain path change, are most important to understand, as for a SPD processed structure every further loading result in a change of the strain path. Preliminary results on this topic are summarized in section 2.1.1.

2.1.1 Boundary migration during a strain path change

A stunning result of the experiments presented in section 2.1 was that the steady state hardness of the cold rolled samples was about 10 % lower (130 HV after CR) than the one after HPT (142 HV). In addition, up to thickness reductions of $\phi = 1$, a pronounced continuous softening occurred, see Fig. 2.5. This is interesting as one would expect an increase in hardness rather than a decrease because the lamellae spacing in ND should become smaller during rolling for geometrical reasons, when the long axis of the grains is aligned parallel to RD.

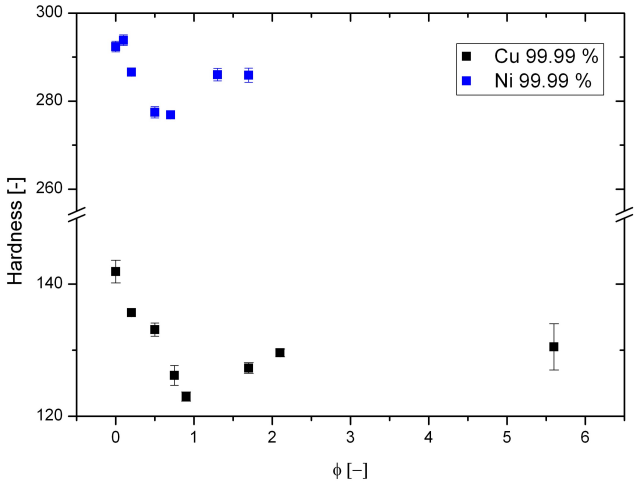

Figure 2.5 Evolution of the microhardness as a function of the applied thickness reduction during CR for UFG Cu and Ni prepared by HPT. Clearly for both materials continuous softening during early stages of cold rolling occurred.

Microhardness was measured at different thickness reductions to document the softening, however, its evolution cannot be attributed to changes in texture with increasing thickness reduction, because measured hardness values are nearly independent of the crystal orientation [65]. Although different yield stresses are observed

even in coarse grained materials due to a change in the strain path as different slip systems will be favored, this cannot account for the measured results either, as hardness decreases continuously to larger strains, see Fig. 2.5. For this reason, the observed decrease in hardness up to thickness reductions of $\phi = 1$ in the case of Cu might be attributed to structural changes. Thickness reductions being larger than $\phi = 1$, lead to an increase in hardness again. Despite that, hardness still leveled off at 10 % lower values than in the steady state of HPT, see Fig. 2.5. This two unexpected results motivated additional work to determine what changes occur in materials with grain sizes in the submicron regime which undergo a strain path change.
Similar rolling experiments as for Cu, with the former torsion axis being aligned in ND and the long grain axis being parallel to the RD, were performed also for Ni to exclude effects of self–heating of the structure due to the high homologous deformation temperature in the case of Cu. From Fig. 2.5 it can be deduced that microhardness as a function of the thickness reduction follows an exactly similar trend as for Cu. This suggests, that the observed softening is unique for HPT deformed fcc metals subjected to cold rolling, when the former torsion axis is aligned parallel to the ND and the long grain axis is oriented parallel to the RD. Microstructural investigations by EBSD of the Cu samples revealed that cold rolling leads to a coarsening of the structure. Fig. 2.6 shows micrographs of as HPT deformed Cu ($\phi = 0$) and samples after thickness reductions of $\phi = 0.75$, both seen in TD direction.

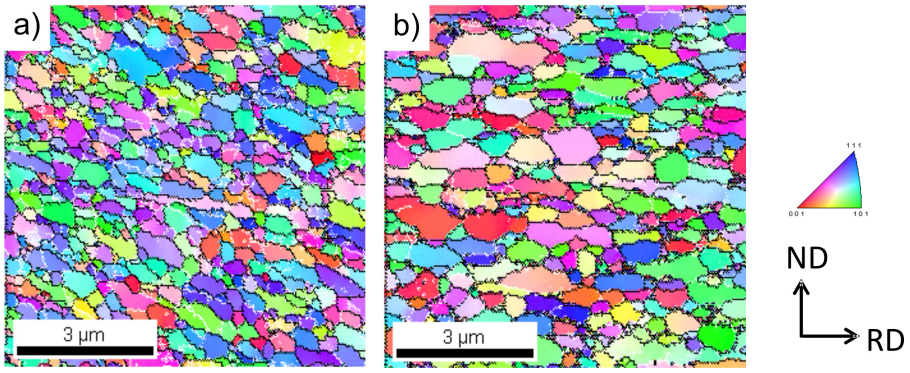

Figure 2.6 IPF maps of UFG Cu produced by a) HPT and b) additionally cold rolled to a thickness reduction of $\phi = 0.75$. Both samples are seen in TD. It is obvious that the structure has coarsened during cold rolling.

To identify the processes that lead to the coarsening during deformation another split specimen was used. Two small HPT deformed Ni samples were prepared as introduced in section 2.1 and cold rolled in several passes to a total thickness reduction of $\phi = 0.54$, with reductions of $\Delta\phi \approx 0.15$ per pass. The experiments showed that, similar as in the steady state, grain boundary migration in ND occurred from the beginning of CR. A sequence of the microstructural evolution of an exemplarily position is shown in Fig. 2.7.

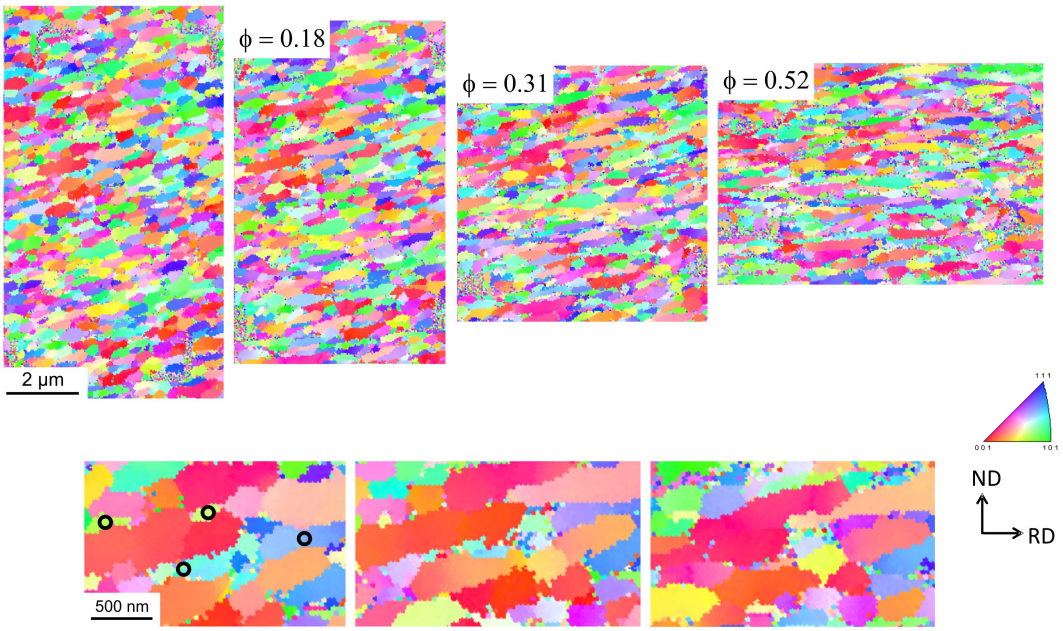

Figure 2.7 Structural evolution of HPT deformed Ni during the early stages of cold rolling. Exemplary positions where changes are visible are zoomed out and circled at the bottom. Similar to the steady state, migration of grain boundaries in ND occurred.

Positions with distinct structural changes are circled in Fig. 2.7. Interestingly, fragmentation of grains and thus the movement of boundaries occurred more frequently than observed in the steady state. In most of the circled regions the grains have completely disappeared during thickness reductions of $\Delta\phi = 0.31$. Because exactly the same recovery mechanism as in the steady state occurred during the chosen strain path change, the essential question to solve is why boundary migration leads to a dynamic equilibrium between refinement and recovery (zero work hardening) in the first case, and to a coarsening of the microstructure in the second case. In the case of Cu where even a slight coarsening of the structure was visible, the refinement caused by plastic deformation, Δx_{def} (increase in boundary length) has to be overcompensated by the movement of the grain boundaries, Δx_{gb} (decrease in boundary length). In other words further refinement or strain hardening of a structure will only be possible if the migration rate of the boundary can be significantly reduced. The reason for this enhanced migration of the grain boundaries at the beginning of cold rolling might be due to the necessary texture change. During rolling the shear texture has to change towards the typical fcc rolling texture. At the beginning of rolling several grains will not be favorably oriented for the new strain path and might be the ones that disappear. As shown in publication B, 20 % of the grains have a Taylor factor that is too large for the distribution that is obtained after cold rolling. Indeed, after large thickness reductions of $\phi = 1.40$ for pure Ni, about 33 % of the grains being larger than the average grain size have orientations close to the

ideal rolling texture components (15 degrees tolerance) while in the HPT starting structure this holds true only for 12 %. Similarly, in many cases it was found in the split specimen experiment, that grains with very large Taylor factors with respect to the neighboring grains disappeared. This proposes that the orientations of the starting structure with respect to the loading direction and the final texture affect the boundary migration rates and thus the extent to which strain can be recovered.

To test this hypothesis, HPT processed samples were again cold rolled but this time with a different load path. Different than in the experiments presented before (see Fig. 2.5), for this set of samples the former torsion axis was now oriented parallel to the TD direction and the long grain axis parallel to ND. Samples cold rolled in that manner are denoted as CR 90 rot in Fig. 2.8. From pure geometric considerations, this should result in a softening, because the elongated grains (as seen in RD direction) will become more and more spherical with increasing thickness reduction, enabling a larger glide path for dislocations. However, in contrast to the samples where the torsion axis was aligned parallel to the ND, hardness remained almost constant over large thickness reductions for both, Ni and Cu samples, see Fig. 2.8. In addition to the fcc metals, Nb as a bcc material was cold rolled in the same manner as the fcc structures and the results are also shown in Fig. 2.8.

For the bcc structures a different behavior than for the fcc ones was found. Softening occurred for the rotated samples, while slight hardening occurred for the samples where the torsion axis was parallel to the ND and the long grain axis parallel to RD. Although this are preliminary results, the pronounced difference between bcc and fcc structures showed, that geometric considerations are not able to predict whether a further refinement or a coarsening of the structure will develop. Of great importance to realize further refinement at the beginning of a strain path change, seems to be the suppression of grain boundary migration by either reducing their mobility (e.g. lower temperature) or by reducing the underlying driving force by a suitable selection of the load path. The difference between fcc and bcc structures might be understood in a way that the starting orientations with respect to the loading direction and the direction towards the final texture directly affects the driving force and so the boundary mobility. This relationship is schematically shown in Fig. 2.9.

Depending if boundary mobility can be suppressed by the new strain path, at the beginning, softening or hardening might occur. Of course, after large strains applied again along the new strain path, all possible paths (e.g. CR normal and CR 90 rot in Fig. 2.8) will end up with the same steady state structure and hardness. The new steady state hardness does not necessarily have to be the same as the one before, as it was the case for Cu (see Fig. 2.5).

To summarize, the results clearly showed that during a strain path change softening or slight hardening can occur, depending on the chosen strain path. As with the same material both responses can be obtained, the absence of hydrostatic pressure can have no pronounced influence. During the strain path change grain boundary migration occurred and once led to a softening and once to constant properties or slight hardening. Thus the local orientations of the grains and the final texture

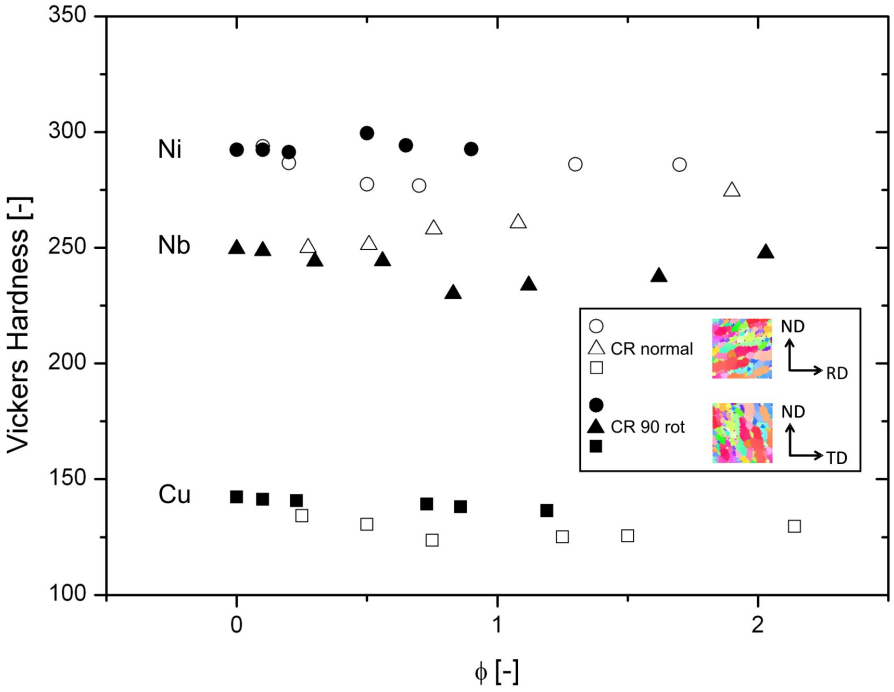

Figure 2.8 Evolution of the microhardness of UFG Cu, Ni and Nb as a function of the applied thickness reduction during CR for two possible strain paths. CR normal denotes samples with the torsion axis being oriented parallel to ND and the long grain axis parallel to the RD. CR 90 denotes samples where the torsion axis was oriented in TD and the long grain axis parallel to ND during rolling.

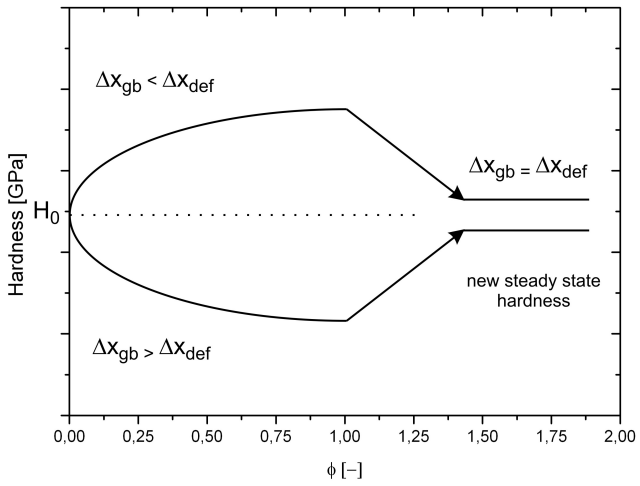

Figure 2.9 Schematics of the hardness evolution during a strain path change. Depending on the balance between refinement and recovery by boundary migration initial hardening or softening will occur. However, after sufficient additional strain, different starting orientations will end up in the same steady state hardness level. This level does not have to be necessarily the same as the starting one.

seem to govern the migration rates. This in turn may lead to an overshooting at the beginning of a strain path change that is possible in both directions depending on the offered driving force for boundary migration, as can be seen in the schematics in Fig. 2.9.

2.1.2 Driving forces for grain boundary motion

Experimental results in the previous sections 2.1 and 2.1.1 clearly showed that boundary migration tend to occur whenever a submicron or nc material is plastically deformed. Although it is well known for several years that high angle boundaries can migrate in UFG or nc metals even at lower homologous temperatures [58–61], details about the driving forces or an understanding which boundaries will migrate and so lead to growth and shrinkage of grains is still incomplete. A reason for that might be that many of the experiments were carried out with TEM samples and no insights into the bulk behavior or an orientation relationship between adjacent grains was gained. Because drastic grain growth in nc and UFG Cu was observed even during indentation creep experiments at 77 K [60], but not for their coarse grained counterparts, the reason for the coarsening was attributed to the high stresses in the fine grained samples. In [58, 59] it was claimed that a high angle grain boundary in a bicrystal was migrating purely due to the applied shear stress. This experiments lead to the notion that the high stresses, present in nc and UFG metals whenever they are loaded, force the boundary to migrate, what was often referred as 'stress–driven' grain boundary migration, see also [62]. In the split specimen described in section 2.1, migration of grain boundaries was found to be the responsible recovery mechanism, enabling a dynamic equilibrium between refinement and restoration during severe straining. At the same time, for both cases, cold rolling and HPT, the expected deformation textures were observed, although grains disappeared continuously, while others grew at their expense. For this reason, it is very unlikely that the boundaries just move due to the high stresses that are applied, but still the expected crystallographic texture would prevail. The advantage of the split specimen technique carried out within this thesis is that beside the identification of boundary migration as the main recovery mechanism the crystallographic orientation between neighboring grains was directly captured using EBSD on bulk samples. The better statistics than in TEM studies, the usage of bulk samples and the knowledge of the grain orientations may deliver useful insights in order to understand boundary migration in UFG and nc metals.

A careful examination of growing and shrinking grains did not show any preferred crystallographic orientation that tended to grow or shrink. This is not surprising, as texture and the intensities of the individual texture components have to remain constant in the steady state or a certain crystallographic texture has to develop during deformation, see publication B. One could argue that the driving force for the migration of the HAGB is a reduction of the grain boundary energy, as the stored energy of the grain boundaries in UFG or nc metals can be estimated to be in the order of Jcm^{-3}. However, a closer look shows that this cannot be the case. When,

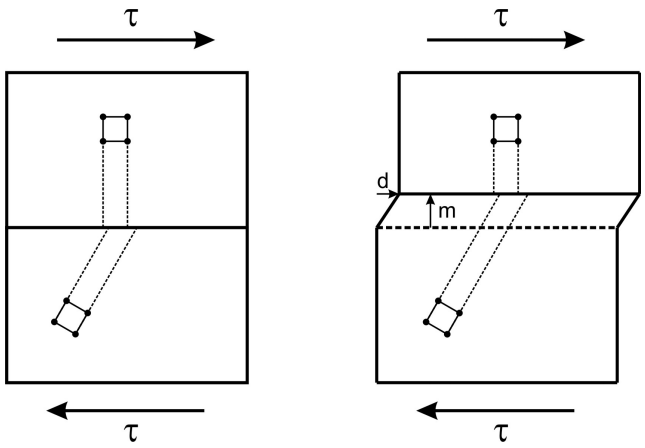

Figure 2.10 Schematics showing that the migration of a grain boundary due to applied shear stresses lead to a migration m of the grain boundary. This migration produces a shear displacement of d [64].

as experimentally observed, boundaries migrate and fragment adjacent grains, the boundary energy is not reduced. Quite contrary, seen at a local scale, for the first step of the fragmentation it is even enlarged due to the formation of an increased boundary surface. Seen on a global scale, the latent energy stored due to boundaries will not change at all, as the crystallite size remains on average constant. A thorough analysis of growing and shrinking grains reveals, that in almost any case the shrinking grain was either unfavorably oriented with respect to its neighborhood or significantly smaller in size. Both, smaller grain size and larger Taylor factors would lead to higher local (yield) stresses. From that point of view, local stress differences and thus a reduction of the systems strain energy by the migration of boundaries, seem to govern the direction of boundary movement rather than the stress level itself as suggested in a vast number of publications, see for example [60,62]. The resulting stress differences can easily be estimated as outlined in publication B by assuming for instance the extreme case of the smallest and largest grains of the grain size distribution being next neighbors. Similar calculations could be performed with two grains having orientations leading to a fairly low and considerably large Taylor factor. As outlined in detail in publication B, such a consideration leads to a difference in the elastic strain energy density between the grains of several MJm^{-3} equal to a driving pressure p on the boundary of several MPa. Although this values seem to be large enough when compared with traditional recrystallization, where p is assumed to be in the same range [63] this leads only to values of $\approx 10^{-3}$ eV per atom. For the migration of a grain boundary transport of atoms or groups of atoms from one grain to the other is necessary. The activation energy for such a transport is in the order of 1 eV [20], the activation energy for self–diffusion. As thermal activation is more and more negligible towards lower deformation temperatures where such recovery processes are still active, the above estimated driving forces seem to be too low.

However, the movement of the boundary itself leads to plastic (shear) deformation, as has been shown experimentally [58, 59, 64]. This situation is schematically illustrated in Fig. 2.10 and is comparable to mechanical twinning or martensitic transformations. The coupling factor β, defined as the ratio between shear displacement d and the lateral movement of the boundary m, determines to which extent shear is produced by the migrating boundary [64]. The coupling factor may depend on factors such as the type of the boundary or misorientation [64]. Taking the average shear stress, τ and calculating the produced shear stain, γ from shear angles typically observed during boundary motion [64] the work done can be calculated. This in turn yields an additional driving force being about $10 - 20$ times larger than the one calculated above. Although these values are about an order of magnitude higher than the ones from the elastic strain energy difference, 10^{-2} eV per atom still seem to be too low to explain boundary migration. For that reason, it is likely, that the large local stress fields of dislocations interacting with the grain boundary are necessary to facilitate the atomic jumps.

2.2 Recovery hardening in severely deformed metals

To clarify the mechanism leading to the frequently observed hardening mechanisms, an in depth study on single phase alloys, as well as pure metals was carried out. The investigated alloys were a commercially available 316L steel (Böhler grade A220), two different PtRu alloys with 5 and 10 wt–% Ru, pure Ni as well as consolidated Ni powders. In the following, only the main findings of these experiments will be summarized, details can be found in publication C, D and E.
HPT of the nc austenitic steel at RT leads to a saturation grain size of ≈ 50 nm as deduced from line interception method [66]. Isothermal (823 K) and isochronal (30 min) annealing treatments up to temperatures of 973 K were carried out on the samples and microhardness was measured to determine changes with respect to the mechanical properties. The results of these measurements are shown in Fig. 2.11 (taken from publication C).

It can be seen that up to annealing temperatures of 823 K hardness increased steadily. Compared to the as–deformed condition hardness increased by 20 %. Above 823 K grain growth occurs, what can be deduced from the hardness measurements and verified by SEM micrographs (see publication A). As seen from the isothermal treatment the hardening occurs rapidly, reaching almost a plateau value after several minutes of annealing. The same trend is visible for annealing temperatures being lower than 823 K. Although the hardness increase is not that pronounced anymore, plateau values are still reached immediately. Interestingly, even at low annealing temperatures of 343 K, a significant hardness change could be detected, see for details publication D. Due to this rapid hardening it was not possible to determine the activation energy of the underlying processes as for the highest annealing temperatures very short annealing times would be necessary what would lead to pronounced scattering of the results. However, additionally to the hardness, remaining constant

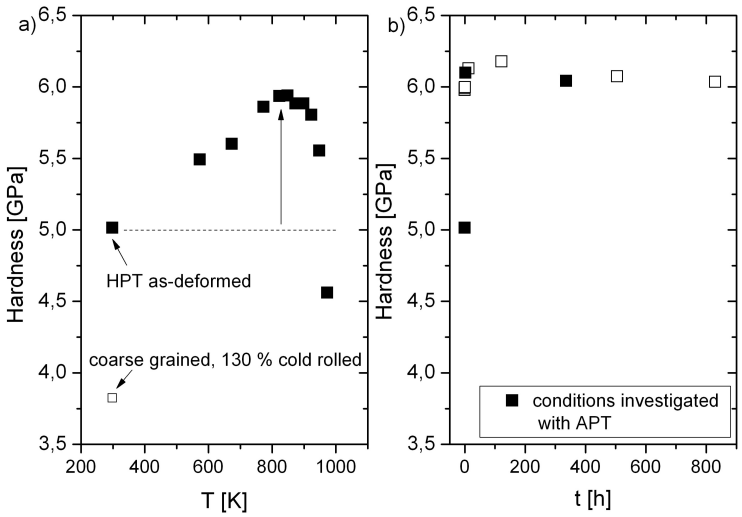

Figure 2.11 Room temperature microhardness of a) isochronally (30 min) and b) isothermally (at 823 K) annealed samples of nc 316L steel. Hardness increased by 20 % when compared to the as–deformed condition after an annealing treatment of 823 K.

over long annealing times of up to 800 hrs, also the microstructure was found to be rather stable (see Fig. 2.12, taken from publication D) in the investigated time interval.

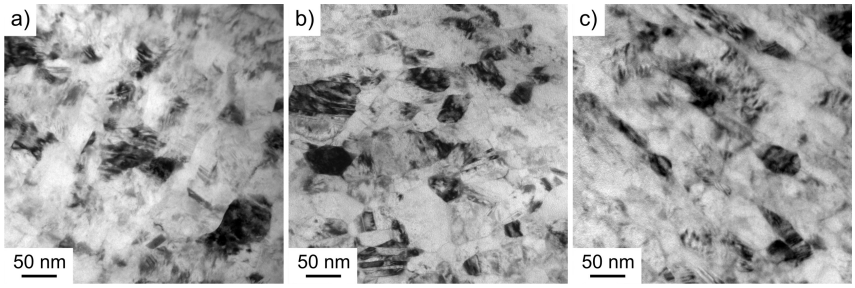

Figure 2.12 Bright field images of HPT deformed 316L steel in the a) as–deformed condition b) additionally annealed for 30 min/823 K and c) additionally annealed for 325 hrs/823 K.

The structural stability opened the possibility to check if boundary chemistry changed with annealing time and enabled to directly link strength with the eventual occurrence of segregations. To do so, APT was carried out on as HPT deformed samples, short time annealed samples (90 min, 823 K) and long time annealed samples (325 hrs, 823 K). Details to the preparation of the APT tips and the measurement parameters can be found in publication C.
The results showed only negligible Si decoration of the as–deformed grain boundaries, with average excess values of $\Gamma_{Si} = 0.15\ \frac{atoms}{nm^{-2}}$. Annealing of the samples for 90 min leads to a slight increase of the average Si excess up to $\Gamma_{Si} = 0.41\ \frac{atoms}{nm^{-2}}$.

Apart from Si only traces of other alloying elements were detected. Drastic changes occurred for long annealing times. In the samples annealed for 325 hrs Mo, Cr and Si rich second phase particles had already formed at the grain boundaries. Additional to the second phase particles a Si excess similar to that after 90 min annealing was measured. However, between 90 min and 325 hrs annealing large amounts of Mo and Cr have to segregate to the boundaries, with no detectable influence on the hardness. From that it could be concluded that additional phases that occur during annealing are not affecting or realizing the hardness increase during annealing, as long as their volume fraction is small enough and no composite behavior is measured, as for example found during the decomposition of a nc high entropy alloy [67]. Furthermore, between annealing times of 90 min and 325 hrs, in addition to the Si excess, Mo and Cr have to segregate to the boundaries. Also this drastic change has no measureable influence on the measured hardness. Unfortunately, effects of Si could not be completely excluded, as for short annealing times both, the Si excess and hardness increased. Nevertheless, a further hint that the boundary chemistry does not play a major role for the strength of nc metals is that cyclically deformed samples of the same austenitic steel showed pronounced cyclic hardening (for details see publication A). Although not investigated in detail, it seems unlikely that deformation induced segregation takes place at RT and rather small plastic strain amplitudes of $\epsilon_{a,pl} \approx 10^{-3}$. Therefore it is likely that such hardening phenomena, independent if caused by cyclic deformation or annealing, are mainly defect based.
A further possibility to clarify the influence of Si would be to analyze samples only annealed for very short times. Nevertheless, such an approach might not lead to an unambiguous result as the Si excess might have already increased even for very low annealing times and also the experimental error is likely to increase for the shortest annealing times. For that reason a different system for the explanation had to be selected. To do so, a simple binary alloy system, where only one solute element might segregate, was targeted. Facilitating further TEM studies the system should also be non–ferromagnetic.
PtRu alloys with two different Ru concentrations, 5 and 10 wt-% were used. In order to study the hardening phenomenon as a function of the grain size both alloys were subjected to HPT at different deformation temperatures (77 K, RT and 473 K). Subsequently the samples were annealed for 30 min up to temperatures of 873 K. Again, room temperature microhardness was measured and the results are presented in Fig. 2.13 (taken from publication E).

It can be seen that, except for the Pt5Ru samples deformed at 473 K, where only a marginal hardness increase occurred, all other samples showed a pronounced hardness change during annealing. Interestingly, independent of the chemical composition both alloys showed the maximum hardness after annealing at 573 K. For higher annealing temperatures pronounced grain growth occurred, as found by EBSD, see publication E for details. No detectable grain growth was found during annealing at 573 K. Selected area electron diffraction (SAED) patterns of the Pt10Ru samples deformed at 77 K showed only reflections belonging to a single fcc phase for both, the as deformed as well as the additionally annealed samples. These samples were

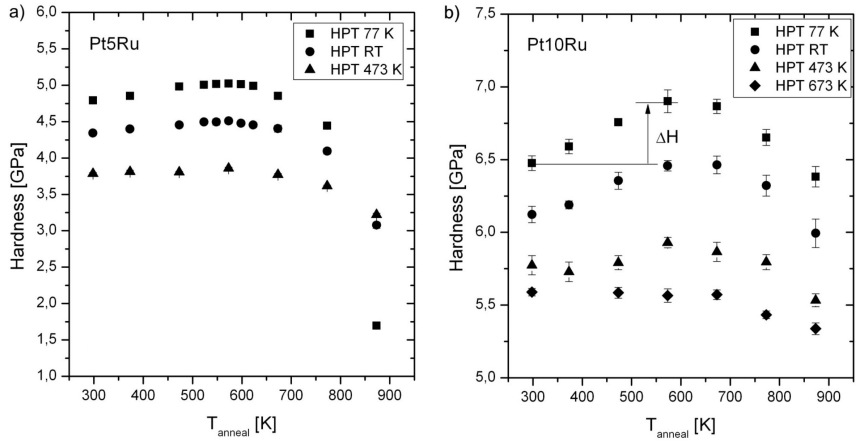

Figure 2.13 Room temperature microhardness of isochronally (30 min) annealed samples a) Pt5Ru and b) Pt10Ru samples.

selected because phase separation during annealing will occur fastest for the samples having the smallest grain size and decomposition of an alloy is most likely to occur at the lowest temperature.

The extent of the hardness increase, labeled ΔH in Fig. 2.13, was more pronounced for the samples deformed at lower temperatures corresponding to smaller grain sizes. This suggests a grain size dependent hardening behavior. To verify this, grain sizes of all samples were measured using a OIM software, based on EBSD data.

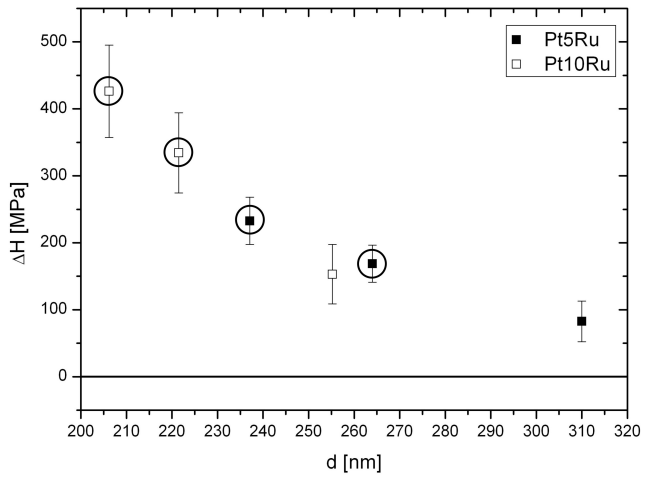

Figure 2.14 Hardness increase, ΔH as a function of the grain size. Below a certain value, a clear dependency of ΔH on the grain size can be deduced. Samples deformed at 77 K and RT are circled. Because the 77 K deformed samples were thermalized at RT these two sets of samples should comprise similar defect contents.

Fig. 2.14 shows the extent of the hardness increase for the PtRu alloys, ΔH as a function of the determined area weighted grain size. Clearly to see, ΔH is a function of the grain size, becoming larger towards smaller sizes. In addition, an extrapolation of this trend suggests, that hardening by annealing can only occur for grain sizes being below a certain value. Of course, as the samples with different grain sizes were synthesized by adjusting the deformation temperature, the resulting defect structures will be different in terms of their defect content and boundary structure, and so could lead to the observed size dependent nature itself. However, as the samples deformed at 77 K were prepared and stored at RT, they can be considered to contain the same defect structure but have different grain sizes than the RT deformed samples because they were already annealed up to and thermalized at ambient temperature. If one takes then into account only the 77 K and RT deformed samples, circled in Fig. 2.14, the size dependent trend is still clearly visible, see Fig. 2.14. Additionally it is possible to synthesize samples with different grain size deformed at the same temperature by adding small particles to the material. These particles shift the minimum grain size achievable towards smaller grain sizes. The easiest way to do this is to compact and subsequently deform metal powders which contain a native oxide layer. This oxide layer fragments during compaction and subsequent HPT deformation leading to fine oxide particles at the boundaries [36]. For noble metals such as Pt which should not form a pronounced oxide layer, the obtainable grain size difference between bulk and powder consolidated samples can be expected to be rather small.
Therefore, instead of Pt, experiments were carried out on bulk Ni and powder consolidated Ni samples with different oxide content. The Ni powder had a particle size of 3 – 7 μm and by annealing the powder in air at 673 K for 10 min, the thickness of the oxide layer could be increased [36]. After HPT deformation at RT the samples were subsequently annealed for 30 min in a temperature range between 373 K and 973 K. It was found that the samples having the largest oxide content and thus the finest grain size ($d \approx 25$ nm) showed the largest hardness increase upon annealing.

Even though, for all Ni samples synthesis of the nc structures was carried out at room temperature still a clear grain size dependency exists. Thus it can be concluded, that hardening upon annealing is a further grain size dependent issue. In addition such phenomena will only occur below a specific value in grain size. For grain sizes larger than this value, hardness will stay constant or will decrease ($H \leq 0$) due to a heat treatment as can be seen schematically in Fig. 2.15. Below a certain value in grain size hardness may increase during a low temperature annealing treatment ($H \geq 0$). According to the experimental results that were summarized schematically in Fig. 2.15, further conclusions about the underlying mechanisms could be drawn, as follows.

In coarse grained materials, especially for hexagonal crystal structures, anneal hardening can occur due to the formation of vacancy clusters acting like dispersoids, see for example [68,69]. This leads to an Orowan type strengthening where the distance

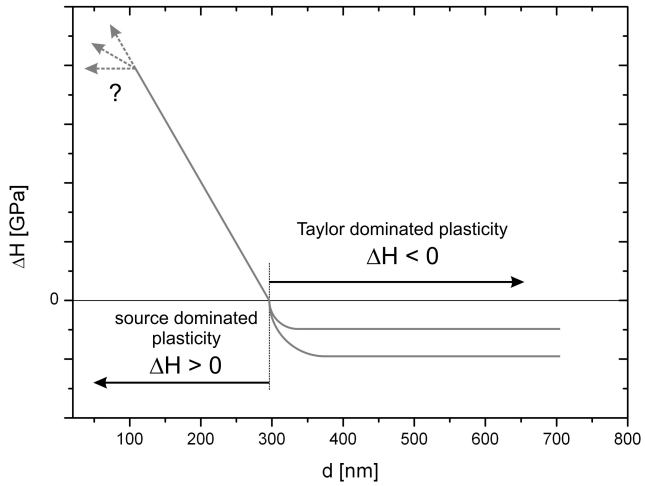

Figure 2.15 Schematic representation of the grain size dependency of hardness increases during annealing. Such phenomena will only occur below a certain value in grain size.

between the vacancy clusters (e.g. dislocation loops), describes the strengthening effect [69]. In that case the internal length scale of the grain is important for the strengthening; thus a grain size dependent hardening should not be observed if vacancy clustering dominates. Moreover, vacancy annihilation at grain boundaries is facilitated for smaller grains, because the sink density is drastically increasing which leads to a reduced supersaturation with vacancies in smaller grains [70]. This in turn should result in a diminishing hardness increase with decreasing grain size.
The experimentally observed grain size dependence of the hardening further questions major contributions of segregated solute to the strength increase during annealing. Larger grain sizes would lead in any case, regardless if interstitials or substitutional atoms segregate, to a similar or even enlarged excess at the grain boundaries, which was estimated on the basis of a simple core-shell model. Details to this estimation can be found in publication E. Similar results as from the simple estimation were experimentally observed. Smaller grains resulted in cleaner grain boundaries [71]. For this reason, a strong solute or impurity interaction with dislocations at the grain boundary should lead to diminishing or at least constant anneal strengthening towards smaller grain sizes. Experimental results gained from an in-situ TEM tensile test point out in this direction. The operation of a boundary source was found to require much larger stress levels than those to overcome an obstacle at the grain boundary, most likely an impurity atom from specimen synthesis [72].

On the other hand, an explanation purely on the basis of defect annihilation seems also questionable, as it will take place below and above the observed threshold value in grain size. The only way, how this transient behavior can be rationalized is that the intrinsic features enabling dislocation based plasticity have to change below a certain grain size. It is reasonable that with decreasing grain size, intragranular dis-

location sources will become less important and grain boundary dislocation sources (intergranular) will prevail. When samples with grain sizes being larger than the critical value are annealed after cold working, hardness will decrease, because dislocation density and so Taylor hardening is reduced. If the applied strain necessitates the activation of dislocation sources, the required activation stress will be also lower in the annealed state as the backstress onto the source is significantly smaller.
With decreasing grain size, the probability of finding a source in the grain interior becomes increasingly unlikely and boundary sources tend to prevail. If the dislocation debris that is originating from the SPD process is lost due to the heat treatment, such boundary sources have to be activated what requires higher stress levels than simply moving already existing dislocations in the material. A transition from sources in the grain interior to boundary sources describes the transient behavior quite well. With this description the grain size dependency is however not *a priori* explained. Two possibilities might lead to the observed behavior. First, the transition from intra- to intergranular sources will be gradual as also the grain size distribution has a certain width. This implies, that the hardness increase becomes significantly larger the more small grains are in the sample. However, this trend would level off as soon as only boundary sources dominate the materials response even in the largest grains of the sample. Second, the character of the boundary source itself might change during the heat treatment. Usually the boundary is in a state of higher energy after SPD processing what is often referred as distorted boundaries or non-equilibrium boundaries [73, 74]. During annealing the boundary structure can relax towards the equilibrium state, e.g. reduction of extrinsic boundary dislocations or reduction of the ledge density [75]. Such relaxation phenomena require atomic shuffling and are supposed to emerge easier in the case of smaller grains due to the enhanced fraction of free volume. If the sample can relax the structure more perfectly, this could result in higher stress levels needed for activating a boundary source. The uncertainty, how and if the trend of increasing ΔH with decreasing grain size will continue for even smaller grain sizes than tested within the thesis is also indicated in Fig. 2.15. Experimental studies on such samples could therefore provide further insights into plasticity of UFG or nc metals.

3
Conclusions

In this thesis, dynamic recovery mechanisms in UFG materials during cold rolling were directly captured and analyzed using a split specimen technique. With the chosen setup grain boundary migration in normal direction was found to be the dominant process. Such a movement of boundaries was identified to take place in both, the steady state regime after severe monotonic strains, as well as during a strain path change in UFG materials. Boundary migration enables the restoration of microstructural features during deformation as certain grains can grow at the expense of others. In addition, by the movement of a boundary a neighboring grain may get fragmented into parts what limits the grain length itself. This recovery of the microstructure can completely balance the geometrical changes that should in principle take place due to a new strain path. Such behavior was found to result in a softening during cold rolling of HPT deformed UFG fcc metals, when the long grain axis was oriented parallel to the rolling direction. When the orientation of the grain was changed by 90 degrees, with the long grain axis being now parallel to the normal direction, this softening could be suppressed. Although this experiments are at their beginning, these preliminary results suggest, that the extent of boundary migration during a strain path change is mainly triggered by the starting texture and its path towards the final texture. Although the estimated driving forces were found to be too low to explain boundary migration, small contributions to the driving force arising from stress differences between the grains could trigger the direction of the movement. From that point of view, local stress fields of dislocations interacting with the grain boundary seem to be necessary to facilitate the atomic jumps. Such an interaction of dislocations with grain boundaries does not only play a role during dynamic recovery, but also during static recovery of severely deformed structures as the enhanced fraction of grain boundaries in nc and UFG materials act as sink for dislocations and might influence the materials properties

there as well. This early stages of (static) recovery of severely deformed materials were investigated in the thesis as well. During such low temperature annealing treatments, an increase of the yield stress and in some cases also of the strength (hardness) was reported. Despite several contradictory explanations given in the literature, this interesting phenomenon does not seem to be completely understood, as several severely deformed materials show such a hardening while others do not. Based on results of several pure metals, binary alloys and a commercially available austenitic steel it was found that a hardness increase upon annealing can only be observed, when the grain size is below a certain limit. Below this grain size that may depend on the material, a grain size dependent hardness increase could be observed getting more pronounced towards smaller grain sizes. This clear grain size dependent behavior and the occurrence of a critical grain size allowed further conclusions. Such a transient behavior can only be explained by a change in the mechanisms leading to dislocation based plasticity, with grain boundary dislocation sources becoming dominant over intragranular ones towards smaller grain sizes. Similar to the observations on small scaled single crystals, such a critical size separates the classical Taylor dominated regime from a source dominated region. The clear grain size dependency of the hardening further rules out vacancy clustering and strong contributions from segregated solute atoms or impurities to be responsible for the strengthening.

Bibliography

[1] Herzer G. Acta Mater. 2013;61:718–734

[2] Dao M., Lu L., Asaro R.J. et al. Acta Mater. 2007;55:4041–4065

[3] Gleiter H. Prog. Mat. Sci. 1989;33:223–315

[4] Valiev R.Z., Islamgaliev R.K., Alexandrov I.V. Prog. Mat. Sci. 2000;45:103–189

[5] Valiev R.Z., Estrin Y., Horita Z. et al. JOM 200;58:33–39

[6] Hughes D.A., Hansen N. Acta Mater. 2000;48:2985-3004

[7] Liu Q., Huang X., Lloyd D.J. et al. Acta Mater. 2002;50:3789–3802

[8] Embury J.D., Fisher R.M., Acta Metall. 1966;14:147–159

[9] Langford G., Metall. Trans. A 1977;8:861–875

[10] Hohenwarter A., Bachmaier A., Gludovatz B. et al. Int. J. Mat. Res. 2009;100:1653–1661

[11] Zhilyaev A.P., Langdon T.G., Prog. Mat. Sci. 2008;53:893–979

[12] Saito Y., Utsunomiya H., Tsuji N. et al. Acta Mater. 1999;47:579–583

[13] Wang J.T. Mater. Sci. Forum 2006;503–504:363–370

[14] Segal V.M., Mater. Sci. Eng. A 1995;197:157–164

[15] Valiev R.Z., Langdon T.G. Prog. Mat. Sci. 2006;51:881–981

[16] Raab G.J., Valiev R.Z., Lowe T.C. et al. Mater. Sci. Eng. A 2004;382:30–34

[17] Tóth L.S., Arzaghi M., Fundenberger J.J. et al. Scripta Mater. 2009;60:175–177

[18] Vorhauer A., Pippan R. Metall. Mater. Trans. A 2008;39:417–429

[19] Hansen N., Mehl R.F. Metall. Mater. Trans. A 2001;32:2917–2935

[20] Humphreys F.J., Hatherly M.: Recrystallization and related annealing phenomena, 2nd edition, Elsevier, 2004

[21] Bay B., Hansen N., Hughes D.A. et al. Acta Metall. Mater. 1992;40:205–219

[22] Hughes D.A., Hansen N. Acta Mater. 1997;45:3871–3886

[23] Hughes D.A., Hansen N. Metall. Trans. A 1993;24:2022–2037

[24] Pippan R., Scheriau S., Taylor A. et al. Ann. Rev. Mater. Res. 2010;40:319–343

[25] Hebesberger T., Stüwe H.P., Vorhauer A. et al. Acta Mater. 2005;53:393–402

[26] Sabirov I., Perez-Prado M.T., Molina-Aldareguia J.M. et al. Scripta Mater. 2011;64:69–72

[27] Valiev R.Z., Ivanisenko Y., Rauch E.F. et al. Acta Mater. 1996;44:4705–4712

[28] Divinski S.V., Padmanabhan K.A., Wilde G. Philos. Mag. 2011;91:4574–4593

[29] Edalati K., Horita Z. Scripta Mater., 2011;64:161–164

[30] Zhilyaev A.P., Swaminathan S., Pshenichnyuk A.I. et al. J. Mater. Sci. 2013;48:4626–4636

[31] Mohamed F.A. Acta Mater. 2003;51:4107–4119

[32] Mishin O.V., Gottstein G. Philos. Mag. A 1998;78:373–388

[33] Mishin O.V., Godfrey A. Metall. Mater. Trans. A 2008;39:2923–2930

[34] Weissmüller J., Krauss W., Haubold T. et al. Nanostruct. Mater. 1992;1:439–447

[35] Weissmüller J. Nanostruct. Mater. 1993;3:261–272

[36] Bachmaier A., Hohenwarter A., Pippan R. Scripta Mater. 2009;61:1016–1019

[37] Chookajorn T., Murdoch H.A., Schuh C.A. Science 2012;337:951–954

[38] Koch C.C., Scattergood R.O., Darling K.A. et al. J. Mater. Sci. 2008;43:7264–7272

[39] Saber M., Koch C.C., Scattergood R.O. Mater. Res. Lett. 2015;3:65–75

[40] Kirchheim R. Acta Mater. 2002;50:413–419

[41] Vo N.Q., Schäfer J., Averback R.S. et al. Scripta Mater. 2011;65:660–663

[42] Shen T.D., Schwarz R.B., Feng S. et al. Acta Mater. 2007;55:5007–5013

[43] Huang X., Hansen N., Tsuji N. Science 2006;312:249–251

[44] Ma E., Shen T.D., Wu X.L. Nat. Mater. 2006;5:515–516

[45] Wang Y.M. Cheng S., Wei Q.M. et al. Scripta Mater. 2004;51:1023–1028

[46] Zhang X.F., Fujita T., Pan D. et al. Mater. Sci. Eng. A 2010;527:2297–2304

[47] Beck P.A. Adv. Phys. 1954;3:245–324

[48] Nes E. Acta Metall. Mater. 1995;43:2189–2207

[49] Johnson L., Ashby M.F. Acta Metall. 1968;16:219–225

[50] Uchic M.D., Dimiduk D.M., Florando J.N. et al. Science 2004;305:986–989

[51] Kiener D, Minor A.M. Nano Lett. 2011;11:3816–3820

[52] Valiev R.Z., Enikeev N.A., Murashkin M.Y. et al. Scripta Mater. 2010;63:949–952

[53] Abramova M.M., Enikeev N.A., Valiev R.Z. et al. Mater. Lett. 2014;136:349–352

[54] Yu. T., Hansen N., Huang X. Proc. Roy. Soc. London Ser. A 2011;467:3039–3065

[55] Yu T., Hansen N., Huang X. Philos. Mag. 2012;92:4056–4074

[56] Yu T., Hansen N., Huang X. Acta Mater. 2013;61:6577–6586

[57] Yu T., Hansen N., Huang X. et al. Mater. Res. Lett. 2014;2:160–165

[58] Winning M., Gottstein G., Shvindlerman L.S. Acta Mater. 2001;49:211–219

[59] Winning M., Gottstein G., Shvindlerman L.S. Acta Mater. 2002;50:353–363

[60] Zhang K., Weertman J.R., Eastman J.A. Appl. Phys. Lett. 2004;85:5197–5199

[61] Jin M., Minor A.M., Stach E.A. et al. Acta Mater. 2004;52:5381–5387

[62] Rupert T.J., Gianola D.S., Gan Y. et al. Science 2009;326:1686–1690

[63] Stüwe H.P.: Recrystallisation of metallic materials, 1978, Dr. Riederer Verlag Stuttgart, Editor: Haessner F.

[64] Rajabzadeh A., Legros M., Combe N. et al. Philos. Mag. 2013;93:1299–1316

[65] Vlassak J.J., Nix W.D. J. Mech. Phys. Solids 1994;42:1223-1245

[66] Scheriau S., Zhang Z., Kleber S. et al. Mater. Sci. Eng. A 2011;528:2776–2786

[67] Schuh B., Mendez-Martin F., Völker B. et al. Acta Mater. 2015;96:258–268

[68] Hampshire J.M., Hardie D. Acta Metall. 1974;22:657–663

[69] Zehetbauer M.J. Key Eng. Mater. 1994;97–98:287–306

[70] Singh B.N., Foreman A.J.E. Phil. Mag. 1974:29(4):847–858

[71] Terwilliger C.D., Chiang Y-M. Acta Metall. Mater. 1995;43:319–328

[72] Mompiou F., Legros M., *Boé* A. Acta Mater. 2013;61:205–216

[73] Nazarov A.A., Romanov A.E., Valiev R.Z. Acta Metall. Mater. 1993;41:1033–1040

[74] Sauvage X., Wilde G., Divinski S.V. et al. Mater. Sci. Eng. A 2012;540:1–12

[75] Priester L.: Grain Boundaries - From Theory to Engineering, Springer, 2013

4
List of appended papers

Paper A
O. Renk, A. Hohenwarter and R. Pippan
Cyclic Deformation Behavior of a 316L Austenitic Stainless Steel Processed by High Pressure Torsion
Advanced Engineering Materials, 2012; 14:948-954

Paper B
O. Renk, A. Hohenwarter, S. Wurster and R. Pippan
Direct evidence for grain boundary motion as the dominant restoration mechanism in the steady state regime of extremely cold rolled copper
Acta Materialia 2014; 72:401-410

Paper C
O. Renk, A. Hohenwarter, K. Eder, K.S. Kormout, J.M. Cairey and R. Pippan
Increasing the strength of nanocrystalline steels by annealing: Is segregation necessary?
Scripta Materialia 2015; 95:27-30

Paper D
O. Renk, A. Hohenwarter, B. Schuh, J.H. Li and R. Pippan
Hardening by annealing: Insights from different alloys
Proceedings of the 36th Risø Symposium on Materials Science

Paper E
O. Renk, A. Hohenwarter, J.H. Li and R. Pippan
Hardening by annealing in nanocrystals: A further grain size dependent issue
Submitted for publication

Remark

In the appended papers, myself, Oliver Renk, performed all experiments, the data analyses and the composition of the publications with the following exceptions:

- In **paper B**
  Prof. Dr. Jozef Keckes and DI Juraj Todt helped performing XRD measurements and calculating fractions of the texture components. Dr. Stefan Wurster contributed to the work with fruitful discussions and FIB milling.
- In **paper C**
  DI Karoline Kormout performed the TEM investigations; APT measurement and data analysis was performed by Katja Eder and Prof. Dr. Julie Cairney
- In **paper D**
  Priv.–Doz. Dr. Jiehua Li arc melted the required PtRu alloys. DI Benjamin Schuh helped with additional APT data analysis
- In **paper E**
  Priv.–Doz. Dr. Jiehua Li arc melted the required PtRu alloys.

- My supervisors, Prof. Dr. Reinhard Pippan and Dr. Anton Hohenwarter participated in all the papers by giving the basic ideas for the publications and with helpful discussions during their preparation.

A

Cyclic Deformation Behavior of a 316L Austenitic Stainless Steel Processed by High Pressure Torsion

Oliver Renk[a], Anton Hohenwarter[a] and Reinhard Pippan[a]

[a]Erich Schmid Institute of Materials Science, Austrian Academy of Sciences, A-8700 Leoben, Austria

Abstract

The influence of severe plastic deformation (SPD) on the fatigue behavior of a modified 316L austenitic stainless steel is investigated. Different ultrafine-grained and nanocrystalline microstructures are obtained by changing the processing parameters and applying a post heat treatment procedure. Samples are fatigued using both, load and strain controlled experiments. High pressure torsion processing makes it possible to reach a saturation microstructure, which is cyclically stable up to a stress level three times higher than the stress level of the coarse-grained structure. Fracture surface investigations and surface damage clearly show that the failure behavior of the SPD states under cyclic loading is different to their coarse-grained counterparts. For these microstructures, localized deformation in shear bands seems to play a major role for crack initiation and propagation.

A.1 Introduction

Bulk ultrafine-grained (ufg) and nanocrystalline (nc) materials produced by various severe plastic deformation (SPD) techniques have gained an increasing interest in the materials research community over the past decades. Most ufg materials are processed via equal channel angular pressing (ECAP) processing, see for example [1,2]. A drawback of ECAP is that medium and high strength materials (e.g., steels, tungsten or chromium) are difficult to process. In contrast, high pressure torsion (HPT) allows larger degrees of deformation and consequently smaller grain sizes than ECAP, which would exhibit higher strength levels. Therefore, HPT is very attractive as a processing technique for several high strength applications such as implants. For instance the 316L austenitic steel is a widely used structural material and has also an exceptional biocompatibility. For such applications, SPD processing would further improve important mechanical properties such as tensile strength and fatigue limit which have been studied recently on ECAP processed material [3]. A distinctive increase in size of HPT tools has made it possible to investigate also mechanical properties like fracture toughness or fatigue properties of such processed samples, which require a certain amount of sample volume [4, 5]. The fatigue properties of a 316L austenitic steel processed by HPT will be analyzed in this study.

A.2 Experimental

Billets from an as received 316L austenitic stainless steel ingot were cold rolled and recrystallized at 950 °C to remove the initial coarse cast microstructure. The chemical composition of the steel used in this study is given in Tab. A.1. The recrystallized billets have an average grain size of 10 mm and were machined into disks with 35 mm diameter and 11 mm in height. These disks were HPT deformed to obtain a nanocrystalline microstructure. The principle of the HPT process and the HPT tool used can be seen in Fig. A.1. Further details of the HPT process can be found elsewhere [6, 7].

Table A.1 Chemical composition of the 316L stainless steel.

C	**Si**	**Mn**	**Cr**	**Mo**	**Ni**	**N**	**Fe**
Max. 0.03	0.30	1.70	17.50	2.70	14.50	0.07	balance

In order to better understand the influence of the microstructure on the fatigue properties of the material, an additional post heat treatment was carried out. Therefore, disks were severely deformed at ambient temperature to obtain a fully nanocrystalline structure. Disks deformed at ambient temperature were then post heat treated at 700 °C for 30 min (bimodal structure). Thus, different ufg/nc microstructures were processed. In all cases, the disks were deformed up to 15 revolutions with an applied pressure of 3.60 GPa, which is equivalent to a strain of $\epsilon = 118$ at a radius of $r = 16$ mm. The equivalent v. Mises strain, applied during the HPT

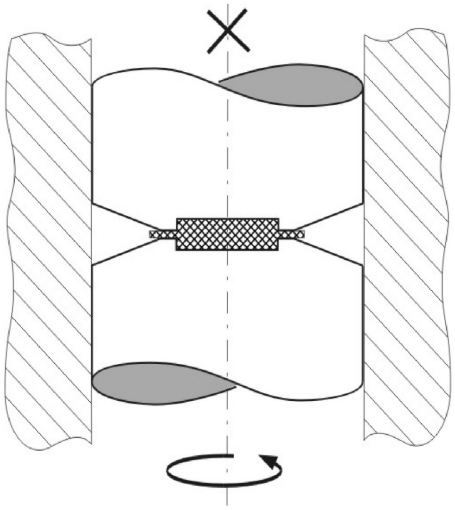

Figure A.1 Principle of the HPT process.

process, can be calculated by Eq. A.1, where n are the number of rotations, r the radius, and t the thickness of the sample.

$$\epsilon = \frac{2\pi r n}{t\sqrt{3}}. \tag{A.1}$$

Such high strains are necessary to obtain a saturated microstructure throughout the disk. Hardness measurements along the radius at the middle of the disks were carried out to make sure that homogenous properties were reached over the whole disk (for $r > 0.5$ mm). From each disk, two round bars were extracted at a radius of 6 mm with the length of the bar along the tangential direction of the HPT disk, see Fig. A.2.
The bars were subsequently shaped into standard round or hour-glass shaped specimens. The standard round specimens with a constant cross section of 3 mm and a gauge length of 4 mm were used for low cycle fatigue (LCF) experiments and tensile tests, and the hour-glass shaped samples with a minimal diameter of 1.4 mm were used for high cycle fatigue experiments (HCF).

All samples were ground mechanically and finally electro-polished to avoid influences from the sample preparation. Despite the small sample size of only 25 mm total length, the dimensions of the samples were selected in accordance with ASTM E606 and ASTM E466 standards [8, 9]. Two tensile tests for each structure were carried out at a constant crosshead speed of 300 μm min^{-1}, which is equivalent to a starting strain rate of $\dot{\epsilon} = 1.67 * 10^{-3} s^{-1}$. The fatigue experiments in the LCF regime were conducted at a stress ratio of $R = -1$ (symmetrical push-pull test) and a frequency of 0.1 Hz on a closed-loop servo hydraulic testing unit under constant total strain amplitude, $\epsilon_{a,tot}$. The strain was measured directly on the sample sur-

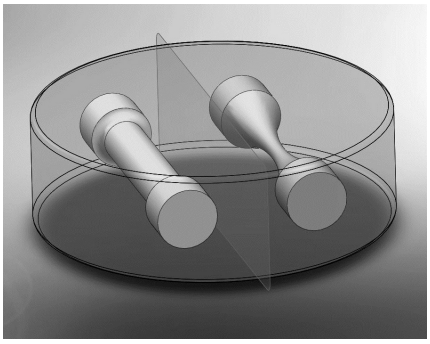

Figure A.2 Extraction of the samples from the HPT deformed disk at a radius of 6 mm.

face using a small clip-on extensometer, Model 3442 from Epsilon Technology. HCF were carried out with the hour-glass shaped samples on an electro-mechanical testing unit under constant stress-amplitude σ_a at a frequency of 100 Hz. To investigate the fracture surface and the fatigue damage on the sample surface a field emission gun scanning electron microscope (LEO 1525) equipped with an EBSD system from TSL was used. For characterization of the nc structures a Philips CM12 transmission electron microscope was used.

A.3 Results

A.3.1 Microstructures after HPT

In Fig. A.3, the different ufg/nc microstructures and the starting microstructure are depicted. Note the different magnifications of the images. Fig. A.3a shows a grain boundary map of the 10 μm coarse-grained (CG) starting material. Fig. A.3b shows a TEM image of the saturation microstructure that can be reached by HPT processing at ambient temperature. The shear direction is indicated with arrows in this figure. In this case, a fully nanocrystalline structure with a grain size of about 50 nm, determined by line interception method, was observed. Deformation twins, visible in some of the elongated grains are encircled in Fig. A.3b. Due to the high strain applied during HPT at room temperature (relatively low homologous temperature), the grain boundaries are not sharp. A post heat treatment of the as deformed disks at 700 °C for 30 min leads to a bimodal grain size distribution consisting of alternating bands of coarse (up to nearly 1 μm) and fine grains (about 100 nm), see Fig. A.3c. The reason for the occurrence of these alternating bands is a fluctuation of the chemical composition in the starting cast material. Energy dispersive spectroscopy (EDS) measurements clearly showed that the chromium, nickel, or molybdenum content in the areas with small grains is about 2 % higher than in the coarse regions. This slightly higher content effectively reduces the grain boundary mobility and disables grain coarsening after recrystallization. In the following, the different structures are termed nc for the nanocrystalline structure, which was HPT

processed at ambient temperature, bimodal for the HPT processed and heat treated samples and cg for the coarse-grained microstructure.

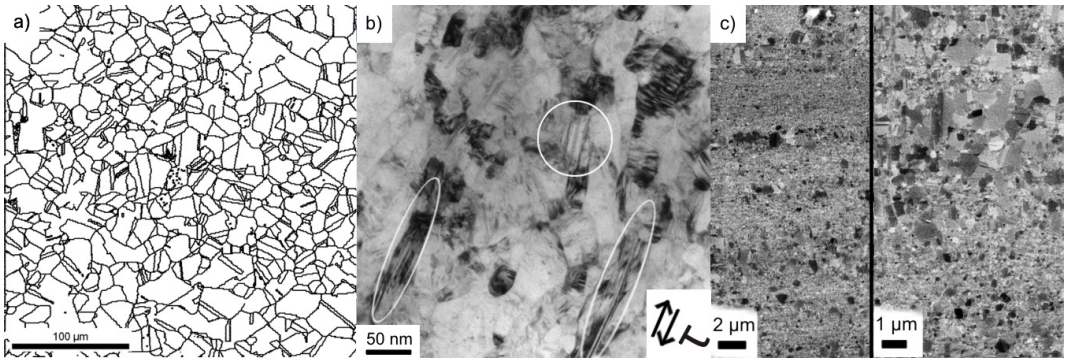

Figure A.3 Overview of the investigated microstructures (a) Grain boundary map obtained by EBSD of the coarse-grained material after cold rolling and recrystallization, (b) TEM image of HPT processed 316L at RT, (c) Back scattered electron images with different magnifications of the bimodal aligned structure after a heat treatment at 700 °C/30 min.

A.3.2 Tensile and Fatigue Tests

A.4 shows the engineering stress-strain curves for the different microstructures measured at ambient temperature. Tab. A.2 contains the values measured in the tensile tests as well as the measured fatigue limits. Fig. A.4 indicates that the tensile strength can be enhanced by a factor of about 3 for the nanocrystalline samples compared with the coarse-grained material.

Table A.2 Mechanical and fatigue properties of the nc, bimodal, and cg samples. σ_{UTS} is the ultimate tensile strength, ϵ the (engineering) elongation to failure, $\sigma_f$the fatigue limit.

Structure	σ_{UTS} **[MPa]**	ϵ **[%]**	σ_f **[MPa]**
nc	1865	11.1/24.4	580
bimodal	1493/1606	8.5/2.3	580/750
cg	622	105.0	250

Although the elongation to failure for the nc as well as for the bimodal structures is inferior to their coarse-grained counterparts, about 25 % of the elongation to failure of the coarse-grained starting material can be reached for the nc microstructure, which is attractive for such high strength materials. Apart from the elongation to failure the ufg/nc microstructures show nearly any hardening capacity. However, for many applications not always the uniform elongation is the parameter of interest, for example for bending or forming under compression the reduction of area is the parameter of interest. It should be mentioned that the values of the engineering elongation are somewhat enhanced due to the small gauge length. As expected, the tensile stresses for the bimodal samples are lower than for the as deformed state

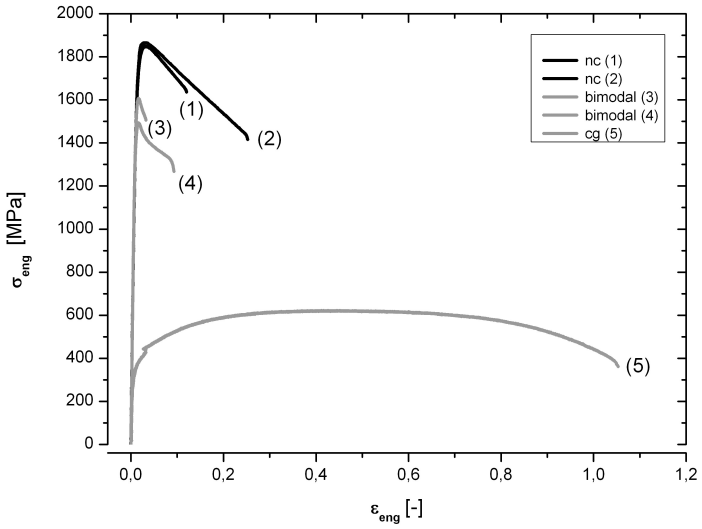

Figure A.4 Engineering stress-strain curves of the different investigated structures.

(nc). However, it was not possible to obtain ductility similar as in the coarse-grained materials. The measured values for the bimodal structure show pronounced scattering of both, tensile strength and elongation to failure. Compared with the coarse-grained samples the nc and bimodal structures show completely different failure behavior. Apart from the typical necking during tensile tests, these structures show strain localization within shear bands, which are inclined at an angle of about 45° with respect to the loading axes. Final fracture also takes place along these shear bands. The fracture surface shows typical features of micro ductile failure. Necking and shear banding is more pronounced for the nc than for the bimodal structures, where early strain localization is evident.
Total strain controlled fatigue experiments were conducted at three different strain amplitudes $\epsilon_{a,tot}$ of 0.8 %, 1 % and 1.5 %. The hysteresis loops for the different conditions, nc, bimodal, as well as the coarse-grained structure, for the largest total strain amplitude of 1.5 % at half of the cycles to failure are shown in Fig. A.5. The results in respect of lifetime are summarized in a total strain fatigue life diagram (Fig. A.6) and a S-N curve (Fig. A.7). As for the tensile tests, one can observe, generally higher stress levels during fatigue tests for the nc and bimodal structures. Furthermore, for these two structures an about three times higher fatigue limit (defined as 10^7 cycles without failure), compared to the coarse-grained state exists. The values of the fatigue limit σ_D of the different states are summarized in Tab.A.2. For the bimodal structures the fatigue limit varies between 580 and 750 MPa.

Although the nc samples exhibited the highest tensile stresses, their fatigue limit of 580 MPa reaches about the minimal value of the bimodal structures. For stress controlled fatigue tests the SPD materials (nc and bimodal structure) exhibit a

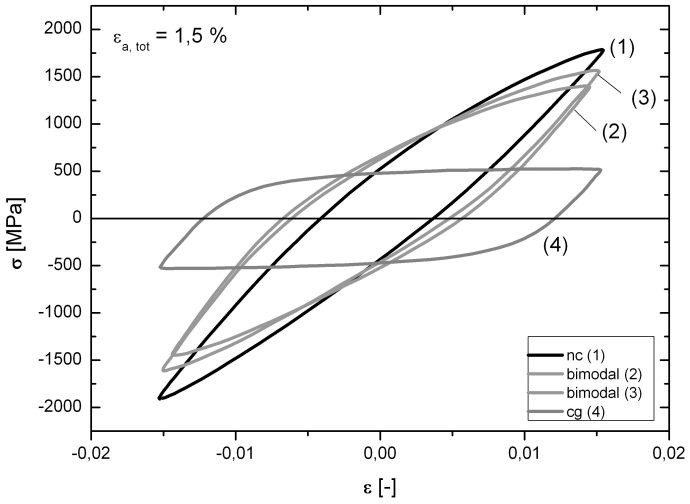

Figure A.5 Hysteresis loops of the different structures observed at half of the cycles to failure at a constant total strain amplitude of $\epsilon_{a,tot} = 1.5\%$.

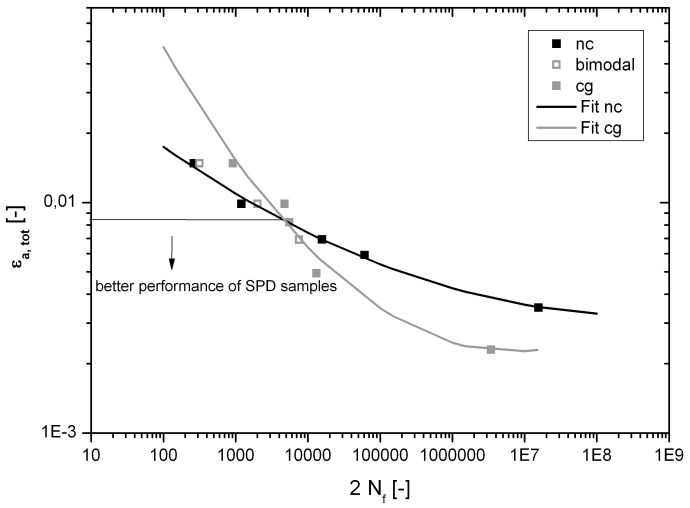

Figure A.6 Total strain fatigue life diagram of the investigated microstructures.

higher lifetime in every case, which is different for strain-controlled fatigue. For the strain controlled tests a critical total strain amplitude exist, above which, the coarse-grained material exhibits a longer lifetime.
This amplitude range is marked in Fig. A.6 and is about $\epsilon_{a,tot} = 8 * 10^{-3}$. The plastic strain amplitude of the HPT samples at the fatigue limit is in the order of $\epsilon_{a,pl} = 2 * 10^{-5}$. This is in agreement with results observed in coarse-grained ductile materials, whereby the plastic strain amplitude at the fatigue limit is in the range of $\epsilon_{a,pl} = 10^{-4} - 10^{-5}$ [10]. Fig. A.8 shows the cyclic deformation curve for the different microstructures, tested with a total strain amplitude of 1.5 %. One can clearly see that the nc samples show cyclic hardening till failure in contrast to the bimodal samples which show some cyclic softening at the beginning of the fatigue experiment. Apart from the softening during the first cycles, the bimodal structures show excellent cyclic stability at a stress level nearly three times higher than for the coarse-grained structure. The high stress levels and the cyclic stability are among the main advantages when compared with coarse-grained, heavily cold worked austenites, which show pronounced softening during cyclic loading [11]. Concerning the failure behavior of the HPT processed 316L steel, completely different mechanisms, compared with the coarse-grained state, appeared. As in the tensile test, fracture occurred along shear bands which are inclined at an angle of about 45° with respect to the loading axis, see Fig. A.9 and Fig. A.10.

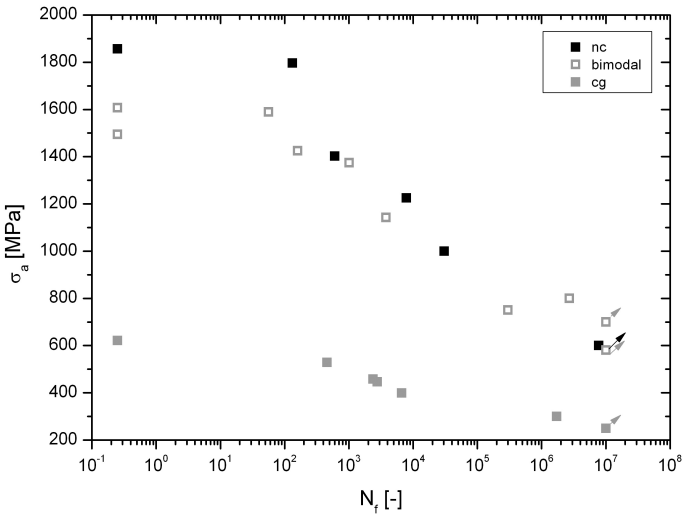

Figure A.7 S–N curve (Wöhler plot) of the investigated microstructures. The fatigue limit is indicated with arrows.

The residual fracture surface shows microductile features. This means that fatigue crack initiation and propagation takes place under mixed mode condition (Mode I and Mode II) which is in contrast to the coarse-grained state. Fatigue cracks initiated

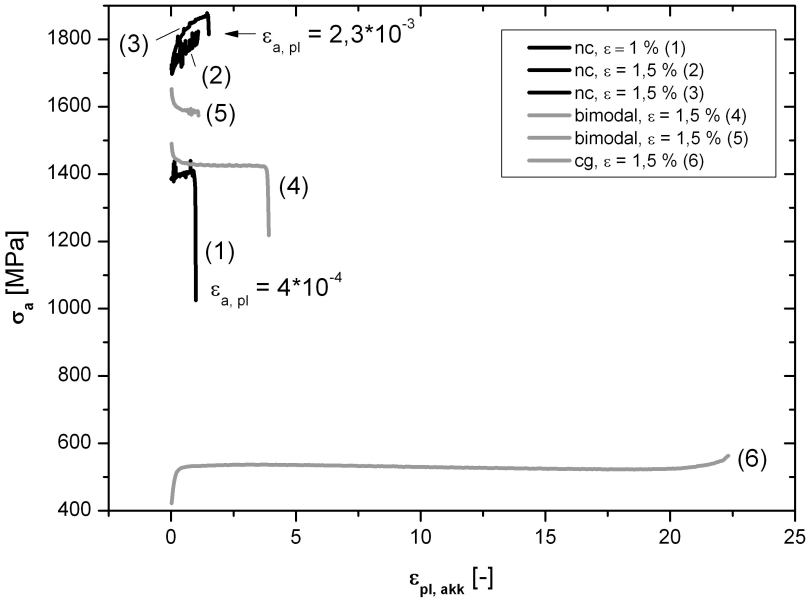

Figure A.8 Cyclic deformation curves for a total strain amplitude of $\epsilon_{a,tot} = 1.5\%$. For the nc structures also a curve for $\epsilon_{a,tot} = 1\%$, as well as the plastic strain for the nc samples are depicted in this diagram.

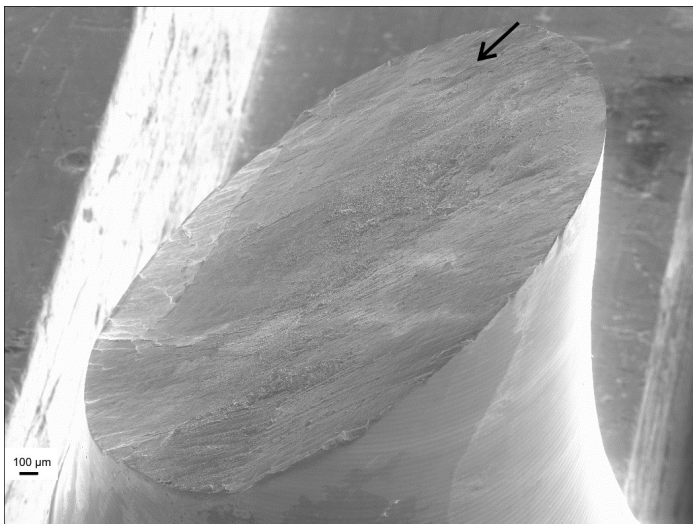

Figure A.9 Fracture surface of a sample with bimodal aligned microstructure fatigued at a total strain amplitude of $\epsilon_{a,tot} = 1\%$. The fatigue crack initiation is indicated with an arrow.

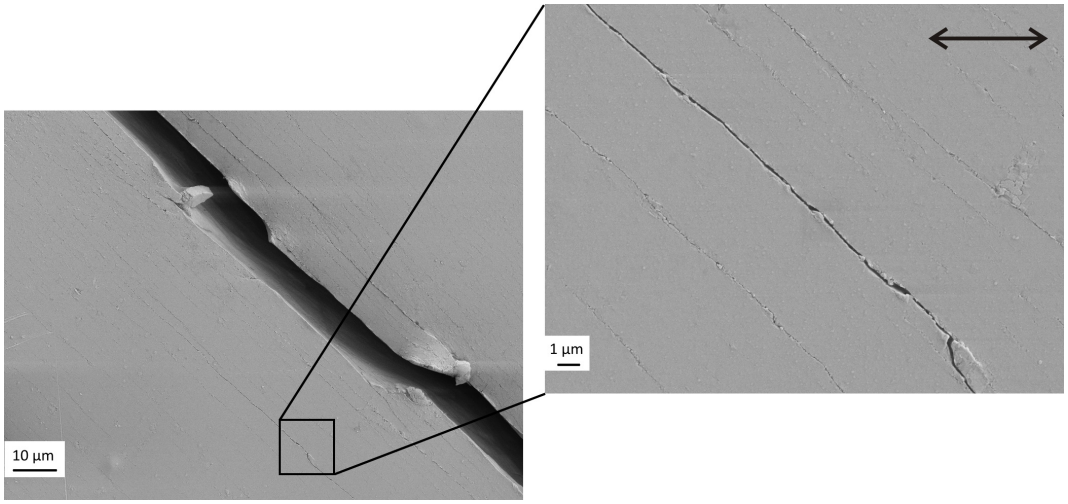

Figure A.10 Fatigue cracks initiated at several shear bands on the surface of a nc sample fatigued with a total stain amplitude of $\epsilon_{a,tot} = 1.5\%$. The loading axis is marked with an arrow.

on the sample surface at one of the shear bands as shown in (Fig. A.9 and Fig. A.10). In fact, this failure behavior has been observed for a variety of ufg or nc materials, see for example Ref. [12–15].

A.4 Discussion

As shown, the tensile strength of the 316L steel could be raised by a factor of three by nanostructuring via HPT processing. Even higher tensile strengths would be possible by processing the 316L steel at higher temperatures, as the saturation hardness values at ambient temperature increase up to HPT deformation temperatures of 600°C [16]. The main problem of most nanocrystalline metals is their limited ductility. In SPD materials, this is mainly because of their lack of work hardening. In fact the tensile strength is reached without significant plastic deformation. The absence of the hardening behavior is attributed to the fact that in submicron or nanocrystalline materials it is nearly impossible to store dislocations within the grains, because grain boundaries can act as sources and sinks for dislocations [17]. Therefore, a potential strategy to regain ductility and work hardening is the application of heat treatments after the SPD processing [14, 18]. However in the present study, the tensile stress for the bimodal structure decreased slightly, but instead of regaining ductility, the elongation to failure decreased somewhat compared with the nanocrystalline, as deformed samples (see Fig. A.4). The reason for this effect is not clear. It seems to be that the hardening of the coarser-grained (about 1 μm grain size) volume fraction is not sufficient to overcome the softening of the fine grained regions with a grain size of about 100 nm. It should be noted that the structure of this fine-grained regions is different to the HPT state, the boundaries

are very sharp and the grains should contain a very low density of dislocations. This difference between the as HPT structure and the nano-grained structure may be the reason for the observed phenomenon. Further studies are necessary to understand this effect on ductility, which should help to develop microstructures with improved ductility. The samples with the bimodal structure also show pronounced scattering of the tensile strength and the fatigue limit, which is a fact of the different amounts of fine and coarse grains in these samples as the chemical fluctuations are not uniformly distributed in the samples. This is also the reason for the occurrence of large differences between the lower and the upper value of the fatigue limit of this structure (see Fig. A.7). Since SPD materials exhibit higher strength levels but reduced ductility, it is evident that the total strain-fatigue life curves of ufg and cg states should intersect [14, 19]. This means that a critical total strain amplitude beneath which SPD states exhibit a higher life time than the coarse-grained material.
Indeed, this behavior was also observed for the 316L stainless steel in this study (Fig.A.6). For coarse-grained materials cyclic hardening or softening can be explained by the formation of typical dislocation arrangements. Their size is dependent on the material itself and the applied stress level. For ufg or nc metals the grain size is in the range or even smaller than the size of those dislocation patterns which can be estimated by Eq. A.2, where d is the size of the dislocation pattern, K a constant, G the shear modulus, b the burgers vector and σ the applied stress [19].

$$d = \frac{KGb}{\sigma}. \tag{A.2}$$

For the 316L steel used in the present study one can calculate with Eq. A.2 a minimum size of the dislocation structures in the nc material of about 100 nm, which is nearly double the grain size. Therefore, cyclic hardening or softening in SPD metals must be explained by other mechanisms. Considering the cyclic deformation curves in Fig. A.8, they show that the nc samples cyclically harden, the bimodal samples cyclically soften. Two basic mechanisms for fatigue softening of SPD metals were proposed, see for example [14,20]. These are softening due to grain coarsening and/or formation of shear bands. Because grain growth during cycling appears by dynamic recrystallization, therefore grain boundary mobility is important [21]. In the investigated nc 316L steel this contribution to cyclic softening should be negligible due to the low homologous testing temperature ($< 0.2\ T_m$), the large fraction of high angle grain boundaries (HAGB) after HPT processing and the high amount (about 35 wt.-%) of alloying elements.
Nevertheless, slight grain coarsening could give a possible explanation for the occurrence of cyclic hardening of the nc samples. In Ref. [16], it has been shown surprisingly, that a higher strength or hardness level at ambient temperature can be achieved if the austenitic steel is processed at higher temperatures, although the grain size increased compared with HPT processing at room temperature. If the grains of the nc samples now coarsened slightly during fatigue testing, the resulting structure should exhibit higher strength. However, it is not clear if the increase in grain size or the more well-defined grain boundaries are responsible for this abnor-

mal behavior. Apart from the cyclic softening during the first cycles, the bimodal structures showed excellent cyclic stability (see Fig. A.8). This is interesting as in a recent work of a 316L steel processed via the ECAP route pronounced and continuous cyclic softening occurred [3]. One reason for this behavior could be that during ECAP processing only a limited fraction of HAGB can be produced. In contrast, HPT processed structures exhibit a large fraction of HAGB which in turn lead to a cyclically stable microstructure [22]. Although the fatigue limits of the as deformed 316L steel (nc) and the bimodal structure reach values comparable with duplex steels or high Mn alloyed TWIP steels, the fatigue limit is slightly below the expectations [3, 23]. In fact, it cannot be fully explained why the nc structure exhibits the same fatigue limit as the minimal values of the bimodal structure, as the tensile strength of the nc samples is higher. One reason for this behavior might be an accelerated fatigue crack initiation in the nc samples. This initiation could be promoted by microyielding at lower stress levels. This assumption is assisted by the fact that the annealed (bimodal) samples with only a small amount of coarsened grains exhibited the highest fatigue limit measured in this study (750 MPa). Therefore, an optimum ratio of strength and fatigue limit could be observed by recovering the nc samples, leading to a grain size of some 100 nm. Finally it should be noted that the rule of thumb from Luk*áš* and Klesnil [10], whereby the fatigue limit of ductile metallic materials is reached within a range of the plastic strain amplitude between $\epsilon_{a,pl} = 10^{-4} - 10^{-5}$ is also fulfilled for the nanocrystalline 316L austenitic steel used in the present study. Therefore, it seems that the phenomena controlling the fatigue limit in nanocrystalline 316L are similar than that in standard microcrystalline metals.

A.5 Conclusions

In the present study, a 316L austenitic stainless steel was HPT processed up to 15 revolutions resulting in a nanocrystalline microstructure. By applying a post heat treatment on the deformed samples an aligned bimodal structure was obtained. These two microstructures along with the coarse-grained initial one were examined with respect of the tensile and fatigue properties. Hence, the following conclusions can be drawn:

- Tensile strength and fatigue limit can be raised by up to a factor of 3 by nanostructuring the 316L steel.
- The annealed (bimodal) structures show excellent cyclic stability due to the high fraction of HAGB generated by HPT.
- Both, the nanocrystalline and the bimodal structure show different failure mechanisms, in tensile as well as cyclic loading, compared with the coarse-grained material. Fatigue crack initiation and propagation till failure takes place in shear bands developed during cyclic deformation.

Acknowledgements
Financial support by the FWF Austrian Science Fund (project $S10402 - N16$ and $24141 - N19$) is gratefully acknowledged.

Bibliography to paper A

[1] Valiev R.Z., Langdon T.G. Progr. Mater. Sci. 2006;51:881–981

[2] Segal V.M. Mater. Sci. Eng. A 1995;197:157–164

[3] Ueno H., Kakihata K., Kaneko Y. et al. Acta Mater. 2011;59:7060–7069

[4] Hohenwarter A., Pippan R. Scr. Mater. 2011;64:982–985

[5] Pippan R., Scheriau S., Hohenwarter A. et al. Mater. Sci. Forum 2008;584–586:16–21

[6] Zhilyaev A., Langdon T.G. Prog. Mater. Sci. 2008;53:893–979

[7] Hohenwarter A., Bachmaier A., Gludovatz B. et al. Int. J. Mater. Res. 2009;100:1653–1661

[8] ASTM Standard E466, 1996 (2002) Standard Practice for Conducting Force Controlled Constant Amplitude Axial Fatigue Tests of Metallic Materials, ASTM International, West Conshohocken, PA

[9] ASTM Standard E606, 1992 (1998) Standard Practice for Strain-Controlled Fatigue Testing, ASTM International, West Conshohocken, PA

[10] Lukáš P., Klesnil M., Polák J. Mater. Sci Eng. 1974;15:239–245

[11] Panzenböck Michael PhD thesis Montanuniverstität Leoben, Ermüdungsverhalten Stickstofflegierter Cr-Mn-Austenite, 1995

[12] Panin A.V., Panina A.A., Ivanov Y.F. Mater. Sci. Eng. A 2008;486:267–272

[13] Wong M.K., Kao W.P., Lui J.T. et al. Acta Mater. 2007;55:715–725

[14] Mughrabi H., Höppel H.W. Int. J. Fat. 2010;32:1413–1427

[15] Malekjani S., Hodgson P.D., Cizek P. et al. Acta Mater. 2011;59:5358–5367

[16] Scheriau S., Zhang Z., Kleber S. et al. Mater. Sci. Eng. A 2011;528:2776–2786

[17] Yu C.Y., Kao P.W., Chang C.P. Acta Mater. 2005;53:4019–4028

[18] Wang Y.M., Ma E. Acta Mater. 2004;52:1699–1709

[19] Mughrabi H. Procedia Engineering 2010;2:3–26

[20] Agnew S.R., Weertman J.R. Mater. Sci. Eng. A 1998;244:145–153

[21] Höppel H.W., Zhou Z.M., Mughrabi H. et al. Philos. Mag. A 2002;82:1781–1794

[22] Niendorf T., Canadinc D., Maier H.J. et al. Inter. J. Fatigue 2008;30:426–436

[23] Hamada A.S., Karjalainen L.P., Puustinen J. Mat. Sci. Eng. A 2009;517:68–77

B

Direct evidence for grain boundary motion as the dominant restoration mechanism in the steady state regime of extremely cold rolled copper

O. Renk[a], A. Hohenwarter[b], S. Wurster[b] and R. Pippan[a]

[a]Erich Schmid Institute of Materials Science, Austrian Academy of Sciences, A-8700 Leoben, Austria
[b]Department of Materials Physics, Montanuiversit Leoben, Jahnstrasse 12, A-8700 Leoben, Austria

Abstract

Ultra-fine-grained high-purity copper (99.99 %) deformed by means of high-pressure torsion into the steady state regime was subjected to additional rolling deformation. The microstructural changes as a function of the applied strain were analysed by means of orientation imaging microscopy. It was found that after a distinctive rolling strain a steady state with respect to microstructural features such as grain size, misorientation distribution and texture evolves again. A special spilt specimen technique was used to perform quasi in situ observations of the microstructure between additional strain increments. Profound insights into the local deformation and restoration processes within the steady state regime were gained. The observations lead to the conclusion that grain boundary migration perpendicular to the rolling direction leads to the disappearance of certain grains, enabling the occurrence of a steady state.

B.1 Introduction

In the last decades, severe plastic deformation (SPD) methods have made it possible to easily apply ultra-high strains to metals at low homologous temperatures. The applied strain leads to enormous grain refinement, resulting in ultra-fine-grained (UFG) or nanocrystalline (nc) materials. However, grain refinement is not indefinite and terminates after a certain amount of strain and the processed materials reach a steady state in deformation regarding microstructural features such as grain size, grain shape or misorientation distribution [1–9]. Additionally, defect densities such as vacancies or dislocations also remain constant. This steady state grain size represents a lower limit for grain fragmentation as additional straining does not lead to further refinement. The occurrence of a distinct minimum grain size for a specific deformation technique at a given temperature and strain rate is confirmed by deforming a material with a starting grain size smaller than the steady state grain size obtained by a certain SPD process. By doing this, the metal coarsens towards the steady state size obtained by deforming a coarse-grained starting material [10]. In contrast to the starting grain size, deformation temperature, amount of impurities and strain rate influence the resulting steady state grain size [1, 2]. In the steady state regime, restoration mechanisms have to take place at the same time in order to keep grain features constant. Estimating the minimum grain size after a certain SPD process is truly a challenging task; however, several attempts with contradicting assumptions have been recently made to predict or model the steady state grain size [11–15]. In Ref. [11] it was suggested that the steady state is a consequence of the equilibrium between grain growth due to adiabatic heating and the refinement caused by straining. Divinski et al. [12] proposed that cracks initiate and propagate during SPD and limit the minimum grain size achievable. If crack initiation can be avoided during deformation, the steady state grain size will be larger than the one calculated by their model. Edalati and Horita developed a model for predicting the steady state hardness of pure metals after SPD as a function of their atomic bond energy and related parameters [13]. Another model proposed that the minimum grain size is a consequence of recovery and generation of dislocations, with the stacking fault energy being one of the most important parameters for the obtainable steady state grain size [14, 15]. In Ref. [1] it was suggested that the mobility of the grain boundaries should be the crucial parameter for the occurrence of a minimum grain size during SPD and larger grains become subdivided again by the formation of low-angle grain boundaries (LAGBs). Despite the vast amount of scientific research in the field of SPD in the last decades and the above-mentioned recently published models for predicting the minimum grain size, the actual deformation and restoration mechanisms within the steady state have not been investigated directly in an experiment due to the obvious experimental difficulties one would have to face. In this contribution these difficulties were overcome by using an innovative experimental technique. The model material, UFG copper, was pre-deformed via high-pressure torsion (HPT) into the saturation regime and deformed further through rolling. The characteristics of rolling allowed for the use of a split specimen and to study quasi

in situ the processes during the steady state, applying for SPD standards very moderate strain increments. The information gained from these experiments will give valuable input for further modelling activities.

B.2 Experimental

UFG copper with an area-weighted grain size of 530 nm was produced by high-pressure torsion. For that, discs of pure copper (99.99 %) with a diameter of 30 mm and a height of 6.5 mm were processed with an applied pressure of 3.5 GPa for 15 revolutions, with a rotational speed of 0.07 rotations min^{-1}. This results in a strain of $\epsilon = 92.1$ at a radius of $r = 11$ mm according to Eq. B.1 with the equivalent plastic strain ϵ, n the number of revolutions, r the radius and t the specimen thickness:

$$\epsilon = \frac{2\pi r n}{t\sqrt{3}}. \tag{B.1}$$

Details concerning the setup of the HPT tool used in this study can be found elsewhere [16]. Microhardness measurements along the radius of the copper disc were carried out to ensure that mechanically homogeneous properties were found across the entire disc, except for the very centre, $r < 0.5$ mm. The UFG copper discs were subsequently cold rolled to different thickness reductions in a conventional rolling mill. The strain rate was kept fairly low. As a consequence, only small incremental thickness reductions and low rolling speeds were allowed in order to minimize self-heating of the copper sheet. The strain rate was estimated from Eq. B.2 [17] to be $\dot{\epsilon} = 10^{-1}\ s^{-1}$, where Δt is the difference in thickness before and after a rolling pass, R is the radius of the rolls, ω is the angular speed of the rolls and ϕ is the logarithmic thickness reduction:

$$\epsilon = \frac{2\omega\phi}{\sqrt{3}\sqrt{\frac{\Delta t}{R}}}. \tag{B.2}$$

The applied rolling strain ϵ (equivalent strain) was calculated according to B.3, with t_1 the thickness of the copper sheet after cold rolling and, t_0 the thickness of the as-processed HPT disc (6.5 mm):

$$\epsilon = \frac{2}{\sqrt{3}} \ln \frac{t_1}{t_0} = \frac{2}{\sqrt{3}}\phi. \tag{B.3}$$

Microstructures after HPT processing and after different amounts of additional cold rolling were captured from electron backscatter diffraction (EBSD) data obtained with a Zeiss LEO 1525 field emission gun scanning electron microscope (SEM). Grain size was calculated from these data using an orientation imaging microscopy (OIM) analysis software package. About 2000 grains were analysed for each condition. Crystallographic texture of the samples was characterized using a Rigaku SmartLab five-axis diffractometer equipped with Cu K_α radiation, a parabolic multilayer mirror in the primary beam and a secondary graphite monochromator. The

Table B.1 Overview of the investigations carried out on samples deformed to different thickness reductions with h the height of the copper sheets, ϕ the logarithmic thickness reduction, ϵ_{CR} the strain applied by rolling and ϵ_{tot} the total strain.

h [mm]	ϕ	ϵ_{CR}	ϵ_{tot}
6.5	0	0	92.1
2.68	- 0.90	1.00	93.1
1.19	- 1.70	2.00	94.1
0.80	- 2.10	2.40	94.5
0.35	- 2.90	3.40	95.5
0.025	- 5.60	6.40	98.5
0.007	- 6.80	7.90	100.0

measurements were performed using a Schultz reflection technique. The collected pole figure data were evaluated using the software package Labotex^{TM} in order to quantify volume fraction of individual texture components.
Throughout this paper, the cold rolled material will be described using rolling direction (RD), transverse direction (TD) and normal direction (ND), see Fig. B.1. In addition to the microstructural and texture investigations, accompanying microhardness measurements with a load of 300 gf were carried out. An overview of the single deformation experiments specifying the geometrical changes and degrees of deformation is given in Tab. B.1.

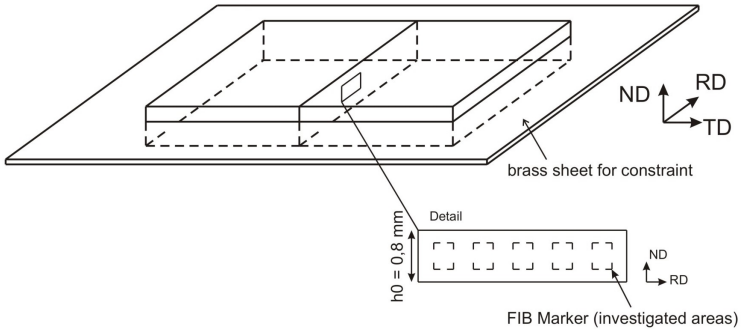

Figure B.1 Schematic of the experimental setup used for the quasi in situ EBSD experiments (inset image not to scale).

As later shown, for a specific deformation regime quasi in situ EBSD experiments were carried out. The principal idea is to obtain OIM data from the same area before and after subsequent rolling steps. To do so, two identical samples were cut out from a copper sheet with a thickness $t = 0.8$ mm, after rolling corresponding to a strain of $\phi = 2.1$. The ND-RD plane of the two samples was ground and electropolished (Elektrolyte D2 from Struers). A LEO 1540 focused ion beam (FIB) dual beam workstation was used to apply markers in the middle of the sheet height

in the ND-RD plane (see schematic drawing in B.1). These markers are suitable to find exactly the same areas after the rolling steps and to ensure that possible drift problems during the EBSD scan are negligible. The height and width of the markers were measured before starting an EBSD scan and compared with the width and height of the markers in the OIM map. To limit the roughness increase along the ND-RD plane during the experiment, which would decrease the quality of the EBSD scans, and to avoid surface effects, the two identically prepared samples were fitted into a brass sheet having a gap that corresponds to the width of the two copper samples. The two polished ND-RD planes were brought into contact with each other and inserted into this gap. Due to the slight expansion of the samples in the TD during rolling, the arising constraint helps the surface roughness to remain negligible and to study the bulk-like behaviour (see Fig. B.1). With the described setup the samples (already a $\phi = 2.1$) and the brass sheet were cold rolled to a total additional thickness reduction of $\phi = 0.7$, with reductions of $\phi = 0.10$ - 0.15 per pass, in the deformation interval from ϕ of 2.1 to 2.8. After each of these rolling increments, the microstructural changes were examined in the FIB marked areas with EBSD scans.

B.3 Results

B.3.1 Microstructural evolution during additional rolling steps after HPT

Microhardness measurements on the as-processed HPT disc showed an almost constant hardness of 142 HV for all radii as the copper disc was deformed to strains that are large enough to reach a steady state. Saturation of the refinement after strains of about $\epsilon \geq 16$ were reported in a large number of papers (e.g. [1, 3–9, 12]). The corresponding area-weighted steady state grain size after HPT processing at room temperature and the given strain rate was found to be 530 nm. To study the change of texture and microstructural evolution during additional cold rolling, EBSD and X-ray diffraction (XRD) measurements as well as microhardness measurements were carried out after various amounts of thickness reduction (see Tab. B.1). Grain boundary maps obtained from OIM data of the microstructures deformed to different thickness reductions can be seen in Fig. B.2.

Fig. B.3 shows the volume fraction of individual rolling texture components as a function of the applied thickness reduction, calculated with an allowed spread of 15°. Additionally, {111} pole figures for the as-HPT-processed material as well as the additionally 90 % and 300 % cold rolled material are inserted. From the pole figures it is obvious that texture is changing from a shear texture after HPT processing into the typical cold rolling texture for copper. From XRD results it can be deduced that texture transition is completed for strains larger than $\phi \geq 2$ where the volume fractions of the individual texture components saturate. At intermediate thickness reductions changes in the volume fraction of the texture components are most pronounced, namely between thickness reductions of about $0.75 \leq \phi \geq 1.25$,

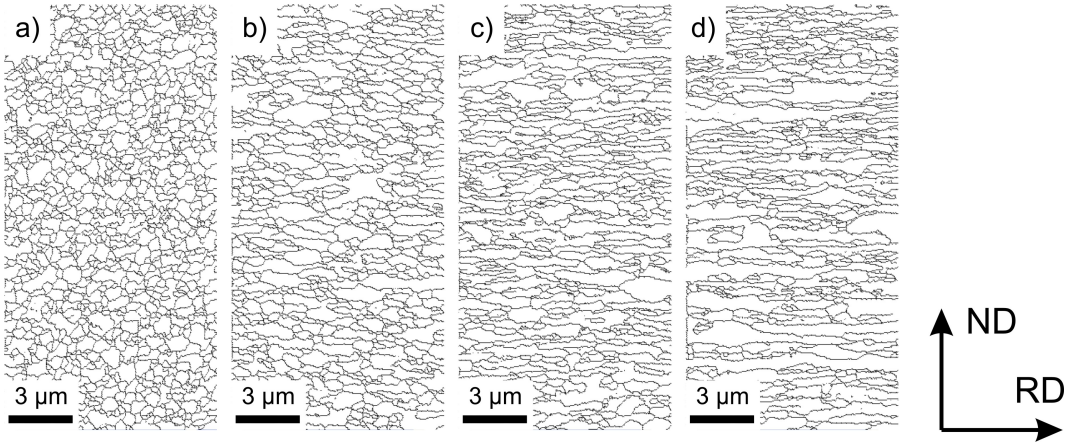

Figure B.2 Grain boundary maps showing the evolution of the UFG microstructure at different thickness reductions: (a) after HPT processing, (b) $\phi = 0.9$, (c) $\phi = 2.1$, (d) $\phi = 5.6$.

which is consistent with marked hardness changes that will be discussed later.

In addition, microstructural parameters such as grain shape were investigated from EBSD scans. The cold rolled structure is elongated, thus the area-weighted half axis of the small (minor) and large (major) axis of the grain were calculated as a measure of the grain size. The results of these microstructural investigations are summarized in Fig. B.4a. The length of the minor axis changed only negligibly during cold rolling, see Fig. B.4a. The length of the long axis increased during cold rolling and reached values of ≈ 1.2 μm at thickness reductions of $\phi \geq 2$.
For larger thickness reductions the length of the major axis remained almost constant (Fig. B.4a). For calculation of the aspect ratio, the area-weighted length of the minor and major axis of the grains was used. This corresponds to an aspect ratio of ≈ 5 for thickness reductions larger than $\phi \geq 2$, which is about two times larger in comparison with a HPT processed sample. An examination of the grain size distribution showed that the lengths of the major and minor axes do not exhibit values larger than 4 μm and 0.75 μm, respectively, in the investigated deformation regime. Therefore, elongated grains have to be fragmented again as otherwise the maximum values of the grain axes would change continuously and exceed the aforementioned maximum values. During cold rolling the grains become longer but not considerably thinner along their minor axis. This indicates that their mean size has to increase compared to that of the as-processed HPT disc. For the sake of volume consistency it becomes clear that certain grains have to disappear during cold rolling. In addition to the microstructural investigations, microhardness measurements were carried out on the ND-RD plane at different thickness reductions. Fig. B.4b shows the microhardness as a function of the applied thickness reduction ϕ. The values measured confirm the above-mentioned results of grain coarsening during cold rolling at low thickness reductions up to $\phi = 0.9$, where the lowest hardness of 123 HV was measured. The hardness decrease has a minimum at this thickness reduction, followed by a slight

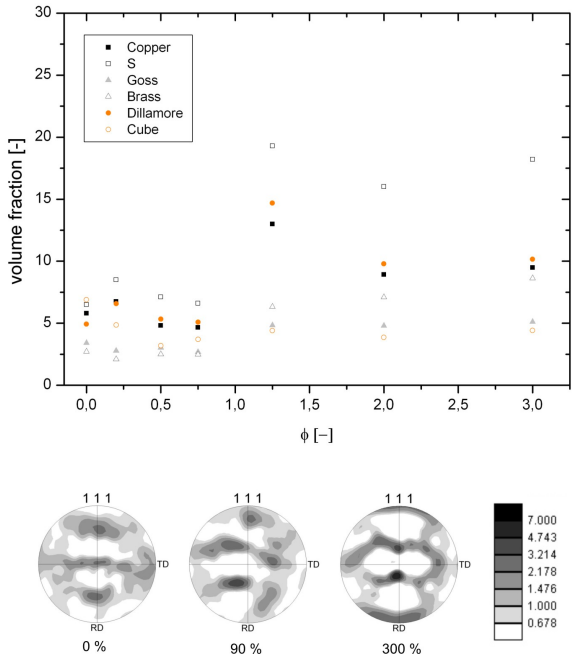

Figure B.3 Volume fraction of texture components as a function of the applied thickness reduction ϕ. The volume fraction was calculated with a spread of 15°. Three {111} pole figures show a transition of the shear texture after HPT processing into the typical fcc cold rolling texture. They were calculated from EBSD data at different thickness reductions.

increase again, levelling off for $\phi \geq 2$ at hardness values of 130 HV. This steady state hardness during rolling is ≈ 10 % lower than the one obtained after HPT processing with 142 HV. The similarity of the texture and microhardness measurements as well as the evolution of the microstructural parameters show that after thickness reductions of $\phi \geq 2$ no distinct changes with further cold rolling are observable. In other words, a steady state was restored, which is in contrast to earlier results on severely cold rolled Ni and Al [18, 19]. Surprisingly, the steady state grain size obtained by cold rolling is marginally larger than the grain size after HPT, which agrees well with the 10 % lower steady state hardness after cold rolling.

B.3.2 Quasi in situ experiments

To scrutinize the microstructural changes within the newly found steady state regime, the aforementioned quasi in situ technique was used. OIMs of six regions of interest, each of them 5 x 11 μm^2 in size, were continuously observed between subsequent rolling steps within the steady state regime starting already with $\phi = 2.1$. The thickness reduction ϕ per rolling increment was ≈ 0.15 - 0.20. In total, four of these rolling steps were carried out, resulting in an additional thickness reduction of $\phi = 0.70$, corresponding to a total thickness reduction of $\phi = 2.8$. Hardness

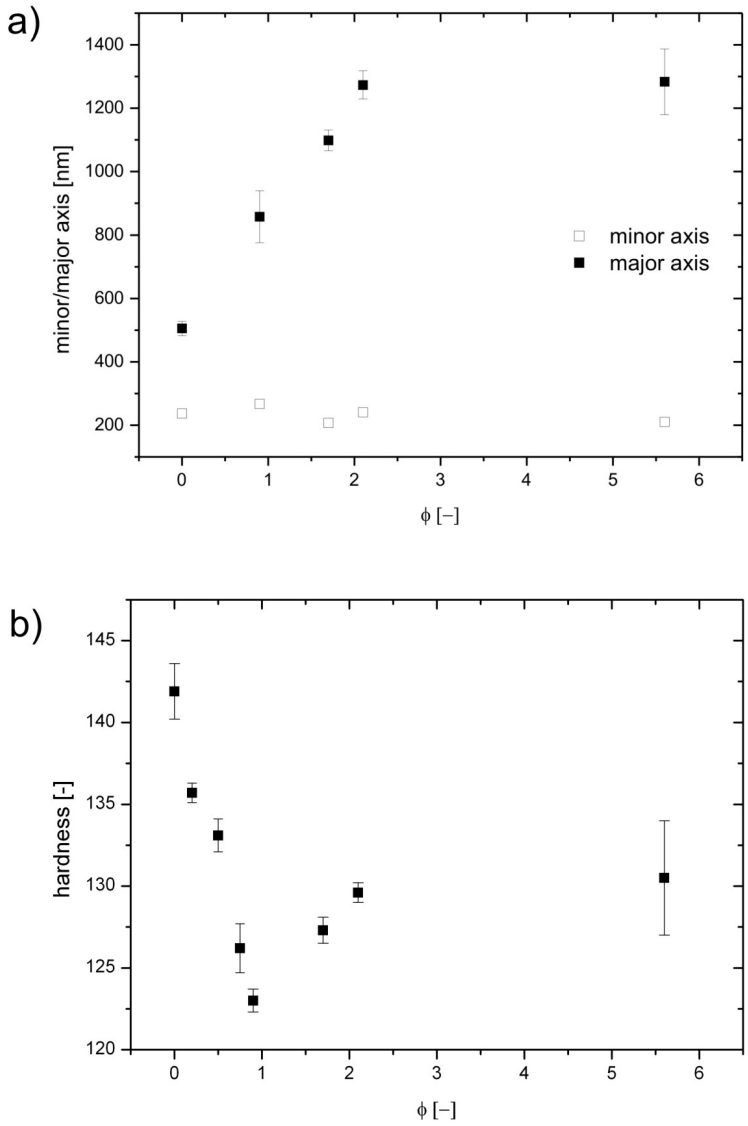

Figure B.4 Changes of microstructural parameters and microhardness during cold–rolling: (a) length of the small and large grain axis as a function of thickness reduction; (b) microhardness as a function of ϕ.

measurements along the ND showed a variation of only 4 %. Although such small gradients are present in the sheet, these will not affect any of our findings as always the exactly same area was investigated (centre layer of the sheet). As an example of the measurements, a sequence of inverse pole figure (IPF) maps of one of the investigated areas at additional rolling increments of $\Delta\phi = 0$, 0.15, 0.30 and 0.50 thickness reductions is shown in Fig. B.5. No clean-up algorithm was applied, as the scan quality was satisfactory enough and clean-ups generally modify the microstructure, especially in grain boundary areas, which would falsify the results. Errors occurring from drift during the scan can also be neglected for this experiment, as the dimensions of the FIB markings were identical in the IPF maps. Changes with respect to the microstructure during the additional rolling increments are clearly visible in Fig. B.5.

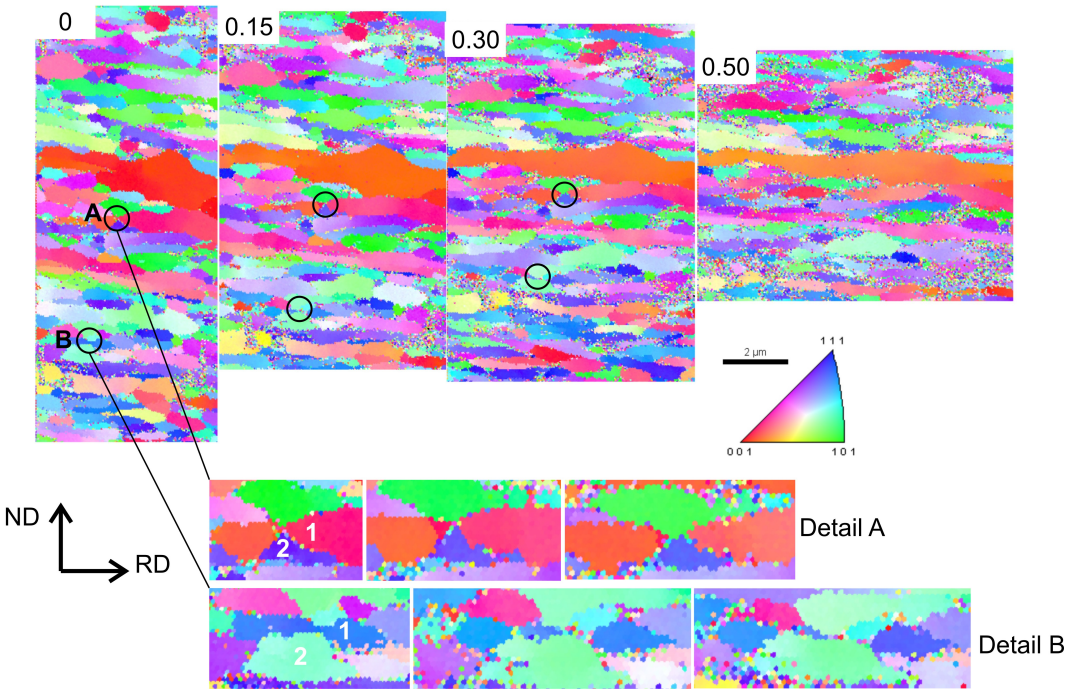

Figure B.5 IPF maps showing the microstructural changes during additional thickness reductions of $\phi = 0$, 0.15, 0.30, 0.50 in the steady state regime during rolling. Two exemplary positions where characteristic changes are visible are circled and shown in larger magnification for the first three rolling increments at the bottom. Grain 1 represents the shrinking grain and grain 2 the growing grain.

Two exemplary positions, labelled A and B, are circled and shown at higher magnifications at the bottom of Fig. B.5. From the experiments it can be seen that a sliding of adjacent grains does not occur on the length scale that is accessible with these EBSD scans. If grain boundary sliding was the dominant mechanism on the atomistic level a pronounced shift of adjacent grains after large thickness reductions should be observable, which is not the case. Therefore, at least for the given defor-

mation temperature and strain rate, other mechanisms have to be responsible for the occurrence of the steady state regime. Quite on the contrary, several grains disappeared during the rolling steps while others grew at their expense. This behaviour is clearly shown in the details of Fig. B.5, where a growing grain (grain 2) splits a grain (grain 1 in detail A, B) first, followed by a possible disappearance during further cold rolling (grain 1 in detail B). This means that the grain boundary of the growing grain moves in the ND. This is surprising as the boundaries aligned in the RD-TD plane are almost planar grain boundaries, thus having no driving force for their movement arising from a reduction in grain boundary energy. Nevertheless, it was shown that shear stresses can lead to the movement of LAGB but also of planar high-angle grain boundaries (HAGBs) [20–22]. A distinct crystallographic relationship between growing and shrinking grains was not observed either, see Fig. B.5. As the two details in Fig. B.5 show, the growing and shrinking grains do not necessarily need to have a similar orientation, see Fig. B.5, detail A.

B.4 Discussion

The results of the present study raise several questions that will be discussed within this section. First of all, it should be discussed in more detail what mechanisms enable the steady state deformation with a constant average grain size. Secondly, the coarsening of the grains, especially at low rolling strains, during the transition of the UFG structure after HPT processing into the cold rolled UFG microstructure will be treated, which finally leads to a larger grain size after cold rolling compared to HPT processing at the same temperature.

B.4.1 Mechanisms enabling a steady state

The occurrence of a steady state during plastic deformation makes restoration mechanisms necessary that, on average, compensate for the refinement caused by additional deformation. Potential mechanisms are schematically shown in Fig. B.6. Such mechanisms could be the movement of grain boundaries leading to the disappearance of certain grains, while others grow at their expense (Fig. B.5) and Fig. B.6a; the movement of triple junctions (Fig. B.6b), which would also enable the growth of neighbouring grains accompanied by a reduction of the aspect ratio; or the sliding of adjacent grains (Fig. B.6c). From the experiments carried out, grain boundary migration along the ND was found to be the dominant restoration mechanism (see Fig. B.5). Therefore, the necessary boundary velocity to balance the refinement caused by plastic deformation should be estimated.
For the experimental conditions with an average thickness reduction of $\phi = 0.15$ per pass ($\epsilon = 0.17$) and an average steady state grain size (boundary spacing) in the ND of 440 nm a refinement of 61 nm per pass can be calculated.
In other words, each boundary has to move 30 nm for a strain increment of $\epsilon = 0.17$ or ≈ 180 nm for a strain of $\epsilon = 1$ in ND to balance the caused refinement. With a strain rate of $\dot{\epsilon} = 10^{-1}\ s^{-1}$ and the mentioned strain increment of $\epsilon = 0.17$ per

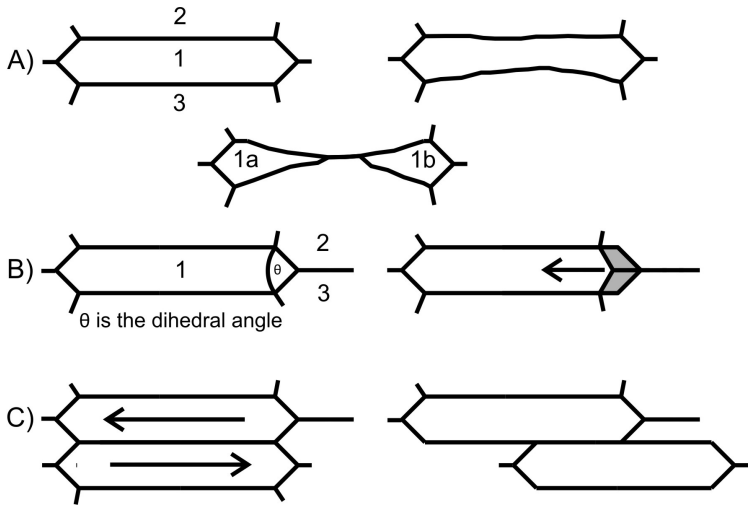

Figure B.6 Schematic of possible restoration mechanisms enabling a steady state: (a) grain boundary motion; (b) triple junction motion; (c) slide event of adjacent grains. Grain 1 represents the shrinking grain, 2 and 3 the growing grains and 1a and 1b are the fragments of grain 1.

pass, the time interval Δt for plastic deformation is ≈ 1.7 s and thus the necessary average grain boundary velocity, v, yields to approximately $v \approx 18$ nm s^{-1}. This seems to be quite a high value for grain boundary migration at room temperature. Nevertheless, grain boundary velocities in the same order of magnitude were experimentally measured in aluminium bicrystals [20]. These relatively high values were attributed to stress driven grain boundary motion. Therefore, the steady state grain size seems to be a consequence of a dynamic equilibrium of grain refinement and mechanically induced grain boundary migration, which was suggested also in [1]. This equilibrium condition must be fulfilled for the entire deformed volume and not only for a single grain. In addition to the mechanically induced boundary migration, triple junction motion was mentioned of being a potential restoration mechanism (Fig. B.6b) and has recently been identified as a recovery mechanism in severely cold rolled aluminium [23, 24]. The driving force for triple junction motion increases if the dihedral angle θ, as shown in Fig. B.6b, decreases. However, triple junction motion can neither be excluded nor confirmed by the experiments carried out in this study as the disappearance of a grain after being split by a migrating boundary could be realized either by further movement of the grain boundary, by triple junction motion, or through a combination of both. With the used experimental technique both possible mechanisms cannot be separated. Results of the mentioned recent studies showed that triple junction motion was not frequently observed at ambient temperature as it is a thermally activated process [23, 24]. Therefore, it is reasonable that their contribution to the restoration of a microstructure within the steady state at low homologous temperatures should not be dominant. Exceptions might occur when grains become thin during deformation, which is also accompa-

nied by a decrease in the dihedral angle θ or at higher homologous deformation temperatures. A more frequent movement of triple junctions and a higher mobility of the grain boundaries at elevated temperature would also explain the observed smaller grain aspect ratio and larger steady state grain size at higher homologous deformation temperatures [1]. As mentioned before, no preferred crystallographic relation was observed between shrinking and growing grains. This local observation is supported by the fact that the volume fractions of the individual crystallographic texture components do not change within the steady state, see Fig. B.3. It is of great importance to think of the driving forces responsible for the movement of the grain boundaries. In principle, UFG or nc structures possess high latent energy due to their large fraction of grain boundaries. An estimation of the energy stored in HAGB yields values of the total grain boundary energy, E_{gb}, of several J cm^{-3}. As a consequence of these high values, a reduction of the grain boundary energy seems likely to be the driving force for the grain boundary movement. A closer inspection, however, shows that this cannot be responsible for the typical rolling structure that consists of a very large grain boundary area parallel to the RD in this study. No grain boundary energy can be saved if an almost planar boundary is moving. It is even enlarged when a shrinking grain is fragmented, see Fig. B.6a, because energy would be only saved when the shrinking grain completely disappears. Recent results suggest that mechanical stresses seem to be important for the movement of (planar) boundaries and often nc or UFG structures showed drastic coarsening when subjected to high stress levels [22, 25–27]. In view of these results combined with our findings, the driving force for the observed grain boundary movement seems to be a result of local stress differences between adjacent grains and not necessarily the high stress levels itself. These stress differences can originate from differences in grain size or Taylor factor. The stress differences yield a difference in elastic strain energy stored during deformation and a difference in the plastic work to be spent to accommodate the external applied strain. In contrast to the grain boundary energy, plastic work or elastic strain energy can also be saved when only a small part of the boundary is moving while the shrinking grain becomes fragmented. Under the assumption of a linear elastic and ideal plastic behaviour of the material that is well fulfilled in UFG metals, the plastic work for deformation scales linearly with the stress. Larger driving forces would result from elastic strain energies, where the energy is proportional to the stress level squared. A simple estimation of the maximum elastic strain energy that can be saved by the movement of a boundary can be performed as follows. Maximum stress differences will arise when a large and a small grain are next neighbours. For simplicity the two grains were regarded as cuboids of 100 nm and 500 nm in thickness, respectively (minor axis), 1000 nm in length (major axis) and 500 nm in width. The values were taken with respect to microstructural measurements as shown in Fig. B.4a and the minimum and maximum values obtained from the distribution of the length of the minor axis. The width was estimated to be the average length measured from OIM recorded along the ND-TD plane. The yield stress of the 500 nm thick grain was taken from literature, having a value of ≈ 440 MPa [28].

Assuming a Hall-Petch type relationship (with an exponent of - 0.5) the yield stress of a 100 nm grain can be estimated to be in the order of 800 MPa. This value is in relatively good agreement with the literature [29]. With these assumptions one can calculate the difference in elastic strain energy density to be $\approx$ 2 MJ m^{-3}, which corresponds with a driving pressure on the boundary of 2 MPa. Literature values for the driving pressures during recrystallization of cold-worked metals are within this range, namely 2 - 20 MPa [30]. The activation energies for the migration of a HAGB are $\approx 10^{-19} J$ or 1 eV per atom. For hot-working or static recrystallization processes it seems clear that this movement is thermally activated. This is not the case for deformation at room temperature and so it is reasonable to assume that plasticity is necessary to overcome this activation barrier. Despite the clarity of this simple estimation, the assumption will bear further scrutiny with suitable experiments.

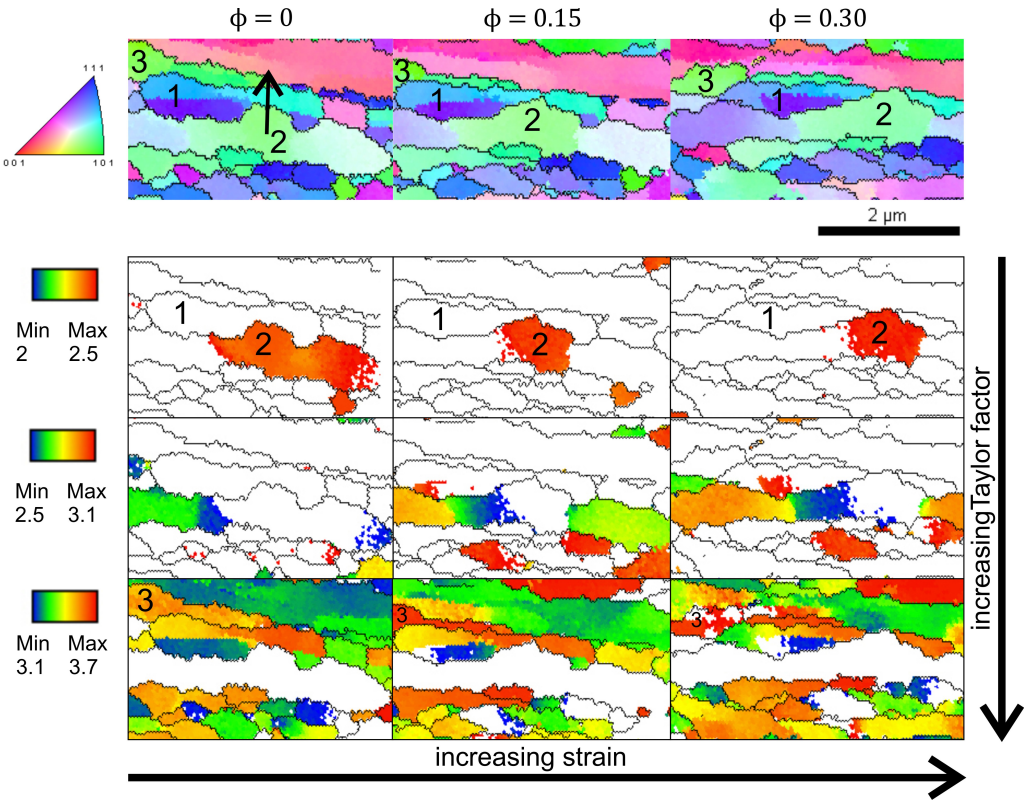

Figure B.7 Possible driving force for grain growth. The IPF maps of a region where a grain shrinks and fragments (grain 1) during additional rolling are shown. The Taylor factors are plotted beneath at different scales for a better visualization of the differences. The growing grain (grain 2) shows considerably lower Taylor factors than the fragmented (grain 1) one.

As previously mentioned, the local stress differences between two adjacent grains could also arise from differences in the Taylor factor. To analyze this, careful investigation of the IPF maps of the quasi in situ experiment in combination with the Taylor factors calculated for rolling were conducted.

The results are shown in Fig. B.7. In the IPF maps at the top of Fig. B.7 it can be seen that grain 1 fragments as grain 2 grows. The direction of the grain boundary movement is indicated with an arrow. Taylor factor maps are plotted underneath, encoded with colours in a rather small factor interval to better visualize their differences.
It can be seen that the fragmented grain (grain 1) has a Taylor factor 50 % larger than the growing grain (grain 2). The same is true for shrinking grain 3, which has a larger Taylor factor than the adjacent grain. Also, for most of the other positions where grains disappeared, stress difference due to different Taylor factors and/or different grain sizes appeared. It should further be mentioned that growing grains could also shrink again as, due to crystal rotation (see Fig. B.5), their Taylor factor is changing during deformation. Additionally, grains could also get into contact with an adjacent grain of similar size or similar Taylor factor, which would also minimize the driving force and lead to refinement again. This is indeed necessary to obtain a steady state grain size distribution and to ensure that grains do not become arbitrarily large. In Ref. [1] it was suggested that larger grains become subdivided again through the increase of LAGBs having a high-angle grain boundary character with increasing strain. However, such a mechanism has not been observed here. On the contrary, it seems that grain boundary motion itself limits the maximum length of the grains.

B.4.2 Structural transition and steady state after cold rolling

Studying the microstructural transition from HPT-processed copper to the steady state structure after cold rolling revealed that a pronounced coarsening up to thickness reductions of $\phi = 0.9$ took place, see Fig. B.4a. The accompanying drop in hardness was followed by a slight increase. The steady state hardness had a value of 130 HV, which is ≈ 10 % lower than the corresponding steady state value after HPT processing (see Fig. B.4b). The observed behaviour during this structural transition that finally leads to the steady state discussed in the previous section can be explained as follows. Texture components have to change from a shear texture after HPT processing into the face centred cubic (fcc) rolling texture. Furthermore, the volume fraction of certain texture components has to increase (see B.3). This process is completed with the onset of the steady state after $\phi \geq 2$. As the same texture occurred for cold rolled coarse grained fcc materials [31], one can conclude that plastic deformation is still dislocation-mediated. A similar behaviour was also observed for cold rolled UFG copper processed by equal channel angular pressing, although smaller thickness reductions were applied [32].

In principle, the texture change can be realized by either crystal rotation and/or shrinkage of grains having an unfavourable orientation for rolling. As coarsening was observed during the initial stage of cold rolling and the minimum hardness measured corresponds well with the formation of rolling texture components (see Fig. B.3 and Fig. B.4b), the latter proposed mechanism seems to be the dominant one although lattice rotation cannot be excluded. This hypothesis is confirmed by comparing the

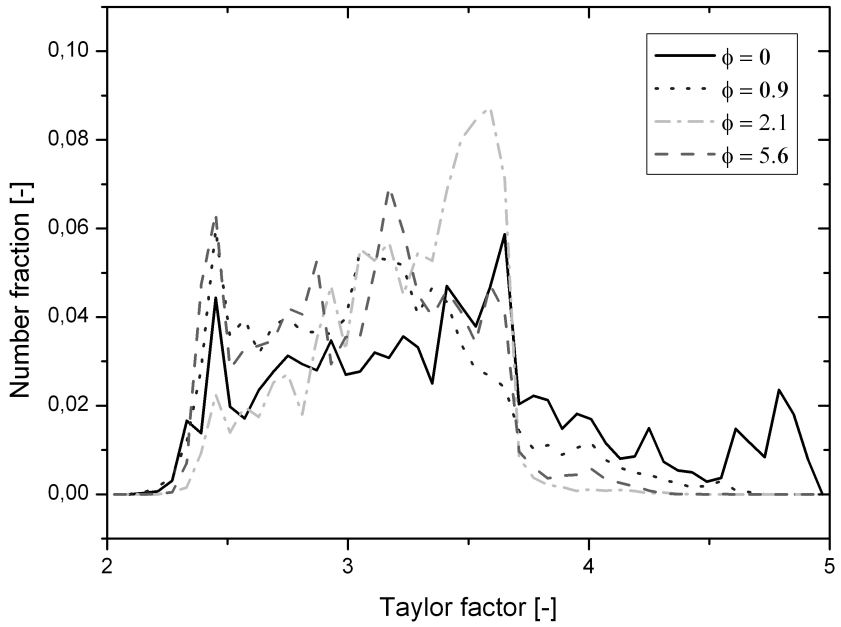

Figure B.8 Distribution of the Taylor factors calculated for cold rolling for microstructures at different thickness reductions.

distribution of the Taylor factor of microstructures deformed to different thickness reductions (see Fig. B.8). From Fig. B.8 it is clearly visible that the UFG structure obtained by HPT is not favourably oriented for cold rolling as ≈ 20 % of the grains have a Taylor factor larger than 3.7. An increasing thickness reduction leads to a decrease in the number fraction of less favourably oriented grains. It has been stated that the driving force for the observed grain boundary motion arises from local stress differences due to different grain sizes or Taylor factors. Regarding the above-mentioned results the latter one seems to be dominant up to thickness reductions $\phi \leq 1$; however, the maximum possible difference in Taylor factor between grains diminishes with increasing strain (see Fig. B.8). This in turn leads to smaller driving forces for the grain boundary movement with increasing thickness reduction. As a consequence the refinement per strain increment is larger than the restoration rate, resulting in a net refinement of the structure until an equilibrium condition between these two competing processes is reached. This explanation is in good agreement with the experimental results (see Fig. B.4b and Fig. B.8).
Despite this, the 10 % lower steady state hardness value after cold rolling is not satisfactorily explained above. A strain rate difference between HPT and cold rolling could principally explain the different steady state grain size [1, 4]. The strain rate during cold rolling $\dot{\epsilon} = 10^{-1}\ s^{-1}$ was, however, larger than in the case of HPT

$\dot{\epsilon} = 10^{-3}\ s^{-1}$, which contradicts this simple explanation. Effects resulting from heating due to plastic deformation are negligible for both processes as well, because the strain rates were rather small. Additionally, more plastic work has to be spent for realizing a certain strain when the sample is deformed by simple shear instead of rolling, and so one could expect even a smaller grain size for cold rolling [33]. The considerations of a dynamic equilibrium between restoration and refinement outlined in chapter B.4.1 lead to the conclusion that in the case of HPT deformation the velocity of the boundaries must be lower than during cold rolling, leading to a smaller amount of growth per strain increment accompanied by a smaller steady state grain size in the case of HPT. One reason for that might be the absence of a large hydrostatic pressure during rolling. There is experimental evidence that hydrostatic pressure impedes the grain boundary mobility [34] and similar effects on the steady state grain size were also reported for copper processed by HPT with different amounts of applied pressure [2,35]. Thus, it is reasonable that for copper a contribution to the enhanced grain boundary mobility during rolling might be due to the absence of hydrostatic pressure.

B.5 Conclusion

In the present work UFG copper was processed by HPT and then cold rolled to strains until another steady state was reached. Afterwards, suitable quasi in situ experiments were carried out to reveal the restoration mechanisms necessary to obtain this new steady state. The main results can be summarized as follows:

- Grain boundary motion along the ND is the dominant restoration mechanism in the steady state regime during cold rolling.
- Stress differences between adjacent grains appear to be the driving force for the observed grain boundary migration.
- The deformation process itself has an influence on the mobility of grain boundaries and as a consequence affects the achievable steady state grain size and hardness.

Acknowledgements
The authors would like to thank Prof. Dr. Jozef Keckes for his support with X-ray measurements.
Financial support by the FWF Austrian Science Fund within project number 24141-N19 is gratefully acknowledged.

Bibliography to paper B

[1] Pippan R., Scheriau S., Taylor A. et al. Annu. Rev. Mater. Res. 2010;40:319–343

[2] Hebesberger T., Stüwe H.P., Vorhauer A. et al. Acta Mater. 2005;53:393–402

[3] Valiev R.Z., Ivanisenko Y., Rauch E.F. et al. Acta Mater. 1996;44:4705–4712

[4] Vorhauer A., Pippan R. Metall. Mater. Trans. A 2007;39:417–429

[5] Sabirov I., Perez-Prado M.T., Molina-Aldareguia J.M. et al. Scr. Mater. 2011;64:69–72

[6] Edalati K., Toh S., Ikoma Y. et al. Scr. Mater. 2011;65:974–977

[7] Popov V.V., Popova E.N., Stolbovskiy A.V. et al. Mater. Sci. Eng. A 2011;528:1491–1496

[8] Pippan R., Wetscher F., Hafok M. et al. Adv. Eng. Mater. 2006;8:1046–1056

[9] Tsuji N., Kamikawa N., Li B. Mater. Sci. Forum 2007;539-543:2837–2842

[10] Yang B., Vehoff H., Hohenwarter A. et al. Scr. Mater. 2008;58:790–793

[11] Zhilyaev A.P., Swaminathan S., Pshenichnyuk A.I. et al. J. Mater. Sci. 2013;48:4626–4636

[12] Divinski S.V., Padmanabhan K.A., Wilde G. Philos. Mag. 2011;91:4574–4593

[13] Edalati K., Horita Z. Scr. Mater. 2011;64:161–164

[14] Mohamed F. A. Acta Mater. 2003;51:4107–4119

[15] Zhao Y.H., Liao X.Z., Zhu Y.T. et al. Mater. Sci. Eng. A 2005;410-411:188–193

[16] Hohenwarter A., Bachmaier A., Gludovatz B. et al. Int. J. Mater. Res. 2009;100:1653–1661

[17] Fritz A., Schulze G., Fertigungstechnik, 9th ed. Springer Berlin; 2010

[18] Hughes D.A, Hansen N. Acta Mater. 2000;48:2985–3004

[19] Liu Q., Huang X., Lloyd D.J. et al. Acta Mater. 2002;50:3789–3802

[20] Winning M., Gottstein G., Shvindlerman L.S. Acta Mater. 2001;49:211–219

[21] Winning M., Gottstein G., Shvindlerman L.S. Acta Mater. 2002;50:353–363

[22] Rupert T.J., Gianola D.S., Gan Y. et al. Science 2009;326:1686–1690

[23] Yu T., Hansen N., Huang X. Proc. R. Soc. A 2011;467:3039–3065

[24] Yu T., Hansen N., Huang X. Philos. Mag. 2012;92:4056–4074

[25] Agnew S.R., Weertman J.R. Mater. Sci. Eng. A 1998;244:145–153

[26] Höppel H.W., Zhou Z.M., Mughrabi H. et al.: Philos. Mag. A 2002;82:1781–1794

[27] Zhang K., Weertman J.R., Eastman J.A. Appl. Phys. Lett. 2004;85:5197-5199

[28] Hohenwarter A., Pippan R. Mater. Sci. Eng. A 2012;540:89–96

[29] Wang Y.M., Wang K., Pan D. et al. Scr. Mater. 2003;48:1581–1586

[30] Stüwe H.P., Recrystallisation of Metallic Materials, Editor: F. Haessner, Dr. Riederer Verlag Stuttgart, 1978

[31] Hirsch J., Lücke K. Acta Metall. 1988;36:2863–2882

[32] Mishin O.V., Gottstein G. Philos. Mag. A 1998;78:373–388

[33] Stüwe H.P. Adv. Eng. Mater. 2003;5:291–295

[34] Hahn H., Gleiter H. Scr. Metall. Mater. 1979;13:3–6

[35] Hebesberger, T., Pippan R., Stüwe H.P. In: Ultrafine Grained Materials II, Editor: Y.T. Zhu, TMS Publications 2002

C

Increasing the strength of nanocrystalline steels by annealing: Is segregation necessary?

O. Renk[a], A. Hohenwarter[b], K. Eder[c], K.S. Kormout[a], J.M. Cairney[c] and R. Pippan[a]

[a]Erich Schmid Institute of Materials Science, Austrian Academy of Sciences, A-8700 Leoben, Austria
[b]Department of Materials Physics, Montanuiversit Leoben, Jahnstrasse 12, A-8700 Leoben, Austria
[c]Australian Centre for Microscopy and Microanalysis, The University of Sydney, Sydney, NSW 2006, Australia

Abstract

Hardening phenomena in nanocrystalline metals after annealing have been widely reported, and the subject of much recent debate. Solute segregation to grain boundaries and dislocation source hardening have been proposed to cause the strengthening. To shed light on the dominant mechanisms, we present results from mechanical experiments and atom probe tomography on samples with similar grain size but different amounts of solute segregation and different boundary chemistries.

Since the pioneering work of Gleiter [1], nanocrystalline (nc) materials have received enormous attention in the past decades. It is well known that this class of material displays not only outstanding mechanical properties, such as high tensile strength or fatigue strength, but also enhanced physical properties, e.g. magnetic properties [2, 3].
The production of nc materials is not only restricted to bottom-up processes such as inert gas condensation or electrodeposition [1]; severe plastic deformation (SPD) methods such as high-pressure torsion (HPT) enable the synthesis of fully dense, bulk nc materials with grain sizes significantly smaller than 100 nm [4]. The advantage of SPD processing is that relatively large bulk samples can be processed, which allows mechanical tests to be performed that require a substantial sample volume, such as fracture toughness or fatigue testing [5, 6]. Although plasticity is still dislocation mediated in the grain size regime of $\approx$ 20 - 100 nm [7, 8], distinct changes are observed in the deformation characteristics when compared with coarsegrained metals. In this grain size regime, grain boundaries act as sinks and sources for dislocations [7,8]. Characteristic dislocation cells, which build up in coarse-grained metals during plastic deformation or fatigue, have not been observed in ultrafine-grained or nc metals, because the grain size is smaller than (or at least of the same order as) these cells [9, 10]. Furthermore, unusual hardening phenomena after annealing treatments well below the temperatures at which grain growth occurs have been observed for nc materials produced by both SPD techniques and bottom-up processes such as electrodeposition (e.g. [11–14]). Although these hardening phenomena have been recognized for several years, the mechanisms behind them are still the subject of much debate in the literature. Some of the explanations are outlined here. For pure nc materials, hardening has been attributed to a significant decrease in the dislocation density within the grains and a relaxation of the boundary structure during heat treatment. The large number of dislocation sinks (grain boundaries) present during annealing may cause a significant reduction in the dislocation density. As a consequence activation of dislocation sources is needed to realize plastic strain after the heat treatment [13, 15]. Similar results were found in MD simulations [16]. The bowing out of a dislocation from a grain boundary that has rearranged into a more equilibrium-like structure is expected to be rather difficult, necessitating high stress levels for the movement of dislocations after annealing [13,15,16]. Interestingly, similar results were obtained during cyclic deformation of nc materials. Experiments and molecular dynamic (MD) simulations showed that plastic strain can cause a similar change in the grain boundary structure to that observed after annealing, leading to cyclic hardening of the samples [17, 18]. Similar behaviour was also observed during cyclic loading of the nc 316L steel used in the present study [19]. Other groups explain the hardening phenomenon on the basis of small amounts of impurity atoms that segregate to the boundaries of the nanocrystallites during annealing. Their contribution to the hardening remains unclear [15]. Segregated solute might supress dislocation emission from the boundaries, pin them or hinder relaxation of the dislocation at the boundaries, all leading to higher stress levels for plastic deformation of the material [15, 20, 21]. Indeed, the hardening behaviour upon annealing was

often attributed to segregated solute for both alloys and metals that contain a certain amount of impurities [22, 23]. Interestingly, the unexpected strength increase in 316L steel was attributed to segregated solute too [24]. In addition, recent MD simulations indicated that solute segregation should lead to enormous strengthening effects [25]. In this paper we present a carefully designed combination of mechanical and microstructural characterization by atom probe tomography (APT) to clarify the question of whether solute segregation or second-phase particles at the boundary can account for the hardening behaviour observed. Annealing treatments of a nc 316L austenitic steel allowed variation of the structure and chemistry of the interface without changing the grain size. By following this methodology, structures with different amounts of solute segregated to the boundaries can be tested mechanically. Linking APT results and the mechanical datasets should clarify whether segregation is necessary for the hardening observed.

Disks of 316L austenitic stainless steel (max. 0.03 C, 0.30 Si, 1.70 Mn, 17.50 Cr, 14.50 Ni, 2.70 Mo, all values in wt.%), 35 mm in diameter and 7.5 mm in height, were severely deformed by quasi-constrained HPT for 15 revolutions at a constant rotation speed of 0.07 rpm with an applied pressure of 3.60 GPa at room temperature, resulting in an equivalent strain $\epsilon = 116$ at a radius of $r = 16$ mm. Details of the setup used and the HPT process itself can be found elsewhere [4, 26]. The HPT process leads to a significant grain refinement down to grain sizes of ≈ 50 nm, investigated by transmission electron microscopy (TEM) and reported in Refs. [19, 27].
To modify the structure as well as the chemistry of the boundaries, isochronal (0.5h) and isothermal heat treatments at 823 K were subsequently carried out on the HPT processed material. Microhardness measurements were conducted on both the annealed and the as-deformed samples to test the influence of the annealing treatments on the mechanical properties.
Microhardness measurements of the isochronally (0.5 h) annealed samples in the temperature range of 573-973 K are shown in Fig. C.1a. Fig. C.1a shows that the hardness increased steadily with increasing annealing temperature up to temperatures of 823 K ($\approx 0.5\ T_m$). In fact hardness increased by 20 % from 5 GPa for the as-HPT-processed material up to 6.10 GPa after the 0.5 h annealing treatment at 823 K. Additionally the hardness values of the nc material are compared with heavily cold-rolled (130 % logarithmic thickness reduction) coarse-grained material in Fig. C.1a. For annealing temperatures higher than 823 K the hardness dropped, which can be attributed to partial grain growth of the structure while parts of the material still remained in the nc state [19].

TEM observations of the material annealed at 823 K showed no evidence of thermally induced grain growth (see Fig. C.2). The grain boundaries of the annealed material (Fig. C.2b) appear sharper when compared to the as-deformed condition (Fig. C.2a), which can be attributed to relaxation of grain boundaries and internal stresses. This is confirmed by a decrease in the full width half maximum (FWHM) values of the {111} peaks obtained by X-ray diffraction by 30 % upon annealing. As the grain size is not changing, this is only possible if defects are annealing out.

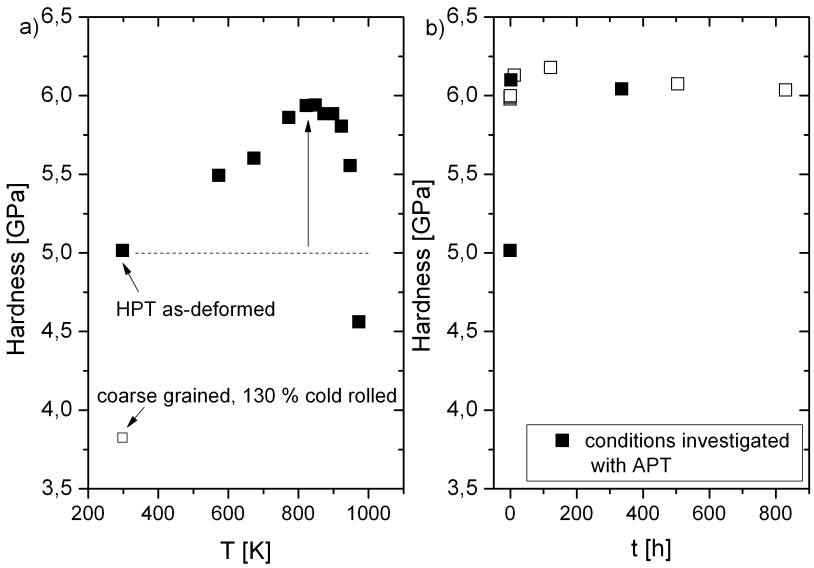

Figure C.1 (a) Hardness of an isochronally (30 min) annealed nc austenitic steel as a function of the annealing temperature. The maximum hardness increase ΔHmax at 823 K is indicated with an arrow. The hardness value of coarse–grained heavily cold-rolled material is given for comparison. (b) Hardness of the nc austenite annealed at 823 K as a function of annealing time.

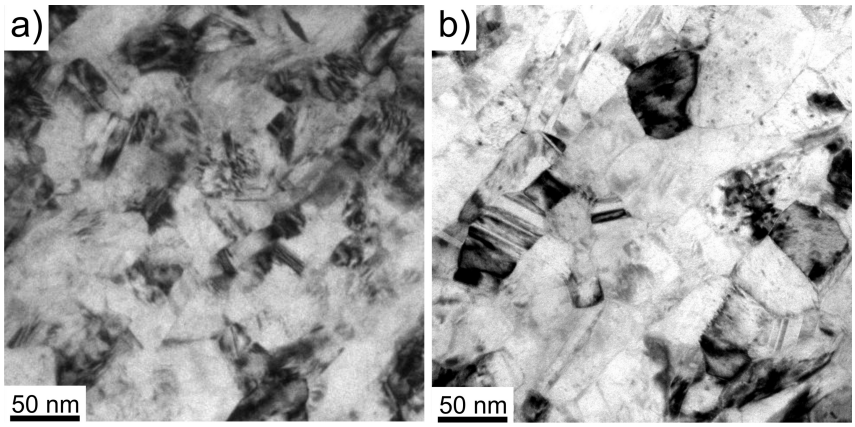

Figure C.2 TEM bright-field images of 316L steel in various conditions: (a) as HPT deformed; (b) HPT deformed + 30 min/823 K.

To study the kinetics of the hardening process, isothermal annealing treatments at 823 K were carried out for different time intervals. The results of these heat treatments on the microhardness are presented in Fig. C.1b. It can be seen that the hardening process takes place rapidly and the maximum hardness value of 620 HV was achieved after 2 h of annealing. Slightly lower values of 610 HV were achieved after 5 min. No change in the mechanical properties was observed, even after annealing the material for 830 h, indicating an unprecedented thermal stability of the nc austenitic steel. To link the mechanical data with possible changes in the grain boundary chemistry due to solute segregation, APT was carried out on as-deformed samples, samples annealed for a short time (1.5 h) as well as samples annealed for a long time (325 h).
For specimen preparation, the samples were dissected into 0.6 mm x 0.6 mm square rods, which were then sharpened via electropolishing to create needles. Rough polishing was conducted with an electrolyte of 25 % perchloric acid in (70 %) glacial acetic acid and a voltage of between 10 and 18 V DC. Fine polishing was performed in 2 % perchloric acid in 2-butoxyethanol at a voltage of 13-18 V DC. The atom probe experiments were carried out on a Cameca LEAP 4000X Si in laser pulsing mode at a specimen temperature of 25 K, a pulse rate of 500 Hz, a pulse energy between 100 and 170 pJ and a target evaporation rate of 1.5 %. IVAS 3.6.4 software was used for the reconstruction and visualization of the APT data. Grain boundaries in the obtained datasets were identified and the Gibbsian interfacial excess of solute (Γ) calculated. Details of the methods for the calculation of Γ can be found in Refs. [28, 29]. Fig. C.3 shows the interfacial excess of Si (Γ_{Si}) of the as-deformed specimen (displayed in red) and the specimen annealed for 1.5 h at 823 K (displayed in blue).

The graph shows the average interfacial excess along 7 selected regions of grain boundaries for the as-deformed specimen and 37 regions for the annealed specimen (each region was a cylindrical volume of data 20 nm in length and 10 nm in diameter). The interfacial excess varied widely, and the error bars show the standard deviation of these measurements. The inset images are regions of datasets obtained showing representative volumes used to determine the interfacial excess values. 14 % of the Si atoms are displayed. The results show very little excess Si on the grain boundaries of the as-deformed specimen. This indicates that, for an austenitic steel, HPT does not lead to deformation-induced segregation as reported previously for several Al alloys [20, 30]. This might be explained by the considerably lower homologous deformation temperature of the austenitic steel. However, segregation can also be diminished again by heavy plastic deformation, as shown for cold-drawn pearlitic steel wires [31].
The samples annealed for 1.5 h showed Γ_{Si} values in the range of 0.2 - 0.64 Si nm^{-2}, indicating significant segregation of Si towards the grain boundaries. The variation of the Γ_{Si} values arises due to inhomogeneous segregation over the length of the grain boundaries. The grain boundaries of the APT datasets were also checked for segregation of all other elements in the sample, but apart from Si, only traces of Mo, Cr and Ni segregated to the boundary. After 325 h of annealing at 823 K,

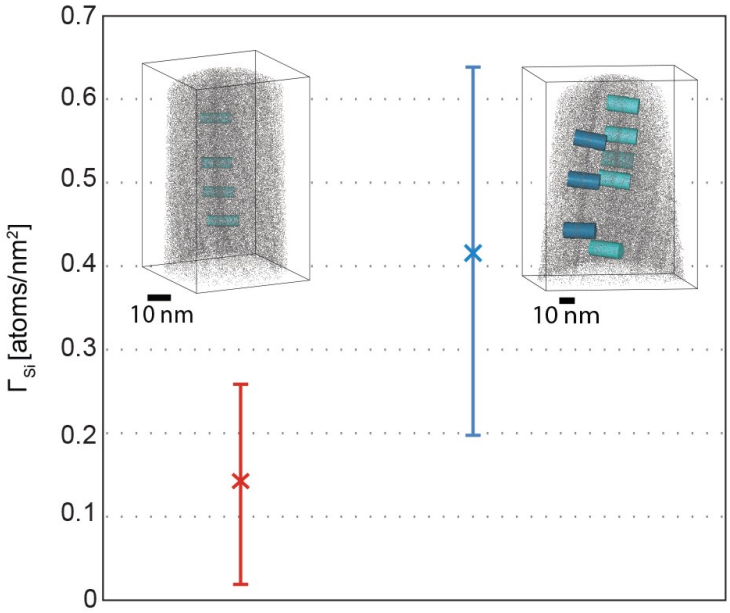

Figure C.3 Interfacial excess of Si (Γ_{Si}) of the as-deformed specimen (red) and the short-term annealed specimen (1.5 h) (blue), with small images of APT reconstructions for each specimen.

in addition to increased Si segregation, Mo and Cr segregated to the boundaries. In these specimens, Mo and Si formed second-phase particles of $\approx$ 5 - 10 nm in thickness and up to 90 nm in length. This can be seen in the APT reconstruction shown in Fig. C.4a and b.

A proxigram [32, 33] showing the composition of all second-phase particles, together with segregation of Cr in the vicinity of the matrixparticle interface, is provided in Fig. C.4c. This plot shows the average composition moving away from an isoconcentration surface (here 14.24 % Mo) in both directions, providing a concentration profile that accounts for the 3-D nature of the grain boundaries. This approach averages any effects from different levels of segregation to different interfaces, as well as any effects that arise from trajectory aberrations in atom probe data when the boundaries are oriented differently with respect to the analysis direction. The proxigram reveals that the secondphase particles contain about 37 at.% Fe, 25 at.% Mo, 10 at.% Si, 23 at.% Cr, 2 at.% Ni, 1 at.% Mn and 0.5 at.% C. In comparison, the matrix consists of 71 at.% Fe, 0.7 at.% Mo, 1 at.% Si, 20 at.% Cr, 5 at.% Ni, 2 at.% Mn and 0.01 at.% C. Fig. C.4b shows a slice of the APT dataset shown in Fig. C.4a, taken in the z direction. Fig. C.4d is a 1-D concentration profile taken from the cylindrical region of interest shown in Fig. C.4b. This profile was taken perpendicular to a second-phase particle. Consistent with the proxigram analysis, it shows that the Cr, Mo, Si and C partition to the second-phase particle, and the particles are lean in Fe, Ni and Mn.

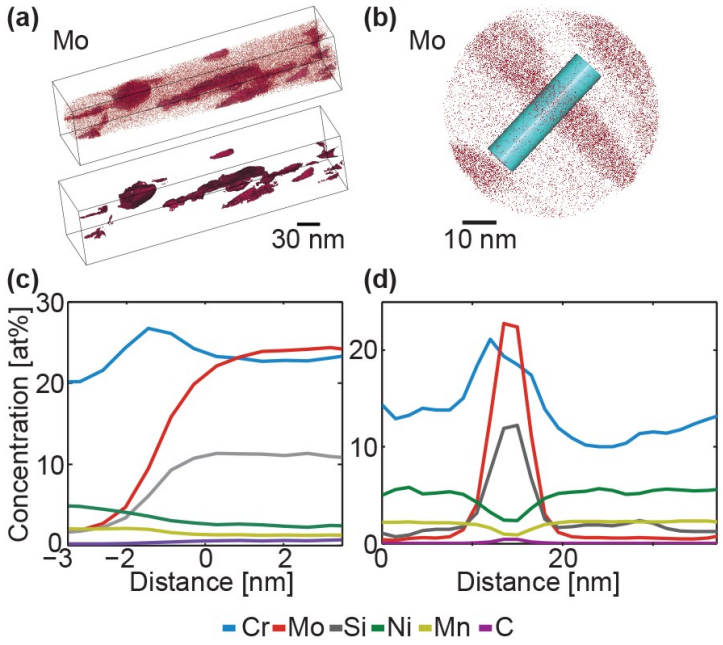

Figure C.4 (a) APT reconstruction for Mo of the long-term annealed sample (325 h). The second APT reconstruction below shows the Mo isoconcentration surfaces of the second-phase particles. (b) Slice of the APT dataset in the z direction with a region of interest (turquoise cylinder) perpendicular to a second-phase particle. (c) Average proxigram from all Mo isoconcentration surfaces (second-phase particles). (d) 1-D concentration profile along the z axis of the of the turquoise cylinder shown in (b).

Beside the particles, additional Si excess $\Gamma_{Si} = 0.36$ Si nm^{-2} was found at the boundary. However, apart from the particles, no Mo, Cr and Ni was found for the 325 h annealed samples which is different to the samples annealed for a short time. Although the annealing temperature of 823 K would be adequate for precipitation of σ–phase, no indication of such phases was found by TEM and transmission Kikuchi diffraction. Additionally the chemical composition of the particles is far from that reported for σ–phase in 316L steel [34]. This further indicates that 316L steel remains fully austenitic also during SPD. The relatively large amount of Si and Mo in the second-phase particles may be explained by the fact that Mo and Si are known to stabilize the ferritic phase. It is likely that these particles would grow further by Ostwald ripening during longer annealing times until the number of particles is too small to stabilize the nc structure against growth. The excellent thermal stability of the nc austenitic steel at 0.5 T_m can be directly attributed to the excess of solute, lowering the grain boundary energy, as treated theoretically in Ref. [35]. For longer annealing times second-phase particles are formed and stabilize the grain boundary, which is sometimes referred as kinetic stabilization [36]. Despite large modifications of the grain boundary chemistry, increasing amounts of Si and Mo segregated to the grain boundary, and finally the formation of second-phase parti-

cles after long annealing times, no changes in the mechanical properties have been observed. If solute strongly influenced the mechanical behaviour, distinct hardness changes would be noticed for the samples annealed for different annealing times. Thus linking APT results and mechanical properties, it can be concluded that the mechanical behaviour of this nc austenitic steel is independent of the amount of solute present at the boundaries. Furthermore the hardening takes place rapidly: after only 5 min of annealing at 823 K the hardness reached values of $\approx 95\%$ of the peak hardness. APT revealed only slight Si decoration even after 1.5 h of annealing at the same temperature, and thus the hardening results are thought to be mainly the result of a dislocation starvation process. The measured hardening effect during annealing can therefore be attributed to the annihilation of relatively mobile dislocations and a relaxation of the grain boundaries, making emission of dislocations or their relaxation at the boundaries difficult. A strong indication for this explanation is the early strain localization during testing of annealed specimens, as the samples will undergo pronounced strain softening, leading to a significantly reduced ductility [13, 15]. Despite these observations, solute segregation is a prerequisite for the observed hardening phenomena but not the actual origin. Segregated solute stabilize the nanocrystallites against grain growth during annealing while competitive processes such as dislocation annihilation and boundary relaxation prevail. These processes, which are thought to be the source for the hardness increase, remain widely unaffected by the boundary chemistry.

To conclude, severely plastically deformed 316L austenitic steel showed an unprecedented increase in hardness by 20 % upon annealing. Combining mechanical data and results from APT revealed that this phenomenon is apparently not related to solute segregation and definitely not to second-phase particles at the boundary. Nevertheless, solute or second-phase particles stabilize the nc structure and therefore allow for the annihilation and relaxation processes necessary for the hardening phenomena during annealing.

Acknowledgements
Financial support by the FWF Austrian Science Fund within project number 24141-N19 is gratefully acknowledged.

Bibliography to paper C

[1] Gleiter H. Prog. Mater. Sci. 1989;33:223–315

[2] Dao M., Lu L., Asaro R.J. et al. Acta Mater. 2007;55:4041–4065

[3] Herzer G. Acta Mater. 2013;61:718–734

[4] Zhilyaev A.P., Langdon T.G. Prog. Mater. Sci. 2008;53:893–979

[5] Hohenwarter A., Pippan R. Scripta Mater. 2011;64:982–985

[6] Hohenwarter A., Pippan R. Mater. Sci. Eng. A 2012;540:89–96

[7] Skrotzki W., Eschke A., Jóni B. et al. Acta Mater. 2013;61:7271–7284

[8] Van Swygenhoven H., Derlet P.M., Frøseth A.G. Acta Mater. 2006;54:1975–1983

[9] Mughrabi H., Höppel H.W. Int. J. Fatigue 2010;32:1413–1427

[10] Boyce B.L., Padilla H.A. Metall. Mater. Trans. A 2011;42:1793–1804

[11] Volpp T., Göring E., Kuschke W.M. et al. Nanostruct. Mater. 1997;8:855–865

[12] Wang Y.M., Cheng S., Wei Q.M. et al. Scripta Mater. 2004;51:1023–1028

[13] Huang X., Hansen N., Tsuji N. Science 2006;312:249–251

[14] Zhang X.F., Fujita T., Pan D. et al. Mater. Sci. Eng. A 2010;527:2297–2304

[15] Ma E., Shen T.D., Wu X.L. Nat. Mater. 2006;5:515–516

[16] Hasnaoui A., Van Swygenhoven H., Derlet P.M Acta Mater. 2002;50:3927–3939

[17] Moser B., Hanlon T., Kumar K.S. et al. Scripta Mater. 2006;54:1151–1155

[18] Rupert T.J., Schuh C.A. Philos. Mag. Lett. 2012;92:20–28

[19] Renk O., Hohenwarter A., Pippan R. Adv. Eng. Mater. 2012;14:948–954

[20] Valiev R.Z., Enikeev N.A., Murashkin M.Yu. et al. Scr. Mater. 2010;63:949–952

[21] Tang F., Gianola D.S., Moody M.P. Acta Mater. 2012;60:1038–1047

[22] Özerinç S., Tai K., Vo N.Q. et al. Scr. Mater. 2012;67:720–723

[23] Shen T.D., Schwarz R.B., Feng S. et al. Acta Mater. 2007;55:5007–5013

[24] Abramova M.M., Enikeev N.A., Valiev R.Z et al. Mater. Lett. 2014;136:349–352

[25] Vo N.Q., Schäfer J., Averback R.S. et al. Scr. Mater. 2011;65:660–663

[26] Hohenwarter A., Bachmaier A., Gludovatz B. et al. Int. J. Mater. Res. 2009;100:1653–1661

[27] Scheriau S., Zhang Z., Kleber S. et al. Mater. Sci. Eng. A 2011;528:2776–2786

[28] Krakauer B.W., Seidman D.N. Phys. Rev. B 1993;48:6724–6727

[29] Felfer P.J., Gault B., Sha G. et al. Microsc. Microanal. 2012;18:359–364

[30] Sha G., Tugcu K., Liao X.Z. et al. Acta Mater. 2014;63:169–179

[31] Li Y.J., Choi P., Goto S. et al. Ultramicroscopy 2013;132:233–238

[32] Hellman O.C., Vandenbroucke J.A., Rüsing J. et al. Micros. Microanal. 2000;6:437–444

[33] Gault B., Moody M.P., Cairney J.M. et al. Atom Probe Tomography, Springer Verlag Berlin, 2012

[34] Hsieh Chih-Chun, Wu W. ISRN Metall. 2012

[35] Kirchheim R. Acta Mater. 2002;50:413–419

[36] Koch C.C., Scattergood R.O., Darling K.A. et al. J. Mater. Sci. 2008;43:7264–7272

D

Hardening by annealing: Insights from different alloys

O. Renk[a], A. Hohenwarter[b], B. Schuh[b], J.H. Li[c] and R. Pippan[a]

[a]Erich Schmid Institute of Materials Science, Austrian Academy of Sciences, Jahnstrae 12, A-8700 Leoben, Austria
[b]Department of Materials Physics, Montanuniversitt Leoben, Jahnstrae 12, A-8700 Leoben, Austria
[c]Institute of Casting Research, Montanuniversitt Leoben, Franz-Josef-Strasse 18, A-8700 Leoben, Austria

Abstract

In contrast to the general notion about the annealing behavior of coarse grained materials, hardening phenomena in nanocrystalline materials can occur. Although the phenomena have already been recognized several years ago, the mechanisms behind are still controversially discussed. For example, the influence of solutes segregated to grain boundaries on the strengthening mechanism is unclear. We present a combination of atom probe tomography and mechanical data to reveal the role of segregations to the strengthening. The results show that despite large modifications of the boundary chemistry the mechanical behavior remains widely unaffected. Additionally, it will be shown that hardening upon annealing can only occur below a material-specific grain size threshold value.

D.1 Introduction

It is well known that cold worked coarse grained materials (where precipitation hardening does not occur) undergo softening during annealing due to recovery and recrystallization. Interestingly, nanocrystalline (nc) materials can show a different behavior - hardening upon annealing instead of a softening. Such phenomena occur at temperatures where significant grain growth of the nc structure can be impeded [1, 2]. Although this behavior has been frequently observed, different hypothesis about the mechanisms and the origin of the hardening have been reported, see for example [1–4]. While the first reports, focusing on very pure metals, attributed the observed strengthening to a reduction in the defect densities during annealing [1, 2], the role of impurities or segregated solute in alloyed systems remained unclear or was expected to cause the hardening [2–4]. Since with decreasing grain size intergranular dislocation sources are thought to become dominant over intragranular sources [5], segregated solute might suppress dislocation emission from the boundaries [4]. Furthermore, as in nc materials dislocations are emitted from the boundary regions and may relax immediately at the opposite boundary, also the relaxation process could be affected by the presence of segregated solute, leading to a different mechanical response.

Nowadays nc and ultrafine-grained materials (UFG) are frequently processed by methods of Severe Plastic Deformation (SPD). After the heavy deformation processes, lattice dislocations will not be completely absorbed at the boundaries and are often stored in the form of dipoles [2]. These dislocations, present in the material before the heat treatment, require lower stress levels for plastic deformation when compared to the activation energy of grain boundary sources [1, 2]. During annealing treatments such segments or dipoles from the interior can be fully absorbed in the boundary leaving a crystal with a low content of mobile defects behind. Additionally, the structure of high angle grain boundaries (HAGB) will change, making the emission of dislocations more complicated, which was also shown in MD simulations [6]. Also the structure of LAGB, mostly present as so called interconnecting boundaries in severely deformed metals will change, and their movement or extraction of dislocations from the boundary will become more complicated [7]. All these processes should lead to increased stress levels to activate dislocation sources after a heat treatment and to the observed hardening. Both, the annihilation of lattice defects and the segregation of impurities or solute will take place simultaneously thus, a separation of their contribution to the hardening seems challenging. Nevertheless, the role of segregations to the strengthening should be investigated further. If they play a key role, an identification of the most effective alloying elements and the interplay between them might lead to the development of ultrastrong materials.

In this study we present a combination of mechanical data of a nc austenitic steel with insights into its boundary chemistry gained by atom probe tomography (APT). These results should lead to a deeper understanding of the role of segregation to the

nc-related hardening mechanism. Furthermore, as hardening upon annealing is not observed in all ufg/nc materials, additional suitable experiments were carried out to gain further insights as to why certain materials do not show the mentioned phenomena.

D.2 Hardening by annealing - is segregation necessary?

The idea to answer the raised question was to compare mechanical data of nc samples with similar grain size but different levels of grain boundary segregation. To do so, we used a standard 316L austenitic stainless steel. Nc structures were obtained by high pressure torsion (HPT) processing. Further experimental details can be found in Ref. [8]. The as HPT deformed structures consist of crystallites with a size of about 50 nm as calculated from several TEM micrographs by the line interception method. The corresponding microhardness was found to be 5 GPa.
An isochronal annealing treatments for 30 minutes in a temperature range up to 973 K showed pronounced hardening up to 6.1 GPa at a temperature of 823 K. Measured room temperature hardness values as a function of the annealing time for the isochronally annealed samples (30 minutes) are shown in Fig. D.1a). For comparison the hardness of heavily cold rolled samples is also shown in Fig. D.1a. To check the thermal stability of the material and to see how fast the hardening process takes place, isothermal treatments were carried out at 823 K, the temperature at which the maximum hardness was obtained.
The results are summarized in Fig. D.1b). The strengthening occurs very rapidly, within 5 minutes the peak hardness values are almost reached. For longer annealing times the hardness only changed slightly before levelling off in a plateau even for long annealing times. Selected area diffraction patterns (SAED) do not reveal any additional Debye Scherrer rings of other phases formed during annealing. As can be expected from the hardness measurements in Fig. D.1b significant grain growth did not occur over the wide range of annealing times. Selected bright field images of the as deformed and the annealed conditions are shown in Fig. D.2. Since grain size and hardness (see Fig. D.1 have not drastically changed but the amount or type of segregated solute might change over time, isothermally annealed samples could be suitable to clarify if segregation contributes to the strengthening. Therefore selected samples were analyzed by APT. A combination of APT data and the mechanical response of the samples should allow one to comment on the contribution of segregated solute to the strengthening. In the following, the major results of the study are summarized, further details of the experiments are outlined in Ref. [8].

Three different sample conditions were investigated by APT, the as HPT deformed samples, samples annealed for 90 minutes and 325 h at 823 K (see also Fig. D.1b). APT results of these three samples are summarized in Fig. D.3. It can be seen that even in the case of the as HPT deformed sample a slight average Si excess at the grain boundaries of $\Gamma = 0.15$ atoms nm^{-2} can be found.

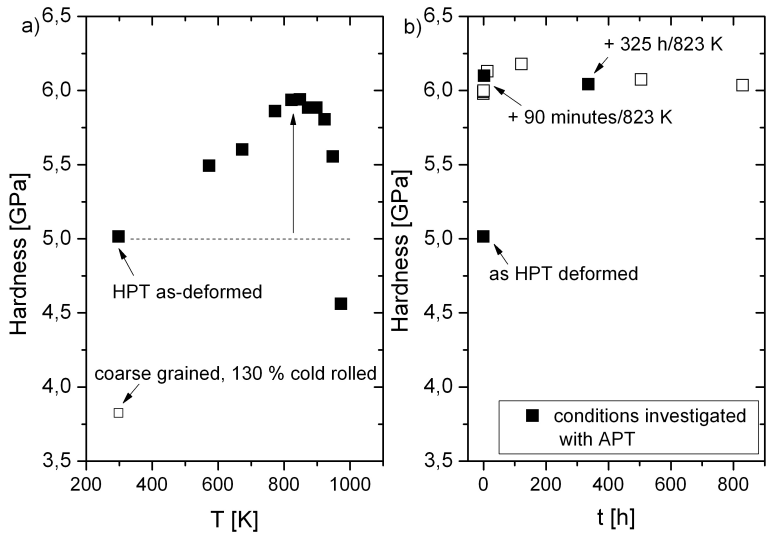

Figure D.1 Room temperature microhardness of a) isochronally annealed samples; b) isothermally annealed nc 316L samples [8].

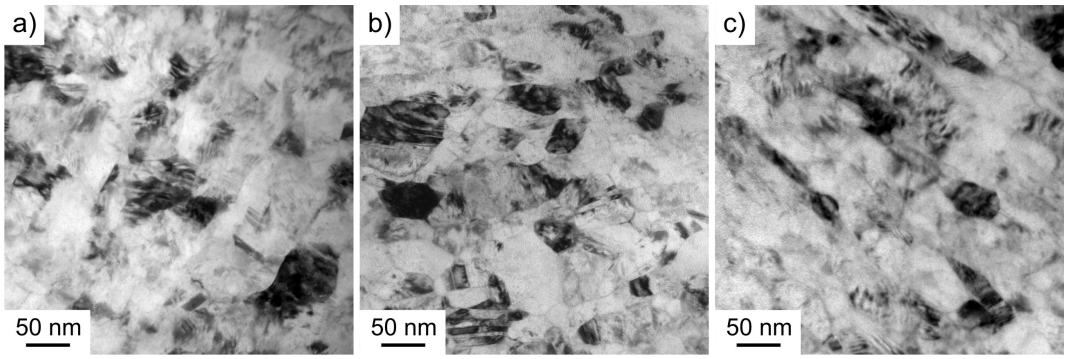

Figure D.2 TEM micrographs of a) as HPT deformed b) 30 minutes/823 K annealed c) 325 h/823 K annealed samples. No significant grain growth was observed during annealing.

Short time annealing of 90 minutes at 823 K leads to an increase of the average Si excess to $\Gamma = 0.40$ atoms nm^{-2}. Apart from the Si, only traces of other alloying elements were found for both samples, the as deformed as well as the 90 minutes annealed sample. For the long term annealed sample (325 h) boundary chemistry has drastically changed. Additionally to a similar Si excess of $\Gamma = 0.36$ atoms nm^{-2} than in the 90 minutes annealed samples, second phase particles could be identified at the grain boundaries. These particles contain mainly Si, Mo and Cr as can be seen in the proxigram in Fig. D.3. Although the temperature range where these particles have formed would suggest sigma phase formation, the average composition of the particles is far from those reported for 316L steels [9]. Further identification of the second phase was not possible from SAED patterns, which only showed reflections that would be referred to a fcc structure.

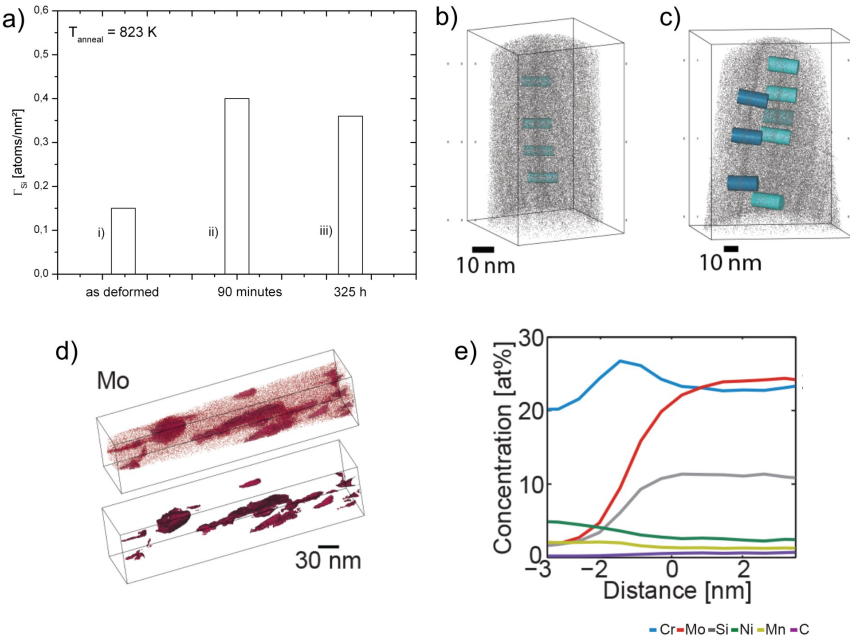

Figure D.3 Results of the samples investigated by APT. a) The average Si excess of several boundaries is displayed for the analyzed samples. b) - d) Reconstruction of the APT tips with Si atoms colored in grey (b and c) and Mo atoms in red (d). d) For the 325 h annealed samples additional particles formed at the grain boundary. e) Their average composition can be seen in the plot [8].

Between annealing times of 90 minutes and 325 h in addition to the segregated Si, Mo and Cr segregate and form particles. Despite this large variation of the boundary chemistry, the mechanical properties remain widely unchanged (see Fig. D.1b). From that it can be concluded that second phase particles at the grain boundary do not influence the strength of a nc material. Furthermore large variations of the type of the segregated element seems also not to have a strong effect on the strength of the material. However, possible effects of small excess values still remain unclear

because during the first 90 minutes, both, the hardness but also the Si excess increased. For further clarification samples either annealed for a very short time or at lower temperatures should be suitable to capture the effects of small excess values. Experimentally, lower temperatures but longer times are easier to realize as one can expect a large scatter when samples are annealed just for very short time intervals. In Fig. D.4 we present the first results of the hardness evolution as a function of the annealing time for temperatures lower than 823 K.

It can be seen that the hardness increase is smaller for lower annealing temperatures. Independent of the annealing temperature, a similar behavior to that at 823 K (see Fig. D.1b) is observed. The hardness rises quickly before it seems that it levels off at a certain plateau value. Surprisingly even at the lowest annealing temperature of 343 K ($\approx 0.2\ T_m$) a significant hardness increase can be observed. Although it is very unlikely that segregation takes place at such a low annealing temperature within 5 minutes, a detailed study has to be carried out to clarify this result. Apart from this study, several other results also suggest, that segregation is not essential for the hardening. For example, nc samples showed pronounced hardening when cyclically loaded at, for nc metals, relatively large plastic strain amplitudes [10]. This behavior was also observed for the nc austenitic steel used in the present study [11]. The reason for the cyclic hardening seems to be an exhaustion of easy mobile dislocations with increasing number of cycles. An in-situ straining TEM study on UFG Al points in the same direction. Stresses to operate a grain boundary source were found to be much larger than those necessary to overcome an obstacle, most likely an impurity [12].

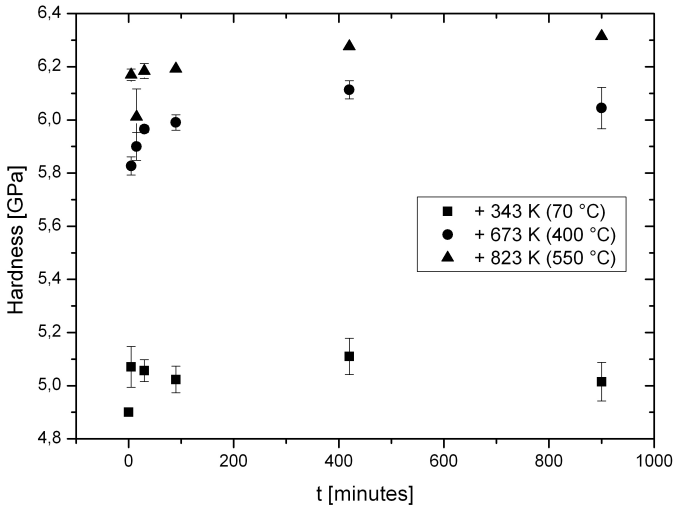

Figure D.4 RT hardness of isothermally annealed nc 316L samples as a function of the annealing time.

D.3 Hardening by annealing - a grain size related phenomena?

As mentioned earlier, hardening by annealing was reported for a wide range of pure metals as well as alloys. Despite this fact, several severely deformed materials do not show a hardness increase upon annealing. In contrast, they show rather constant hardness values until grain growth takes place. One example is UFG high purity Ni (99.99 %) processed by HPT, where no hardening occurs during annealing, see Fig. D.5.

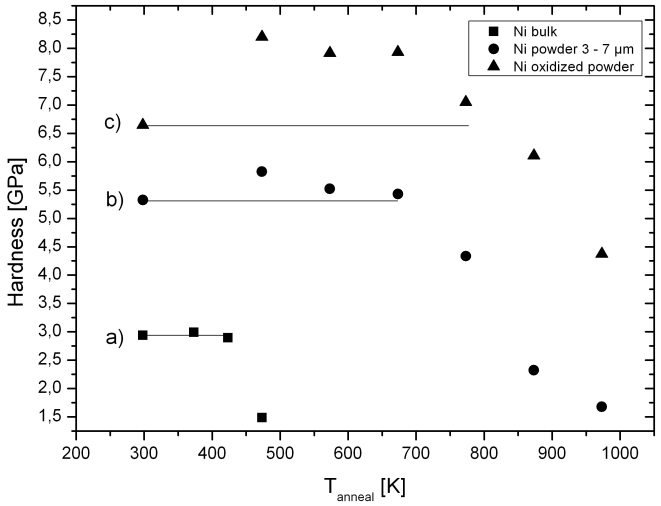

Figure D.5 Room temperature hardness of HPT deformed a) bulk Ni b) Ni powder c) oxidized Ni Powder samples as a function of the annealing temperature. For all temperatures the annealing time was kept to 30 minutes.

When Ni powder (3 - 7 μm particle size) was consolidated and subsequently HPT deformed a slight hardening during annealing takes place. The higher initial hardness of the powder consolidated samples indicates a smaller grain size for this set of samples, as impurities and oxides on the powder surface slow down boundary mobility, thus shifting the minimum grain size achievable by HPT to smaller sizes. Annealing of the Ni powder in air (400 °C for 10 minutes) results in an increase of the oxide content of the powder and to a further reduction of the grain size after HPT. Interestingly, these samples showed an even larger hardness increase upon annealing. From these results one could expect hardening by annealing to be a grain size dependent phenomenon. However, the impurity level of the powder and the bulk material were different. Although the results in section D.2 indicate that this might not explain the different extent of hardening, experiments on samples of the same impurity/alloying content would be more meaningful to interpret. As the mini-

mum grain size achievable in HPT can also be modified by changing the deformation temperature, samples of identical nominal composition but a different grain size can easily be processed. To do so, a Pt5Ru (concentration in wt-%) alloy produced by arc melting was deformed by HPT at 77 K, RT and 573 K. The alloy contains only a single phase after deformation as confirmed by TEM. SAED patterns captured after annealing also did not show signs of the formation of additional phases. Grain sizes of the three samples were calculated by analyzing EBSD data. After deformation, the samples having different grain sizes but the same composition were subjected to isochronal heat treatments (30 minutes) in a temperature range up to 773 K. The results are summarized in Fig. D.6.

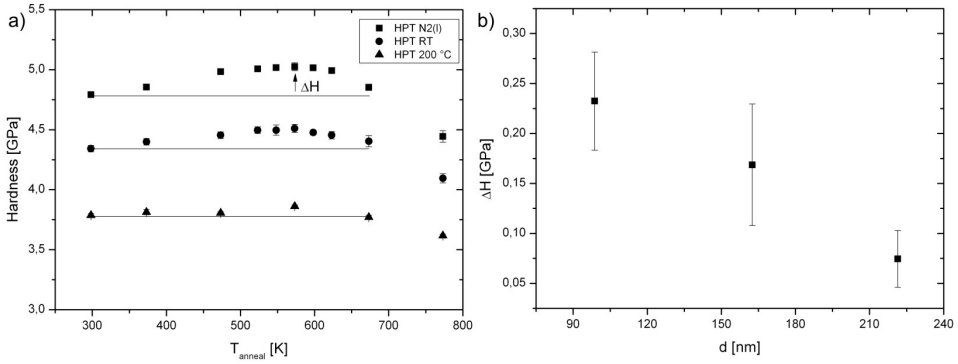

Figure D.6 a) RT hardness values for the isochronally annealed Pt5Ru samples. b) Hardness increase as a function of the grain size.

It can be seen that with a decrease of the deformation temperature also the hardness of the alloys increases, which is in good agreement with grain size measurements. Upon annealing, for the samples deformed at 77 K and RT pronounced hardening can be seen, whereas for the samples deformed at 573 K the hardness increase is almost negligible. Similar to the results in Fig. D.5, the relative hardness increase ΔH is increasing with decreasing grain size. By plotting the hardness increase ΔH as a function of the grain size, a clear dependency can be seen as shown in Fig.D.6b. These results strongly indicate that hardening by annealing will only occur below a threshold value of the grain size, which is 220 nm for the Pt5Ru alloy under investigation. As can be expected from Fig. D.5, also for Ni, hardening will occur only below a certain grain size.

The occurrence of the hardening mechanism only below a specific grain size might further rule out a strong contribution of segregation to the strengthening. Since for all Pt5Ru samples the global composition remains the same, only the excess values of segregated solute might be different. For a given annealing temperature one can expect the diffusion length, i.e. the distance from which solute can be transferred to the grain boundaries, to be similar for all three sets of samples. Only the surface area over which the solute can be distributed drastically increases with decreasing

grain size ($\approx 1/d$). Based on this estimation one would expect larger solute excess values for the samples having the largest grain size. The estimation of 'smaller is cleaner' was also experimentally validated [13]. In the case of a strong correlation between segregation and strengthening, one would expect a significantly enhanced strengthening of the samples having the largest excess of segregated solute - the opposite of what is observed, see Fig. D.6.
The reason for this grain size dependent behavior is yet not clear. It seems that this transient behavior must be related to intrinsic features of crystal plasticity being dominant in the grain size regimes below and above the observed threshold value. One could expect, for grains coarser than a critical value, intragranular sources to be still active after the heat treatment, while with decreasing grain size a transition to intergranular dislocation sources takes place. As outlined above, this requires much higher stress levels.

D.4 Conclusion and Outlook

Hardening by annealing is frequently observed in nc materials. Although this phenomenon has been known for several years the role of segregated impurities or solute to the strengthening is yet not clear. Additionally, several UFG materials show hardening by annealing while others do not. The present study presents experimental findings to clarify the raised questions. The findings lead to the following conclusions:

- Formation of second phase particles and large variations of the type of segregated solute do not have an influence on the mechanical properties of the investigated nc steel
- Hardening by annealing can occur at relatively low homologous temperatures
- Hardening by annealing occurs only in materials with grain sizes below a material specific threshold value

Although the combination of APT and mechanical datasets provided deeper insights to rationalize the origin of the strengthening, the effect of small excess values still remains unclear. However, as significant hardening within short time intervals occurs, further in depth studies are promising to resolve this question. Apart from these observations the impact of this hardening mechanism, specifically of different boundary chemistries, on other mechanical properties such as ductility or fracture toughness will bear further scrutiny.

Acknowledgements
Financial support by the FWF Austrian Science Fund within project number 24141-N19 and the European Research Council under ERC Grant Agreement No. 340185 USMS is gratefully acknowledged.

Bibliography to paper D

[1] Huang X., Hansen N., Tsuji N. Science 2006;312:249–251

[2] Ma E., Shen T.D., Wu X.L. Nat. Mater. 2006;5:515–516

[3] Shen T.D., Schwarz R.B., Feng S. et al. Acta Mater. 2007;55:5007–5013

[4] Valiev R.Z., Enikeev N.A., Murashkin M.Yu. et al. Scr. Mater. 2010;63:949–952

[5] Van Swygenhoven H., Derlet P.M., Frøseth A.G. Acta Mater. 2006;54:1975–1983

[6] Hasnaoui A., Van Swygenhoven H., Derlet P.M Acta Mater. 2002;50:3927–3939

[7] Li J.C.M. Phys. Rev. Lett. 2006;96:215506

[8] Renk O., Hohenwarter A., Eder K. et al. Scr. Mater. 2015;95:27-30

[9] Hsieh Chih-Chun, Wu W. ISRN Metall. 2012

[10] Moser B., Hanlon T., Kumar K.S. et al. Scr. Mater. 2006;54:1151–1155

[11] Renk O., Hohenwarter A., Pippan R. Adv. Eng. Mater. 2012;14:948–954

[12] Mompiou F., Legros M., Boé A. et al. Acta Mater. 2013;61:205–216

[13] Terwilliger C.D., Chiang Y.-M. Acta Metall. Mater. 1995;43:319–328

E

Hardening by annealing in nanocrystals: A further grain size dependent issue

O. Renk[a], A. Hohenwarter[b], J.H. Li[c] and R. Pippan[a]

[a]Erich Schmid Institute of Materials Science, Austrian Academy of Sciences, Jahnstrae 12, A-8700 Leoben, Austria
[b]Department of Materials Physics, Montanuniversitt Leoben, Jahnstrae 12, A-8700 Leoben, Austria
[c]Institute of Casting Research, Montanuniversitt Leoben, Franz-Josef-Strasse 18, A-8700 Leoben, Austria

Abstract

Nanocrystalline metals can exhibit a pronounced strengthening during annealing treatments. Different explanations for this phenomenon have been introduced with no dominant theory. This phenomenon has been systematically studied for the first time here. The results show that hardening upon annealing occurs only below a specific threshold grain size. Below the threshold the extent of hardening by annealing scales with the grain size. The results suggest starvation of dislocations to be responsible for the hardening.

Rising demands for structural materials with respect to their strength and ductility stimulated intense research in the field of Severe Plastic Deformation (SPD) in the last decades [1]. Due to the microstructural refinement during the SPD process, the strength of the materials can be enhanced typically by a factor between two and five compared to the starting material, which can be explained by the limited glide path of dislocations available in such nanostructured (NS) and nanocrystalline (NC) materials. Nevertheless, these strength values still only reach about 1/10 of the theoretical strength. Up to now, beside whiskers, only one single example exceeds these values. Heavily drawn pearlitic steel wires, applicable as structural materials, reach strength values of about 30 % of the theoretical strength after the severe wire drawing process [2]. Beside SPD processing annealing treatments of NC structures have shown to be another intriguing and feasible strategy to further increase strength in NC metals and alloys. At first glance, one would assume this approach to cause softening due to recovery and recrystallization processes, well known from traditionally coarser grained materials. However, several studies have already discovered a hardness increase in the course of heat treatments on systems, where no additional phase occurred during the anneal [3–8]. As an example, the strength of NC austenitic steel samples, could be altered by 20 % by making use of suitable heat treatments [5].

Surprisingly, the origin of such strength increases is still controversially discussed. Based on the fact that in NC materials grain boundaries act as sources and sinks for dislocations it was proposed that heat treatments lead to a continuous decrease in the defect density within a grain - comparable to what is referred as 'defect starvation' in micron and nano scaled single crystalline samples which normally do not contain any intended alloying elements [3, 4, 9, 10]. Under these conditions, plastic deformation of the annealed material requires the activation of dislocations sources, which increases the required stress levels compared to the inherent dislocations present in the material after SPD-processing [3, 4]. Additionally, the grain boundary structure is thought to change during annealing which complicates any dislocation activity, as found by MD-simulations [11], which should result in an increase of strength consequently. While this explanation would hold true for perfectly pure metals, the hardening anomaly was also observed in NC alloys, and the strengthening was related to segregates. Solute present at the boundaries might supress dislocation emission or hinder the relaxation of the lattice dislocations, both increasing the stresses necessary for plastic deformation [6, 12]. Recent MD simulations, which typically study, due to computational reasons, smaller grain sizes than reached by SPD processes, point out into a similar direction [13].

A sound identification of the underlying mechanisms responsible for the unconventional strengthening would permit an optimization of the extent of possible hardening. For example, if segregation would be crucial, the identification of the most efficient solute or their interplay would represent an enormous potential for the design of ultra-strong materials. Nevertheless, untangling the contributions of the mentioned processes is challenging, because segregation of residual impurities can

even occur in high-purity nanocrystals [7,8] while defect annihilation will also occur in alloyed systems. In view of these considerations, the present study was motivated to gain a clear identification of the mechanisms leading to this hardening effect in nanocrystals. For an unambiguous investigation, an alloy system remaining a true single solid solution phase after SPD and consecutive annealing was targeted. For this, PtRu alloys with a nominal content of 5 and 10 wt–% Ru were used. The PtRu alloys were produced by repetitive arc melting to ensure a homogenous solute solution before SPD-processing. The pure metals were purchased from Ögussa (Pt) and smart-elements (Ru). The coarse grained structures were subsequently deformed by quasi constrained high pressure torsion (HPT) [14] to obtain nanostructured materials. Disks having 8 mm in diameter and 0.75 mm in thickness were used and deformed under an applied pressure of 7.8 GPa for 5 rotations, resulting in an equivalent v. Mises strain of $\epsilon_{eq} = 72.6$ at a radius of $r = 3$ mm. Such strains are sufficient to ensure homogenous properties throughout the disk except for the very centre ($r < 0.5$ mm) [15].

As the minimum grain size achievable in SPD is mainly affected by the boundary mobility [16, 17], changing the deformation temperature allows to study the annealing behaviour in samples with different grain sizes without altering chemical composition. Therefore, the deformation temperatures were varied between 77 K and 673 K. A detailed description of the used setup and the equipment used for cooling and heating can be found elsewhere [14, 15]. After HPT deformation, the samples were subsequently annealed at various temperatures up to 873 K for 30 min. TEM investigations carried out on a Philips CM12 on Pt10Ru samples deformed at 77 K and additionally annealed ones (30 min/573 K) were used to clarify whether unknown phase separation processes appeared during HPT deformation and subsequent annealing. These samples were selected, because in the thermodynamic equilibrium state of a binary system the driving force for phase separation is higher at low temperatures. Furthermore, in the case of phase separations, the decomposition kinetics and so the detectability would be maximized by investigating the finest grain sizes present for low temperature deformation. The recorded selected area electron diffraction (SAED) patterns show for both samples a sequence of Debye Scherrer rings fully consistent with the expected FCC phase with no additional reflections (see supplementary section). Microhardness measurements were carried out at room temperature on the as deformed samples as well as on the various annealed ones to capture mechanical changes caused by the annealing treatments. Grain sizes of the PtRu alloys were determined from electron backscatter diffraction (EBSD) data in radial direction (see Fig. E.1 for definition of the principal viewing directions) obtained with a Zeiss LEO–1525 field emission gun scanning electron microscope (SEM). Grain sizes were calculated from EBSD data using an OIM (Orientation Imaging Microscopy) analysis software package. About 2000 grains were analysed for each condition. The measured hardness evolution of both PtRu alloys deformed at three different deformation temperatures and post-annealed up to 873 K for 30 min are shown in Fig. E.1. These values are the average values of at least six measurements with the standard deviation as the error bar. The values at the low-

est temperature (293 K) represent the as-deformed hardness (H_{def}) without further annealing treatment. For a given deformation temperature hardness values of the as deformed condition (293 K) are shifted to higher levels with increasing amount of solute content as well as for decreasing deformation temperature, what is in good agreement with grain size measurements. All investigated samples show a noticeable hardness increase for annealing temperatures below 573 K, except the Pt5Ru samples deformed at 473 K, which exhibits only a marginal increase in hardness and the Pt10Ru samples deformed at 673 K which showed no hardness increase. Peak hardness values were reached after annealing at 573 K, independent of the composition of the alloys, demonstrating a satisfying thermal stability of the nanostructures up to temperatures of 0.27 T_m. Higher annealing temperatures lead to a continuous decrease of the hardness values due to the beginning of significant grain growth, as shown later. Hardness values measured for the as-deformed (H_{def}) as well as the peak aged samples (H_{max}) are summarized in Tab. E.1.

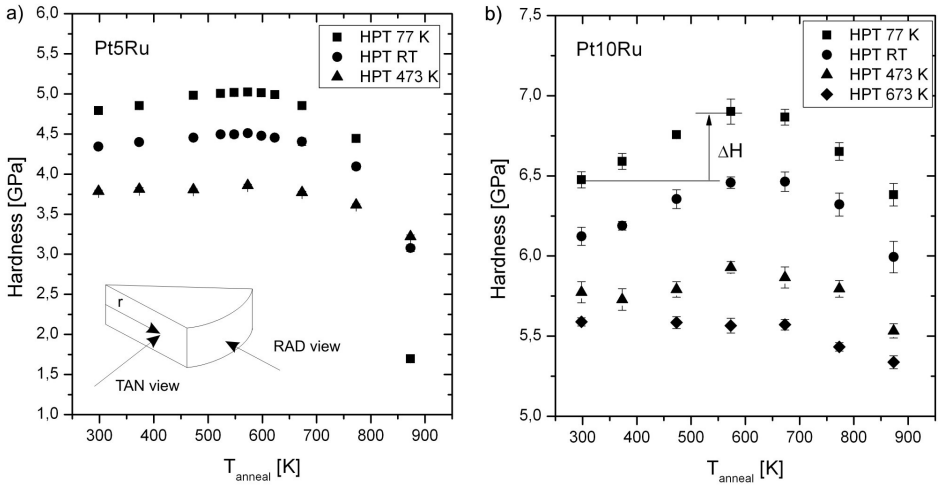

Figure E.1 Room temperature microhardness of isochronally (30 min) annealed a) Pt5Ru and b) Pt10Ru samples as a function of the annealing temperature. The inset image in a) shows the principal viewing directions used to describe the different orientations in the HPT specimen.

For both alloys, the extent of the hardness increase, ΔH, defined as the difference between peak hardness, H_{max}, and hardness of the as-deformed samples H_{def}, is more pronounced for decreasing deformation temperatures, see Fig. E.1b and Tab. E.1. As grain size decreases with decreasing temperature, this proposes that hardening upon annealing is directly related to the grain size, becoming more pronounced for smaller grain sizes. Indeed, the calculated average grain sizes (area weighted), listed in Tab. E.1, clearly confirm this trend. Plotting the extent of the hardening ΔH as a function of the determined grain size, a clear correlation between the hardness increase and the grain size is visible with increasing ΔH values towards smaller grain sizes.

Table E.1 Overview of the properties of the PtRu alloys under investigation. T_{def} is the HPT deformation temperature, H_{def} the hardness of the as–deformed conditions, H_{max} the maximum hardness obtainable after a heat treatment, ΔH the hardness increase and d the average grain size obtained from OIM data in radial direction (RAD).

	T_{def} **[K]**	H_{def} **[GPa]**	H_{max} **[GPa]**	Δ **H [GPa]**	**d [nm]**	$\frac{H_{max}}{H_{def}}$ [–]
Pt5Ru	77	4.79	5.03	240	237.1	1.05
	298	4.34*	4.51	170	264.0	1.04
	473	3.79	3.86	70	310.0	1.02
Pt10Ru	77	6.48	6.90	420	206.2	1.07
	298	6.12	6.46	340	221.5	1.06
	473	5.77*	5.93	160	255.2	1.03
	673	5.59	5.59	0	293.9	1

An extrapolation of the data points in Fig. E.2 reveals, that a certain threshold in grain size exists only below which hardening by annealing occurs (ΔH $>$ 0).
For the PtRu alloys, this threshold value lies at grain sizes of somewhat larger than 300 nm. As the grain size variation was accomplished by SPD at distinct deformation temperatures this grain size dependence might be just a consequence of different inherent defect structures that might change with processing temperature. This argument can be mitigated by reviewing Fig. E.2. Focusing only on the samples deformed at 77 K and RT the behaviour described above is still valid. These two sets of samples can be considered to have similar defect structures as the samples deformed at 77 K were stored at RT after SPD processing for longer times.

Investigating the thermal stability of the investigated structures, it appeared that up to 573 K the microstructures of the samples remained completely stable, without any grain size changes, see Fig. E.4. In addition the fraction of low angle (LAGB) and high angle boundaries (HAGB) did not change up to that point. For higher annealing temperatures, significant grain growth occurred. Although hardness is decreasing at that point still values comparable to the as–deformed condition can be reached, compare Fig. E.1a and b. This implies that a certain fraction of the softening caused by grain growth must be compensated by the observed hardening mechanism of the still fine grained fraction.

The occurrence of a distinct threshold grain size separating the positive (Δ H $>$ 0) from a negative (Δ H $\leq$ 0) annealing response and the clear grain size dependency of ΔH below this critical grain size, allows further conclusions about the underlying mechanisms. The clear grain size dependency questions segregated solute or impurities being responsible for the strengthening. If his would be the case, the relative hardness increase $\frac{H_{max}}{H_{def}}$ (see Tab. E.1) should be more pronounced for samples showing larger excess of segregates at the boundary. The excess can be estimated

* The difference in hardness despite similar grain sizes can be explained by the difference in the Young's modulus [18] and the significant enhanced friction stress [19, 20].

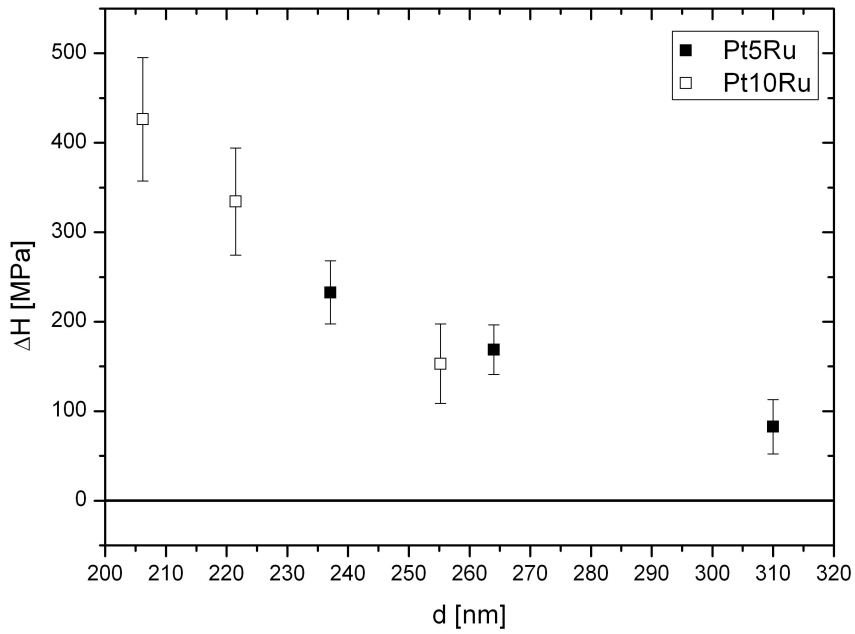

Figure E.2 Hardness increase upon annealing for the two PtRu alloys as a function of the grain size. Clearly, the hardness increase ΔH is related to the grain size, becoming larger towards smaller grain sizes.

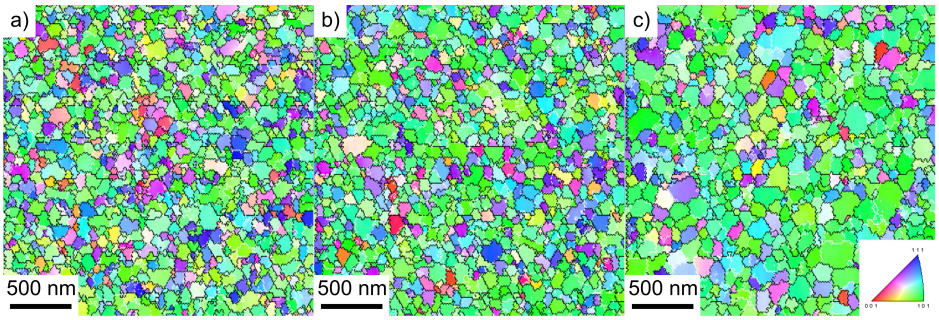

Figure E.3 Inverse Pole Figure (IPF) maps of the Pt10Ru samples a) deformed at 77 K; b) deformed at 77 K and annealed at 573 K/30 min; c) deformed at 77 K and annealed at 873 K/30 min. The structures are seen in tangential direction (TAN, for definition see Fig. E.1) at a radius $r = 3.9$ mm.

in the following simple model. Let us assume the grains to be spheres of diameter d_1 and d_2, with $d_1 < d_2$. During the heat treatment solute can be transferred to the boundaries out of a shell with thickness x. x is proportional to the diffusion length feasible for the given temperature and so independent of the grain size. An average excess Γ [atoms nm^{-2}] of segregates on the boundary can be estimated by dividing the number of segregated solute atoms by the surface of the sphere, A_{sphere}, representing the grain boundary area. The number of segregated solute atoms can be calculated by multiplying the volume of the shell, V_{shell}, with the molar volume V_M, the Avogadro constant N_A and the global solute concentration c in at–%. Additionally a constant f can be inserted, that accounts for the fraction of solute atoms that segregated out of the shell, with $0 \leq f \leq 1$. These considerations lead to the relation as in Eq.E.1.

$$\Gamma \cong \frac{c\ V_{shell}\ N_A\ f}{A\ V_M} \cong C * \frac{V_{shell}}{A} \cong C * \left(x - \frac{2\ x^2}{d} + \frac{4\ x^3}{3\ d^2} \right) \tag{E.1}$$

For $x << d$, what is the case for substitutional alloying elements and low homologous annealing temperatures, as for the PtRu samples, the excess values will be almost independent of the grain size, see Eq. E.1.
In case of mobile interstitial impurity atoms like C or N, the diffusion length might become similar to the grain dimensions, and so the estimation of the excess becomes grain size dependent – with smaller grains having cleaner surfaces. Experimental results support this simple estimation of smaller grains obtaining cleaner boundaries [21, 22]. Additionally, an in-situ straining TEM study showed that stresses, necessary for a dislocation to overcome an obstacle at the boundary, most likely an impurity, were significantly smaller than those needed to operate the grain boundary source [23]. Therefore, if segregates would dominate the strengthening, its extent should decrease for smaller grain sizes or be almost independent of the size, however, exactly the opposite is observed, see Fig. E.2. Although these considerations suggest that segregates do not contribute to the strengthening actively they play an important role for the structural stability during annealing. Through them the boundary energy can be reduced [24] and grain growth diminishes. The strong grain size dependency only below a certain grain size also rules out effects of vacancy clustering, often attributed to a strength increase in coarse grained materials [25, 26]. Such a strengthening mechanism would depend on the distance between such clusters (e.g. loops) and their size and rather be independent of the grain size. Further, because of the increased sink density, for smaller grain sizes annihilation of point defects will be facilitated. This would be in clear contradiction to the threshold-like behaviour as observed here.

The annihilation of lattice defects occurs in the entire grain size regime, below and above the threshold. Thus, the reduction of defect densities itself cannot explain the experimental results either. The transition from hardening to softening can therefore only be attributed to a fundamental change in the basic mechanisms

governing dislocation plasticity. To our notion this transient behaviour separates the traditional grain size regime with intra- and intergranular dislocation sources from a regime where boundary sources (intergranular) prevail as the probability for having a source in the grain interior is diminishing towards smaller grain sizes. Such a transition was suggested earlier [27], however could not be verified experimentally. In the coarse-grained regime dislocation–dislocation interaction is known to be a significant hardening mechanism, also referred as Taylor hardening. For grains with $d > d_{th}$, annealing will lead to a softening, because dislocations re-arrange or annihilate and reduce in this way Taylor hardening. If the remaining dislocations are not sufficient to realize the enforced deformation, the stress for source activation is lowered due to the reduced back stress exerted by the remaining dislocations.
Although similar processes will also occur in the grain size regime below the threshold ($d < d_{th}$) where boundary sources dominate, a reduction in defect densities results in an increase of strength. The most significant and plausible reason explaining this hardening is the loss of dislocations or dislocation debris originating from the synthesis process, in our case SPD processing. This lack of mobile dislocations, which operate at comparably low stresses than the one required for the operation of sources lead to the strengthening, as observed here with the hardness increase. It should be mentioned, that such a starvation process, leading to the hardening, is not a phenomenon exclusively appearing in SPD-processed materials. Inherent and grown-in defects will also occur in other synthesis processes such as found for electro–deposited materials [7]. Beside the changes within the grain interior, the boundaries are thought to change their structure during annealing. A transition, from a distorted state of higher energy, often referred as non-equilibrium boundaries [28] directly after deformation, to a relaxed one after the heat treatment, as also seen in MD simulations [11]. In this way a threshold like behaviour can be rationalized; however with these considerations the grain size dependency on the hardening, experimentally observed in the source dominated regime, is not fully clear and could depend on more than one mechanism.
The behaviour could be attributed to an increasingly hindered activation of boundary sources with decreasing grain size, because in a smaller grain, the structural changes of the boundaries during annealing can be thought to be facilitated. This is due to the increasing free volume possible. On the other hand the size dependent nature of the hardness increase might be just a consequence of a continuous and not abrupt transition from an intragranular to a boundary source dominated behaviour.

In summary, it has been shown, that significant hardness increase can occur during annealing of nanostructured materials when the grain size is below a certain limit, with the extent of the strengthening being invers proportional to the grain size. Considering different possibilities that may cause this strengthening, only a starvation of dislocations and a transition from the classical Taylor dominated regime to a source dominated regime are able to explain the results.

Acknowledgements
Financial support by the FWF Austrian Science Fund within project number 24141-N19 and the European Research Council under ERC Grant Agreement No. 340185 USMS is gratefully acknowledged.

E.1 Supplementary Material

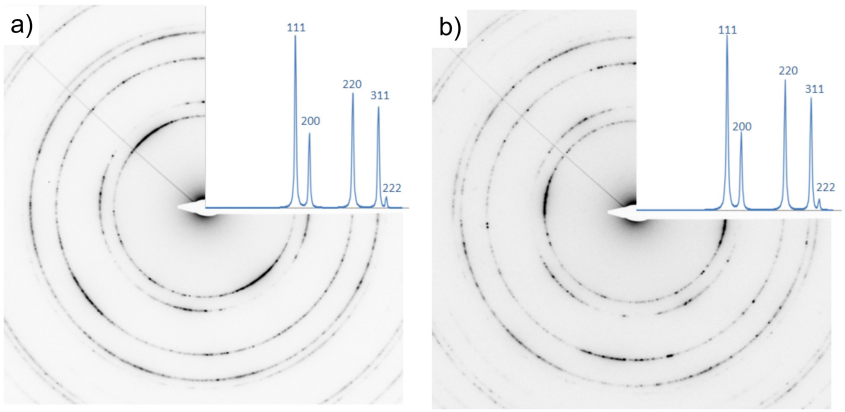

Figure E.4 a) SAED patterns for the Pt10Ru samples deformed at 77K; b) the same samples but additionally annealed at 573 K for 30 min. In both cases only reflections expected for the fcc lattice occurred.

Bibliography to paper E

[1] Valiev R., Islamgaliev R., Alexandrov I. Prog. Mater. Sci. 2000; 45:103–189

[2] Li Y., Raabe D., Herbig M. et al. Phys. Rev. Lett. 2014; 113:1–5

[3] Huang X., Hansen N., Tsuji N. Science 2006;312:249–251

[4] Ma E., Shen T.D., Wu X.L. Nat Mater. 2006;5:515–516

[5] Renk O., Hohenwarter A., Eder K. et al. Scripta Mater. 2015;95:27–30

[6] Shen T.D., Schwarz R.B., Feng S. et al. Acta Mater. 2007;55:5007–5013

[7] Wang Y.M., Cheng S., Wei Q.M. et al. Scripta Mater. 2004;51:1023–1028

[8] Zhang X.F., Fujita T., Pan D. et al. Mater. Sci. Eng. A. 2010;527:2297–2304

[9] Uchic M.D., Dimiduk D.M., Florando J.N. et al. Science 2004;305:986–989

[10] Kiener D., Minor A.M. Nano Lett. 2011;11:3816-3820

[11] Hasnaoui A., Van Swygenhoven H., Derlet P. Acta Mater. 2002;50:3927–3939

[12] Valiev R.Z., Enikeev N.A., Murashkin M.Y. et al. Scripta Mater. 2010;63:949–952

[13] Vo N.Q., Schfer J., Averback R.S. et al. Scripta Mater. 2011;65:660–663

[14] Hohenwarter A., Bachmaier A., Gludovatz B. et al. Int. J. Mater. Res. 100:1653–1661.

[15] Vorhauer A., Pippan R. Metall. Mater. Trans. A 2008;39:417–429

[16] Pippan R., Scheriau S., Taylor A. et al. Annu Rev Mater Res. 2010;40:319–343

[17] Yu T., Hansen N., Huang X. et al. Mater. Res. Lett. 2014;2:37–41

[18] Hyun S., Kraft O., Vinci R.P. Acta Mater. 2004;52:4199–4211

[19] Biggs T., Taylor S.S., Van Der Lingen E. Platin Met. Rev. 2005;49:2–15

[20] Raykhtsaum G. Platin Met. Rev. 2013;57:202–213

[21] Terwilliger C.D., Chiang Y-M. Acta Metall. Mater. 1995;43:319–328

[22] Li J.C.M. Phys. Rev. Lett. 2006;96:2–5

[23] Mompiou F., Legros M., Boé A. et al. Acta Mater. 2013;61:205–216

[24] Saber M., Koch C.C., Scattergood R.O. Mater. Res. Lett. 2015;3:65–75

[25] Hampshire J.M., Hardie D. Acta Metall. 1974;22:657–663

[26] Zehetbauer M.J. Key Eng. Mater. 1994;97–98:287–306

[27] Cheng S., Spencer J.A., Milligan W.W. Acta Mater. 2003;51:4505–4518

[28] Nazarov A.A., Romanov A.E., Valiev R.Z. Acta Metall. Mater. 1993;41:1033–1040